CALIFORNIA INSTITUTE OF TECHNOLOGY

EARTHQUAKE ENGINEERING RESEARCH LABORATORY

NEAR-FIELD GROUND MOTION FROM THE LANDERS EARTHQUAKE

BY

XIAODONG CHEN

REPORT NO. EERL 95-02

PASADENA, CALIFORNIA

1995

Near-Field Ground Motion from the Landers Earthquake

Thesis by

Xiaodong Chen

In Partial Fulfillment of the Requirements

for the Degree of

Civil Engineer

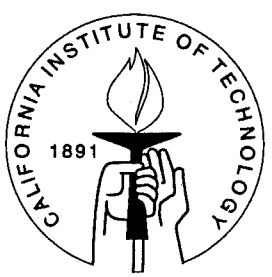

California Institute of Technology

Pasadena, CA 91125

1995

(Submitted by May 8, 1995)

Acknowledgments

I would like to give my sincere gratitude and appreciation to my advisor, Professor W. D. Iwan, for his guidance and encouragement throughout the course of this study. Without his support, this thesis would not have been possible. My sincere gratitude also goes to Professor D. E. Hudson for his encouragement on the investigation of the Landers earthquake and the experimental test of the SMA-2/EMA instrument. I also wish to thank Dr. Thomas H. Heaton from USGS, Professor R.F. Scott and J.F. Hall for the valuable discussions and suggestions.

Many thanks go to Dennis Ostrom of Southern California Edison company for his help in obtaining the Lucerne Valley data and in providing the SMA-2/EMA instrument for testing. Thanks are also given to Rod Merril, John Diehl and other staff members of Kinemetrics Inc. for their generous help during the instrument test. Thanks are also due to Raul Relles for his assistance with the experimental investigation.

Thanks are extended to all the other faculty and staff members in the Civil Engineering and Applied Mechanics departments who helped me in obtaining the excellent education during my graduate studies.

I am sincerely grateful for the financial support from the California Institute of Technology and the National Science Foundation, Clifford Astill, Program Manager. The support in conducting experiments from the Albert Niu Lin Laboratory of Structural Dynamics and the Earthquake Engineering Research Laboratory are particularly acknowledged.

Finally, I wish to dedicate this thesis to my mother and father, Suqin Yu and Keyu Chen, for their love throughout my life and constant support throughout my education.

Abstract

In order to investigate near-field ground motions, an important Lucerne Valley record from the Landers earthquake was studied. The Lucerne Valley record was recorded on the Kinemetrics SMA-2/EMA instrument located 2 km from the fault. Since the characteristics of the SMA-2/EMA instrument were not completely understood and the conventional data processing procedures have difficulty in recovering long-period information from near-field earthquake accelerograms, an instrument test on the SMA-2/EMA was conducted and a new data processing procedure was developed to perform the instrument and baseline corrections.

For an electro-magnetic transducer, an additional parameter of corner frequency, other than natural frequency, electronic damping ratio and sensitivity, should be considered during instrument correction of the SMA-2/EMA recorded accelerograms. For this purpose, a special instrument correction filter was derived in support of instrument correction and a laboratory test of the SMA-2/EMA accelerograph was conducted for obtaining the characteristic parameters of the instrument. The possible error sources in data recording and playback procedure were also examined and an appropriate baseline correction scheme was formulated for effectively removing the nonphysical trend involved in the earthquake data.

The new data processing procedure was verified by a set of SMA-2/EMA simulated long-period accelerograms and then applied to the Lucerne Valley record. The results of new data processing revealed the important features of near-field ground motion, which were a displacement offset parallel to the fault and a large pulse-like motion perpendicular to the fault. The response spectra and Fourier spectra were also calculated and compared to those of the conventionally processed record. With these investigations, a number of important conclusions are obtained and several suggestions for future studies are given.

Table of the Contents

List of Figures

List of Tables

Chapter 1

Introduction

1.1 Motivation

Study of structural response to a large earthquake has been an important topic in earthquake engineering. The calculation of the response spectra of structures to an earthquake is a way of establishing design criteria for structural engineers to carry out earthquake resistant design. However, the correct calculations of response spectra are based on correct ground input information, which is strong ground motion recorded during an earthquake.

Strong-motion acceleration records, or accelerograms, are recorded on strong-motion accelerographs. Because of the limitations of the instrument architecture, various errors are involved in the recorded data. Hence, the data retrieved from the instrument needs to be corrected.

The data which is directly retrieved from the instrument is called raw data or uncorrected data. Correction of the raw data is an important step in data processing. The purpose of the data processing is to correct the raw data into the data which represent the real earthquake ground motion. Therefore, it is necessary to design an effective data processing scheme to recover real ground motion information from earthquake records.

Data processing schemes are mainly focused on two aspects. One is instrument correction and the other is baseline correction. Design of an effective data processing scheme is based on an understanding of the instrument structure, being aware of the sources of noise contamination in the recorded data, and being able to remove

distortions from the data. Although much effort has gone into studies, and various data processing schemes have been constructed since the 1960's, the problem of recovering long-period information from earthquake records still exists. DC offsets are not present in the displacement time histories and long-period components may also be removed from data processed using conventional methods (or conventionally processed records). Overcoming this problem is important, especially for the data processing of near-field earthquake records.

Near-field ground motion from an earthquake on a strike-slip fault has two important characteristics; a permanent displacement offset along the fault direction and a pulse-like motion perpendicular to the fault. These characteristics are more associated with the rupture process of the earthquake than with seismic wave propagation from the earthquake source. The study of the dynamic behavior of structures located in the near field of an earthquake fault has recently attracted the attention of the engineering community. Unfortunately, few near-field earthquake records are available for response analysis and the existing data processing methods have difficulty in recovering long-period information from the records which do exist.

An important near-field earthquake record, the Lucerne Valley record, was recorded on a Kinemetrics SMA-2/EMA instrument during the Landers earthquake of June 28, 1992. To study this record, the author first applied an integration to the acceleration record. The integrated transverse component was found to have a large velocity pulse with a peak value over 100 cm/sec. This value is much greater than that of the conventionally processed record, which showed a peak velocity of 48.94cm/sec. Using the special curve-fitting baseline correction scheme, the preliminary integrated displacement components were obtained to have large displacement offsets which were not present in the conventionally processed record. Since the conventional data processing did not give reasonable geological behavior of the Lucerne Valley station during the Landers earthquake, a new data processing method was developed to correct the Lucerne Valley record. In the meantime, it was also found that the characteristics of the SMA-2/EMA accelerograph were not completely understood. The use of traditional instrument correction induced a displacement offset opposite to what was observed from the Lucerne Valley site. Therefore, a special instrument correction formulation was derived for the electro-magnetic transducer (EMA) and an experimental test on the SMA-2/EMA was conducted to obtain the

characteristic parameters of the instrument. Finally, a new data processing scheme was formulated and verified using simulated earthquake records.

In summary, the work is motivated by the need to correctly interpret near-field ground motion through the data processing of the Lucerne Valley record from the Landers earthquake. In order to do this, the author conducted a field investigation, performed experimental tests of the SMA-2/EMA strong-motion accelerograph, and developed a new data processing scheme which can recover long-period information from near-field earthquake records. The final objective of the work is to give a corrected version of the important Lucerne Valley record as well as to provide a means to obtain reliable strong-motion records, especially records from near-field ground motions, so that structural engineers and researchers can perform reliable dynamic response studies of structures with properly processed earthquake data.

1.2 Brief Review of the Work

The work in this thesis consists of four parts: 1) formulation of a special instrument correction filter for the SMA-2/EMA, 2) calibration of the SMA-2/EMA instrument, 3) development of a new data processing scheme which can recover long-period information from near-field earthquake records, and 4) data processing of the Lucerne Valley record from the Landers earthquake.

In Chapter 2, a brief description of earthquakes is given from the seismological point of view. The characteristics of near-field ground motion are also described based on an understanding of the nature of earthquakes. The chapter also presents several photographs taken from the field investigation of the Lucerne Valley site after the Landers earthquake. The photographs show the geological features of the Lucerne Valley station, the SMA-2/EMA instrument which recorded the Landers earthquake data, and the surface rupture near the Lucerne Valley site.

Chapter 3 gives a brief review of strong-motion accelerographs and a description of the SMA-2/EMA instrument. A detailed description of the electro-magnetic transducer design is given to derive a special formulation for instrument correction of the SMA-2/EMA. It is concluded that conventional instrument correction does not apply to the electro-magnetic transducer. Besides the natural frequency, damping ratio and sensitivity, an additional parameter, called the corner frequency, must be

considered in the electro-magnetic type instrument correction. The new instrument correction corrects the low frequency errors introduced by the EMA transducer.

Chapter 4 presents the instrument test on the SMA-2/EMA strong-motion accelerograph. The chapter describes the experimental setup and the equipment used during the test. The major part of the test was to perform a transfer function test on each of the horizontal transducers. By applying a curve fit technique on the test results, the natural frequency, electronic damping ratio, sensitivity, and corner frequency (or time constant) of the instrument are obtained. A set of simulated earthquake records were also generated manually by moving the instrument in its longitudinal and transverse direction for later applications.

Chapter 5 summarizes the detailed procedure of the new data processing scheme. The possible error sources are scrutinized for every step of the recording and retrieving procedures of the earthquake data. The data processing procedure includes instrument and baseline corrections to an earthquake record. Instrument correction is used to correct the errors brought about by imperfections in transducer design. The baseline correction is mainly correcting the noises introduced by the instruments as well as the environment. Based on the fact that the corrections should be consistent with the physical behavior of the ground motion, a new data processing scheme is developed. To verify the new data processing method, laboratory simulated earthquake records are used as test samples. In data processing of simulated earthquake records, the instrument correction formula derived in Chapter 3 and the instrument parameters obtained in Chapter 4 are used for the instrument correction. The processed results show that the new data processing method works well for correcting the simulated earthquake records. Therefore, it is concluded that the new data processing scheme can also work well on real earthquake records.

Chapter 6 presents the new data processing of the Lucerne Valley record (newly processed record). The results of new data processing are compared with the results of conventional data processing. The response spectra and Fourier spectra of the newly and conventionally processed records are also calculated and plotted in the figures. The differences between the newly and conventionally processed records are shown in the low and high frequency range of both the response spectra and Fourier spectra. The results also show that the response spectra of the newly processed record

are consistent with the long-period ground motion while those of the conventionally processed records are not.

Chapter 7 summarizes the results of this thesis. Some recommendations for the future work and the extended application of the Lucerne Valley record are also given.

Chapter 2

Nature of the Near-field Ground Motion

2.1 Nature of Earthquakes

An earthquake is the result of a rupture process suddenly occurring along a geological fault in the crust of the earth. The rupture emanates seismic waves in all the directions. When the waves propagate to the surface of the earth, the ground shakes. This is called an earthquake.

According to the elastic rebound theory [1], the fractures, or faults, in the earth's crust are caused from the breaking of the weakest portions of the rock when the elastic stress in the rock gradually builds up and exceeds the competence of the rock. The strain in the rock is generated by the tectonic movement of the earth's crust, which may take hundreds and even thousands of years. Most earthquakes are associated with ruptures of existing faults. Some are the result of new faulting. The tectonic movement of the earth's crust continuously accumulates strain energy in the rock, and an earthquake is a process to release this strain energy.

2.1.1 Seismic Waves

The strain energy in the rock is released as heat and elastic waves. After an earthquake, two types of elastic waves are generated from the earthquake focus. They are primary waves (P-waves) and secondary waves (S-waves). Both of these are body waves. The P-waves are dilatational waves which propagate in the same direction of the particle motion. The S-waves are shear waves which propagate in the direction perpendicular to the particle motion. Since there are two directions of the particle motion (horizontal and vertical) which can be perpendicular to the wave

propagation direction, the S-waves are also classified as the SH-waves and SV-waves. When the P-waves and S-waves reach the interface of different materials, they are reflected and refracted. The P-waves can be reflected or refracted as P-waves and SV-waves. The SV-waves can be reflected or refracted as P-waves and SV-waves. Unlike the P and SV-waves, the SH-waves can be reflected or refracted only as SH-waves. By wave theory, the reflection angle of a wave is equal to the incident angle of the wave, while the refraction angle of a wave is not equal to the incident angle of the wave due to the different material constants on both sides of the boundary. The material constants include Lamé elastic constants λ, μ and the mass density ρ. On the free surface of the ground, no refracted waves are considered. Hence, there is no critical angle for a P-wave, but there is a critical angle for a S-wave. When the incident angle of SV or SH-waves exceeds the critical angles, the reflected waves are then "trapped" and propagate along or in a thin layer of the free surface. These types of waves are called surface waves.

Surface waves on the free surface of the ground are also classified as of two types: Love waves and Rayleigh waves. Love waves are the SH-waves traveling within a thin layer of a free surface. The particle motion of the Love waves is perpendicular to the wave propagation direction. Rayleigh waves are coupling of P-waves and SV-waves traveling along a free surface. In this case, the particles perform a circular motion in a vertical plane.

In summary, there are four types of waves that can be recorded from a strong-motion earthquake. They are P-waves, S-waves, Love waves and Rayleigh waves. Of the two body waves, the P-waves travel faster than S-waves. Of the two surface waves, the Love waves travel faster than Rayleigh waves. And in general the body waves travel faster than surface waves. Therefore, the arrival orders of the P-waves, S-waves and surface waves can be identified from an earthquake record.

The P-wave and S-wave velocities are given by the following equations:

$$c_P = \sqrt{\frac{\lambda + 2\mu}{\rho}} \tag{2.1}$$

$$c_S = \sqrt{\frac{\mu}{\rho}} \tag{2.2}$$

where c_P and c_S are the P-wave and S-wave velocities, λ and μ are the Lamé constants of an elastic solid, ρ is the density of the solid material. When the properties of the solid material are known, the values of the P-wave and S-wave velocities can be obtained. In granite, the S-wave velocity is about 3.0 km/sec and the P-wave velocity is about 5.5 km/sec.

The surface wave velocities can be estimated by the following two inequalities:

$$c_L < 0.92 c_S \tag{2.3}$$

$$c_{S_1} < c_R < c_{S_2} \tag{2.4}$$

where c_L and c_R are the Love wave and Rayleigh wave velocities, c_{S_1} and c_{S_2} are the S-wave velocities in the surface and deeper layers.

By reading the time delay of the P-waves and S-waves on the seismic recordings from different stations, the position of the earthquake center can be calculated. The depth of an earthquake can also be determined by the arrival time of the wave front.

2.1.2 Magnitude and Intensity

The earthquake magnitude is a measure of the energy release from an earthquake. It is commonly determined from the seismographic readings. In 1935, Charles Richter of Caltech developed a method to measure the local earthquake magnitude M_L. He defined the magnitude of a local earthquake as the logarithm to the base ten of the maximum seismic wave amplitude (in thousandths of a millimeter) recorded on a standard seismograph (Wood-Anderson type) at a distance of 100 kilometers from the earthquake center. This method is used for measuring the local earthquakes in Southern California area. The type of the seismic wave which has the maximum amplitude is not specified in this method. It can be any type of wave from the horizontal components, whether a body wave or a surface wave.

For a shallow earthquake of larger epicentral distance (over 600 kilometers), the size of the earthquake is measured by surface-wave magnitude M_s. The surface wave magnitude is defined by the logarithm of the maximum combined horizontal ground amplitude (in microns) for surface waves with periods near 20 seconds produced at the given distance by a standard shock taken as magnitude zero [1].

Another magnitude scale, which is not affected by the focal depth, is body-wave magnitude M_b. It is determined from the amplitude of the body waves of an earthquake. Earthquakes that have deep foci usually give very different seismographs from those having shallow foci, even though the total amount of energy release in each event might be the same. In particular, deep-focus earthquakes do not present as significant surface wave trains as do shallow earthquakes. So, to give a better measurement of overall size of an earthquake, a moment magnitude M_w is introduced. The moment magnitude gives a consistent measure of an earthquake size from various ground motion records. In common practice, usually more than one magnitude is calculated to give a global view of an earthquake's size.

Though the magnitude measures the size of an earthquake, it is not sufficient to describe the severity of the ground motion that is observed at different sites. For example, the damage potential of an earthquake to the structures decreases with distance from the earthquake source. So the concept of earthquake intensity is used to indicate the level of damage potential of an earthquake in an area which sustains an equal level of shaking. For the same earthquake, the intensities in different earthquake zones are different. The first intensity scale, which ranged from I to X, was developed by M.S. de Rossi of Italy and Francois Forel of Switzerland in the 1880s. Later, the Italian scientist G. Mercalli constructed an intensity scale with twelve values. In California and most of the United States, an abridged Modified Mercalli Intensity Scale (ranging from I to IIX), developed by H.O. Wood and Frand Neumann, is used to fit the construction conditions of those areas.

2.1.3 Earthquake Faults

As mentioned in the beginning of this chapter, fracture will occur in the crust of the earth at the time of an earthquake. The fractures, or offsets of the geological structure are called faults. The length of a fault may range from a few meters to many kilometers. The rupture velocity of a fault is generally 2.5 km/sec.

There are five basic types of earthquake faults: strike-slip fault, normal fault, reverse fault (or thrust fault when dip is small), horizontal fault (dip angle=0°) and vertical fault (dip angle=90°). Most earthquake faults are a combination of these five types. They are called oblique-faults. A strike-slip fault can also be classified

as a right-lateral fault or a left-lateral fault, based on the motion directions on two sides of the fault.

The study of earthquake faults is very significant for near-field ground motion. Sometimes earthquake damage is not only affected by the shaking of the ground but also by the rupture process and displacement offset of the earthquake faulting.

2.1.4 Recording of Earthquakes

In order to investigate an earthquake in detail, the resulting ground motion needs to be recorded. For this purpose, a special instrument was designed to measure the ground motion.

The first earthquake recorder was invented by a Chinese scientist and philosopher Chang Heng in 136 A.D. [2]. It was a bronze sphere attached with eight dragons oriented evenly in eight directions, each holding a ball in its mouth and face down to eight open-mouthed frogs. The ball was believed to be held by a level device connected to a pendulum inside the hollow bronze sphere. When an earthquake occurred, one of the pendulums swung sufficiently to knock a ball out of the dragon's mouth and fall into the facing frog's mouth. The frog then would vibrate to indicate the approximate epicenter direction of the earthquake. Since such a device did not record the complete time history but only gave the direction of the earthquake, it cannot yet be called a seismograph, but rather a seismoscope.

The first effective seismograph was constructed just before the beginning of the twentieth century [3]. The basic principle of a seismograph is that a device with a mass freely suspended from a frame attached to the ground will vibrate due to inertia, when the supporting frame is shaken by the earthquake ground motion. A pen attached to the mass then records the relative motion of the mass on a paper that is wrapped around a rotating drum.

Nowadays, various types of modern instruments are developed for different purposes. For example, seismographs are developed for seismology study and accelerographs are developed for engineering studies. But no matter what types of instruments and no matter how complex they are, the basic principles of these are similar to the first one.

In a highly seismic area, usually a group of instruments are placed so that a group of earthquake records can be collected for an overall investigation of an earthquake. *Seismograph Arrays* or *networks* are used to record an earthquake at different stations on the same time base. This technique makes it possible to quickly determine the epicenter of an earthquake, to identify different types of the seismic waves (P-waves, S-waves, etc.), to calculate the depth of the soil by the velocity of the seismic wave fronts, and to observe the variation of earthquake intensity in that area.

2.2 Near-field Ground Motion

Near-field (or near-source) ground motion refers to the earthquake ground motion within a distance of a few kilometers from the fault. For a large earthquake, the near-field ground motion is largely affected by the displacement offset and the rupture process of the earthquake faulting. Study [1,4] and field observation have shown that the displacement offset resulting from the earthquake faulting is greatly reduced with increasing distance of the site from the fault. Hence, far-field earthquake ground motion consists mainly of the vibration of the ground resulting from the seismic waves propagating from the earthquake source. The amplitudes of the far-field seismic waves may be amplified or attenuated according to site condition. Compared with the far-field ground motion, near-field ground motion is dominated by the details of the earthquake faulting. In addition to the vibration of the ground motion, the large rapid displacement of the ground near the fault contributes more damage potential to the strong ground motion.

2.2.1 Characteristics of Near-field Ground Motion

Two particular features of near-field ground motion are: 1) permanent displacement offset, and 2) large pulse-like motion. The permanent offset appears parallel to the fault slip direction and the large pulses appears perpendicular to the fault. Usually each pulse represents one event of slip. If several events happen successively, an equal number of pulses may occur.

A permanent offset along the fault can be roughly explained by the elastic rebound theory. After a long process of tectonic movement builds up a certain amount of strain energy in the earth's crust, the rupture occurs along the fault and the energy is then released. As a result, the displacement offsets will occur on both sides

of the fault. At a close-in location, the displacement is dominated by a linear ramp that represents the actual static displacement of a point adjacent to a strike-slip fault [5]. The scale of the displacement offset usually decreases with the reciprocal of the square of the station-to-fault distance.

The large pulse-like ground motion can be explained by the directivity of the seismic waves or "Doppler effect" [1,6]. As mentioned, the seismic waves are produced by the rupture process. The shear waves that propagate to the station are greatly enhanced when the rupture front travels in the direction towards the station. The station then records shorter duration and hence higher amplitude ground motion than the observers located opposite to the direction of rupture propagation.

2.2.2 Synthetic Near-field Accelerograms

Two years before the Landers Earthquake, Heaton and Hartzell [4] simulated several sets of synthetic near-field earthquake accelerograms for investigation of near-field ground motions. The simulation was based on a right-lateral strike-slip earthquake model constructed by Heaton [7]. The station-to-fault distance was assumed to be a few kilometers. Each set of synthetic accelerograms included two horizontal components of velocity time history. One was parallel to the fault trace and the other was perpendicular to the fault trace. After integration of each component, the fault-parallel displacement showed a permanent offset and the fault-perpendicular displacement showed a large pulse. The pulse width or the ramp duration was about the period of the raise time. In 1991, Iwan and the author [8] first studied structural effects of the near-field ground motion by employing those synthetic accelerograms. The study results showed that the large strain in the structures due to the near-field ground motion might cause serious damage to the structures. The maximum strain in a structure was greatly affected by the large pulse-like ground shaking. The study concluded that the investigation of near-field ground motion was very important to engineering practice.

2.2.3 Important Landers Earthquake Data

During the Landers earthquake, an important near-field accelerogram was recorded at the Lucerne Valley station. To obtain a corrected acceleration, velocity and displacement time histories, a proper data processing scheme needed to be

applied to the record. Since the near-field ground motion had not been taken into serious account in the past, the customary data processing schemes were not designed to be able to recover typical near-field earthquake information. This thesis develops a new data processing scheme which can recover long-period information for near-field ground motion. The processed Lucerne Valley record by the new method shows typical near-field ground motion behaviors. The result of the velocity and displacement component are surprisingly similar to the synthetic earthquake waves generated by Heaton and Hartzell. The processed result of the Lucerne Valley record further proves that a large pulse-like motion perpendicular to the fault trace and a displacement offset parallel to the fault trace exist in the near-field ground motion from an earthquake generated by a vertical strike-slip fault.

2.3 The Lucerne Valley Record from the Landers Earthquake

Since the Landers earthquake is the first large event which gave a near-field earthquake record, the author believes it is necessary to give a detailed study of this near-field earthquake record. This important record will no doubt be used for many seismological and engineering purposes in the future.

2.3.1 Geometry and Mechanism of the Landers Earthquake

The Landers earthquake occurred on June 28, 1992 at 4:57am PDT. It was the largest event (M_L 7.4, M_s 7.5) in California since 1952 (Kern County earthquake M_s 7.7). The quake was centered at $34°13'N$, $116°26'W$ with a depth of 1 to 3 km (Reference [9] reported focal depth of 3-8 km).

The Landers earthquake was the result of a right-lateral strike-slip along a vertical fault over 70 km long. The total length of the fault is made up of a combination of several faults. They are Johnson Valley fault, Homestead Valley fault, Emerson fault and Camp Rock fault. The rupture started on the Johnson Valley fault and propagated toward the north. It then took an easterly step across to the Homestead Valley fault propagating northward, slightly turning to the northwest. The rupture stepped further east on the Emerson Fault and propagated in a northwest direction, finally propagating along and to the end of the Camp Rock Fault. The details of the geological format of the Landers earthquake are shown in Figure 2.1.

The field investigations by Kerry Sieh *et al.* show that the fault slip is > 2 m on Homestead Valley fault and > 4 m on Emerson fault. The maximum slip of 6 m occurred at Galway Lake Road. More detailed fault slip information for the Landers earthquake may be found in Reference [10].

2.3.2 Field Investigation of the Lucerne Valley Site

The Lucerne Valley station was the closest station to the fault of the Landers earthquake. The station was located at $34°34'N$, $116°37'W$ within a distance of 2 kilometers from the fault trace and 42 kilometers from the epicenter. It was very close to the region where the largest surface displacement occurred and was clearly within the near-field region of the earthquake. Since the Lucerne Valley station recorded a very important accelerogram on an SMA-2/EMA strong-motion accelerograph, a field investigation was undertaken soon after the Landers earthquake.

On October 1 1992, the author went to the Lucerne Valley site with a staff member from the Caltech Earthquake Engineering Research Laboratory and the Southern California Edison company. The station was on hard soil. The SMA-2/EMA instrument rested in a concrete vault covered by a 40 inches$\times$40 inches steel plate (Figure 2.2). The thickness of the steel plate was 0.125 inches and the thickness of the concrete vault was about 5.5 inches. The concrete vault was embedded 2 feet deep into the ground. The SMA-2/EMA strong-motion accelerograph was placed on a flat surface at the bottom of the concrete vault. A level showed that the bottom surface was still level (Figure 2.3). A compass measurement showed that the instrument is oriented in the direction $N15°W$, which indicated a positive motion of the longitudinal transducer in that direction. Figure 2.4 shows a photograph of the SMA-2/EMA instrument which is a tape recording instrument powered by a set of batteries. When the ground shakes, the masses of the three transducers in the instrument vibrate and send electronic signals to the tape recorder.

Driving roughly perpendicular from the station to the fault, the odometer showed a driving distance of 1.3 miles. Since the driving path was not exactly straight, the actual distance between the station and the fault was estimated to be 1.2 miles. The direction of the fault segment, which was the closest to the station, was measured to be $N50°W$. The cracks along the fault trace were clearly seen on the ground (Figure 2.5). The photograph in Figure 2.5 also shows that the fault went right through a

bush. This can be seen more clearly from the photograph in Figure 2.6: the bush was torn apart into two pieces. The positions of two parts of the bush showed a right-lateral slip of the fault, and the distance between two parts of the bush was measured to be 32 to 34 inches (81 to 86 cm). The vertical offset was not very obvious in that region. Only certain segments of the fault showed a vertical offset (Figure 2.7). The maximum vertical offset in that area was measured to be 13 inches (33 cm). Since the photograph was taken looking northwest, the offset indicated a downward motion on the southwest side or an upward motion on the northeast side.

In some other areas near the Lucerne Valley, a much larger horizontal and vertical offset were observed. Figure 2.8 shows a several meter horizontal offset across the road. Figure 2.9 shows a significant vertical offset of about 6 feet with the east side up and west side down.

From the field investigation, significant surface ruptures from the Landers earthquake were observed, and a set of fault-displacement and -orientation data was collected. This information can be used as a reference in analysing the recorded strong-motion data.

2.3.3 The Lucerne Valley Record from the Landers Earthquake

Lucerne Valley record was recorded on a Kinemetrics SMA-2/EMA instrument which was owned by the Southern California Edison company. After the Landers earthquake, the data was immediately retrieved by the SCE and processed by Kinemetrics, Inc using the conventional data processing method. The processed results are shown in Figure 2.10. The peak accelerations of the uncorrected data are 0.88g, 0.63g and 0.68g for longitudinal, transverse and vertical components respectively. The Fourier spectra of these accelerograms (Figure 2.11) also show that the ground motion at the Lucerne Valley site has a broadband frequency content. Unlike some other earthquake records, the Lucerne Valley record does not appear to have an obvious dominant frequency. The Fourier spectrum of the transverse component also shows a portion of a large amplitude low frequency content. It implies that long-period information is significant in the Lucerne Valley record.

Since the instrument direction measured at the Lucerne Valley station was oriented in $N15°W$ while the fault near the station was aligned at $N50°W$, the longitudinal component is roughly parallel to the fault and the transverse component is

roughly perpendicular to the fault. Because of the proximity of the station to the fault, the processed record should present the characteristics of the near-field ground motion.

2.3.4 Conventional Data Processing of the Lucerne Valley Record

The results of conventional data processing of the Lucerne record are shown in Figure 2.10. They were performed using the standard CIT Vol II method [11]. A filter with a band limit of 0.2 Hz to 25 Hz was applied. The choice of the band limit was based on test results of Robert C. Dullien conducted in 1972 [12]. With this band limit, information with a frequency content under 0.2 Hz and beyond 25 Hz was filtered out. For structural response analysis purpose, the frequency range of interest is usually under 25 Hz. So the choice of a high frequency limit of 25 Hz is acceptable. However, the choice of a low frequency limit of 0.2 Hz, implies that the earthquake waves with periods greater than 5 seconds will be filtered out. Such waves could be important for large or low frequency structures.

The choice of low frequency limit is critical when there is a significant low frequency content in the record. Usually, large amplitude long-period waves occur in an earthquake record for two reasons, 1) long-period waves are amplified when seismic waves travel through soft soil, and 2) the record is recorded in the near-field of a large earthquake. Here, the discussion is focused on the near-field effect since the Lucerne Valley record is recorded at close distance from the earthquake fault. For this particular record, a large pulse-like wave of more than 5 seconds should be recorded. This can be seen from the results of direct integration of the record without applying filters. A permanent offset should also be shown in the displacement component as observed from the field investigation.

Unfortunately the conventional data processing method was not able to recover the long-period information from the record. For example, the results in Figure 2.10 do not show permanent offsets, and the large pulse with a period of more than 5 seconds is missing. In addition, the low frequency response properties of the SMA-2/EMA strong motion accelerograph were unknown before the instrument was completely studied. Since the data processing of an earthquake record includes instrument correction, an instrument test on the SMA-2/EMA also needed to be

conducted. Therefore, a new data processing scheme should be formulated in order to perform better data processing on earthquake records, especially to recover long-period information in near-field earthquake records.

2.4 Discussions and Conclusions

Based on geological observations and earthquake mechanism studies, the characteristics of near-field earthquake ground motion are recognized as a permanent offset along the fault and a large pulse perpendicular to the fault. The pulse-like motion in the perpendicular direction from a large earthquake is believed to be potentially destructive to structures. The study of near-field ground motions is very important to both the seismological and engineering communities.

The Lucerne Valley record from the Landers earthquake is one of the most important near-field earthquake accelerograms. Since there are very rare opportunities to collect near-field earthquake data, the study of the Lucerne Valley record is especially important.

The application of existing data processing procedure to the Lucerne Valley record does not show a capability for recovering long-period information from near-field earthquake records. The preliminary investigation of the record and the study of the instrument show that the existing data processing procedures need to be modified and a new data processing scheme needs to be developed.

In summary, the primary investigation of the near-field earthquake record - Lucerne Valley record brings us the following tasks:

(1). To conduct an instrument test to support the formulation of a new data processing scheme. For this particular record, the instrument used is the Kinemetrics SMA-2/EMA strong-motion accelerograph. The characteristics of this type of instrument were unknown before this study. To precisely obtain the response of the instrument in the low frequency range became particularly important.

(2). To develop a new data processing scheme so that long-period information can be recovered from near-field earthquake records.

(3). To process the Lucerne Valley data with a proper method and therefore to provide reliable near-field earthquake data to seismologists and engineers.

The following chapters will give detailed descriptions of the SMA-2/EMA strong motion accelerograph, the test procedure and test results of the instrument, the development of the new data processing scheme, and the data processing of the Lucerne Valley record using the new method.

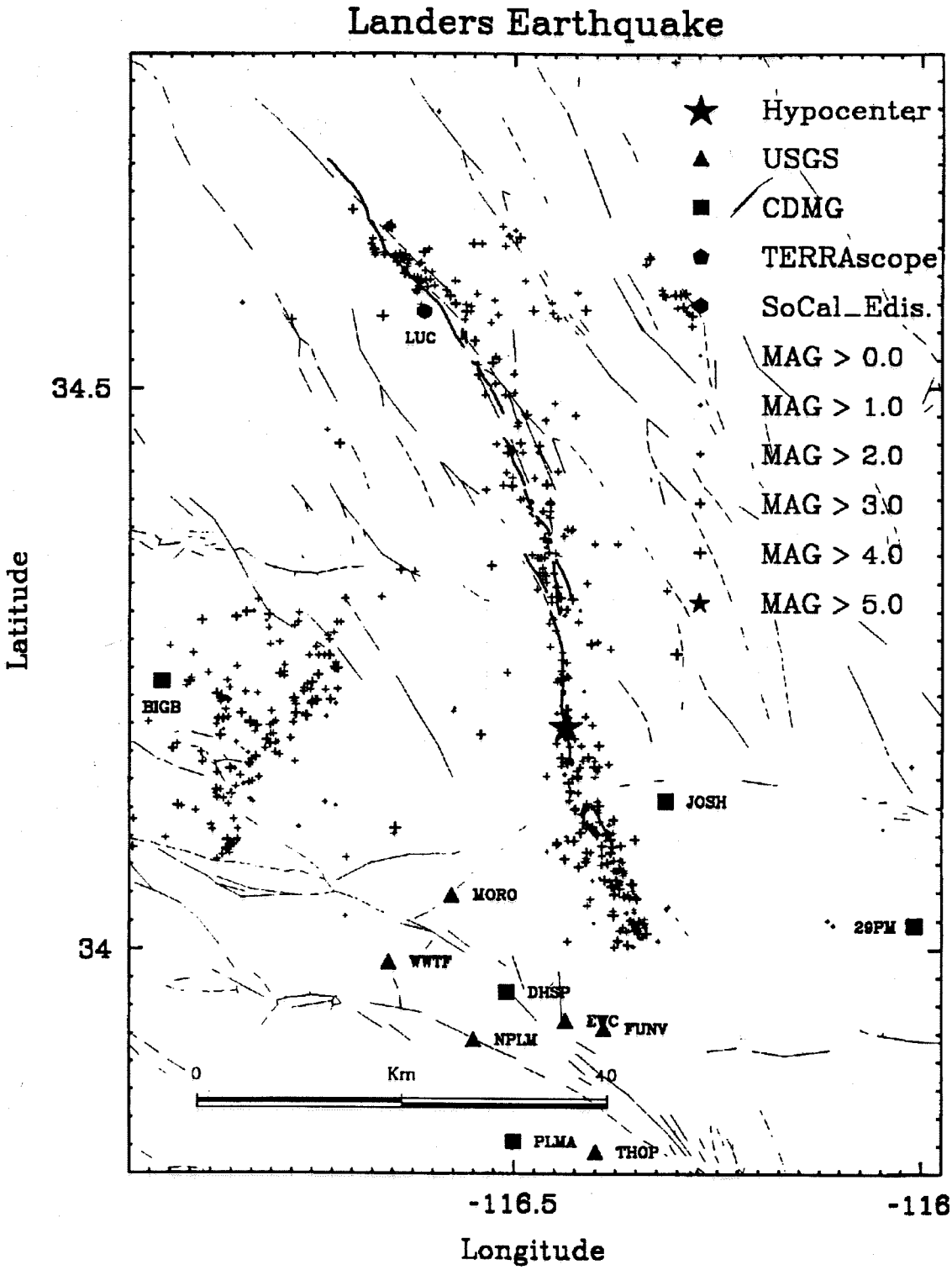

Figure 2.1 Locations of the Landers Surface Rupture and Lucerne Valley Station.

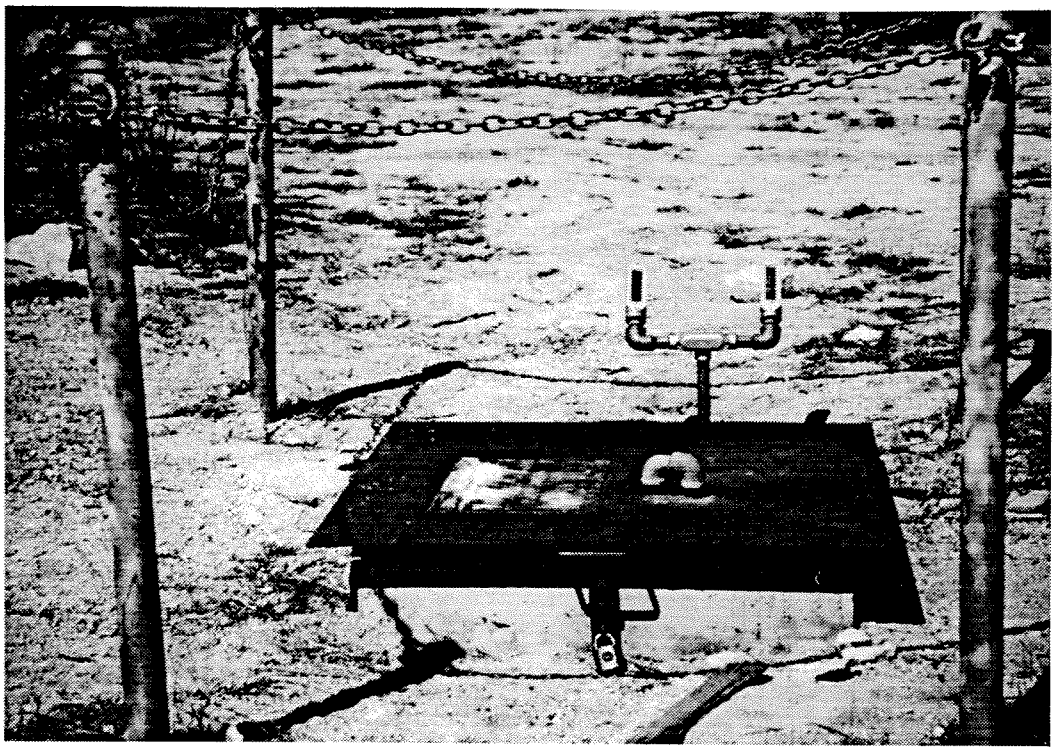

Figure 2.2 The Lucerne Valley Station.

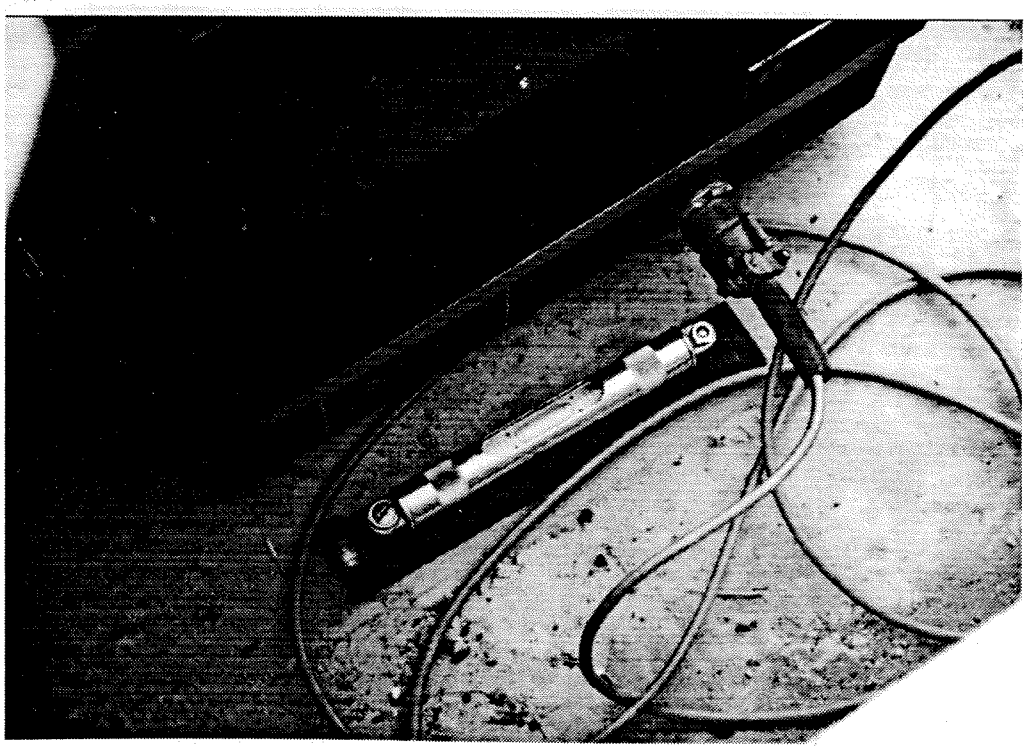

Figure 2.3 The SMA-2/EMA Instrument Sitting on a Level Surface.

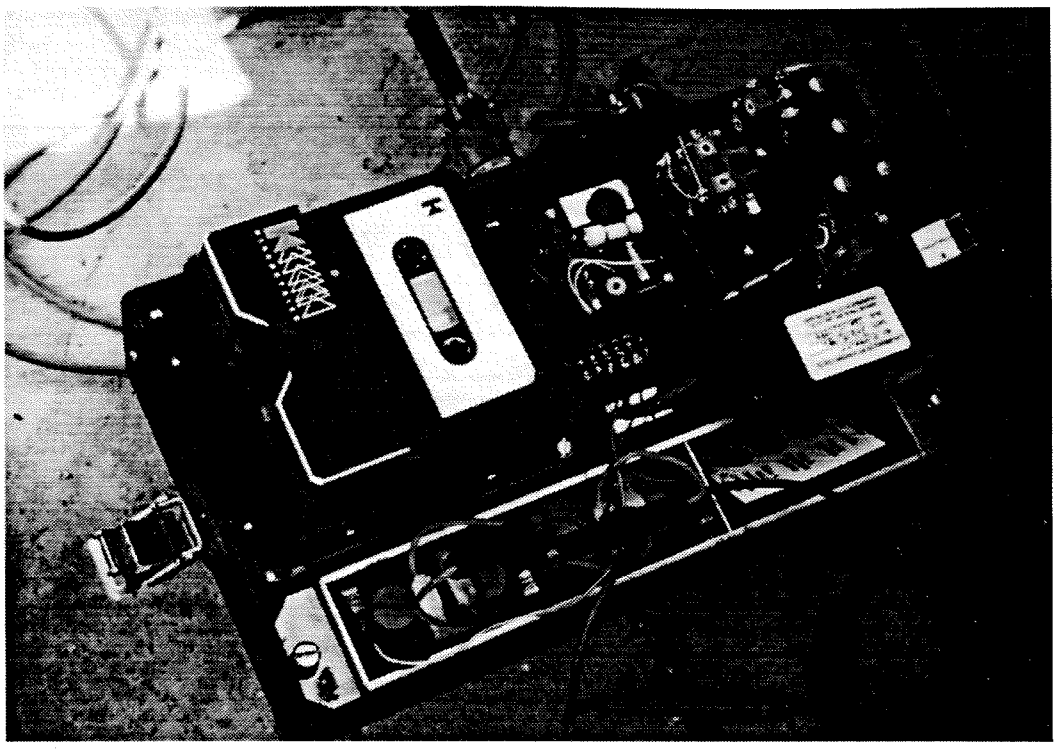

Figure 2.4 The SMA-2/EMA Strong Motion Accelerograph at the Lucerne Valley Station.

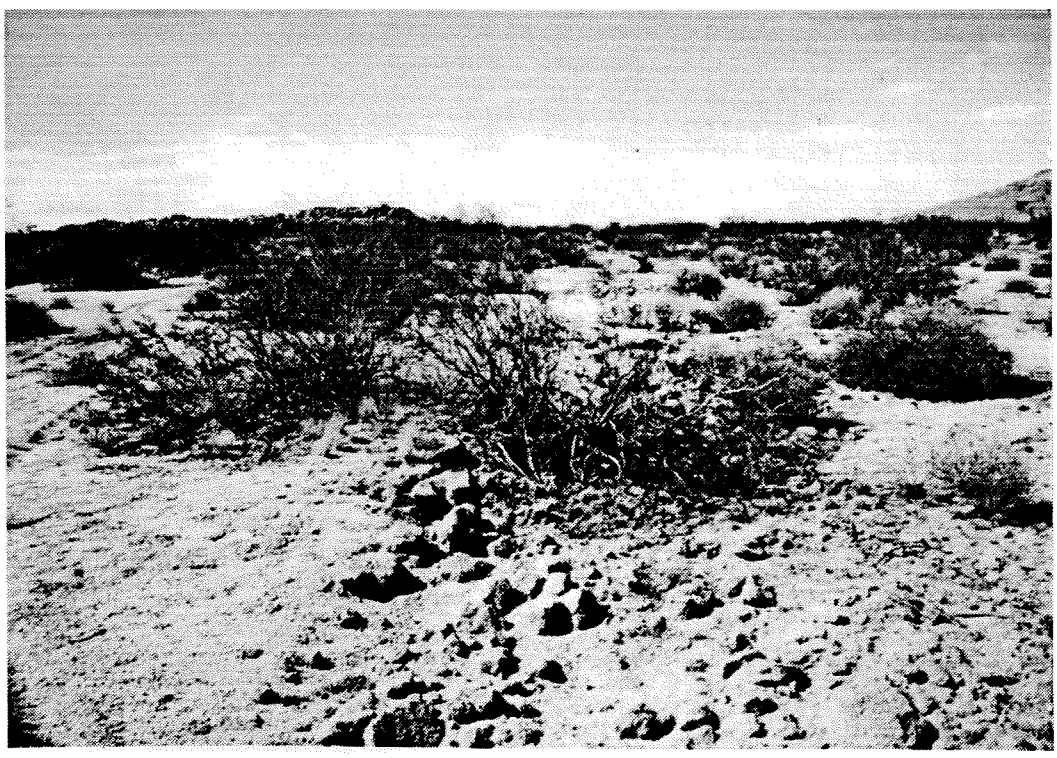

Figure 2.5 Cracks on the Fault Show the Fault Trace Went Through a Bush (Viewing in the Fault Trace Direction).

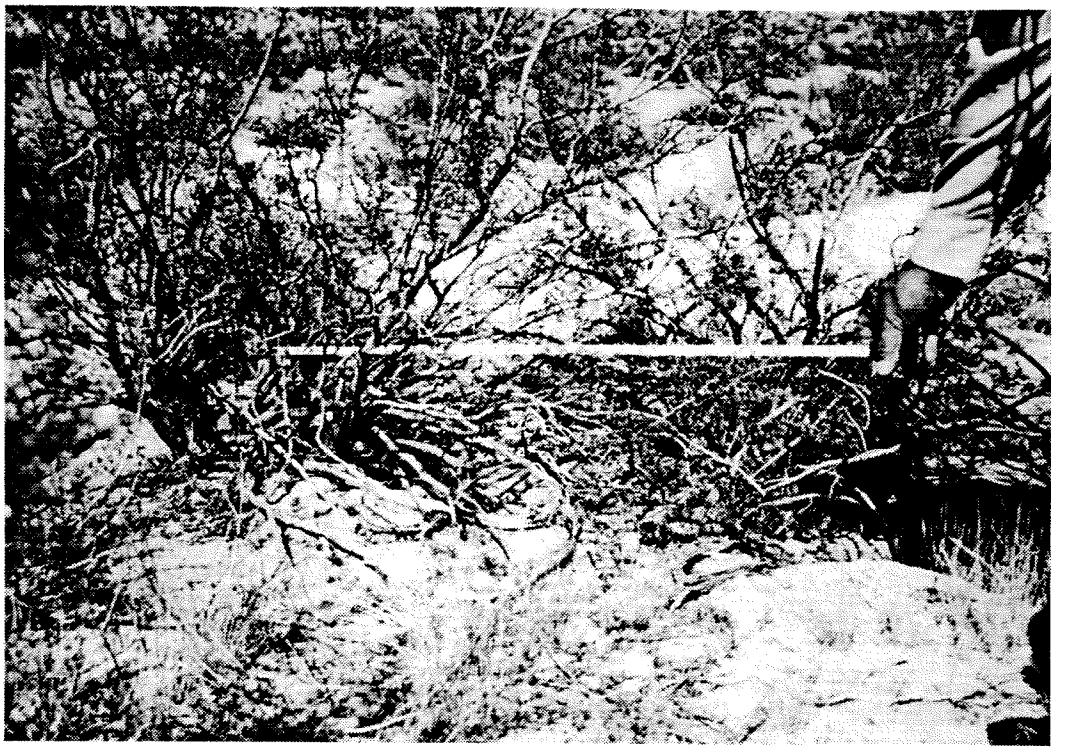

Figure 2.6 The Bush on the Fault Was Torn Apart by the Two Sides of the Fault (Viewing Perpendicularly to the Fault Trace).

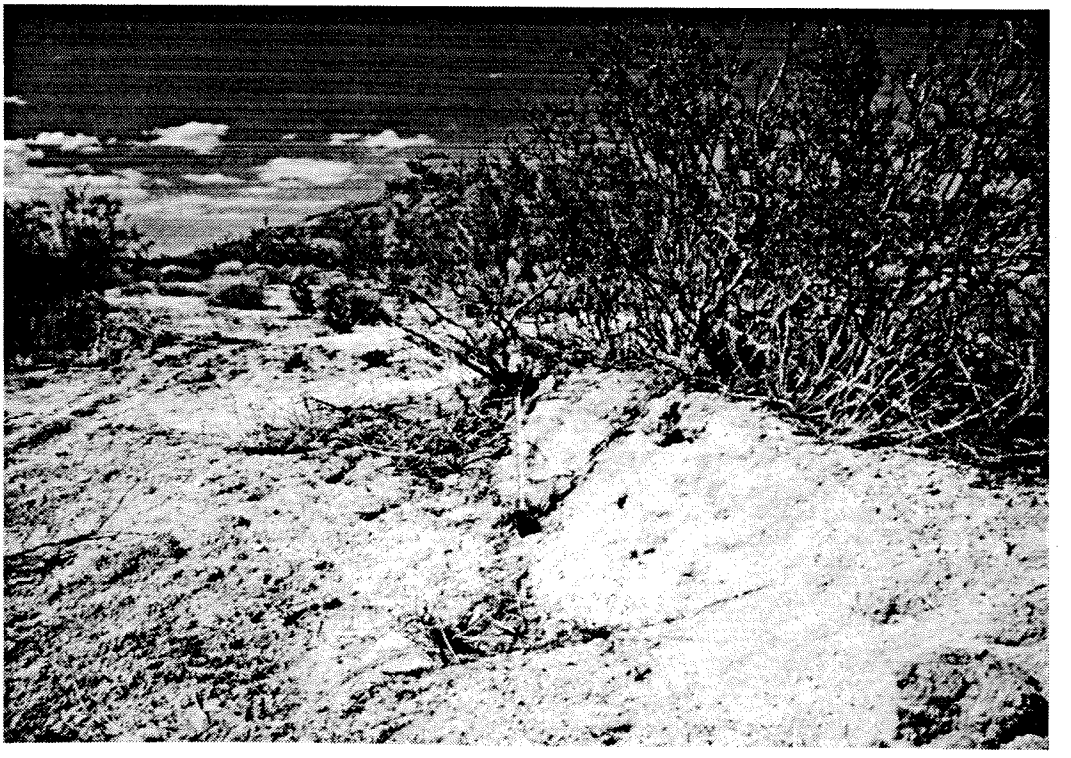

Figure 2.7 Vertical Offset on the Fault Near the Lucerne Valley Station.

Figure 2.8 A Several Meter Horizontal Dislocation on a Road.

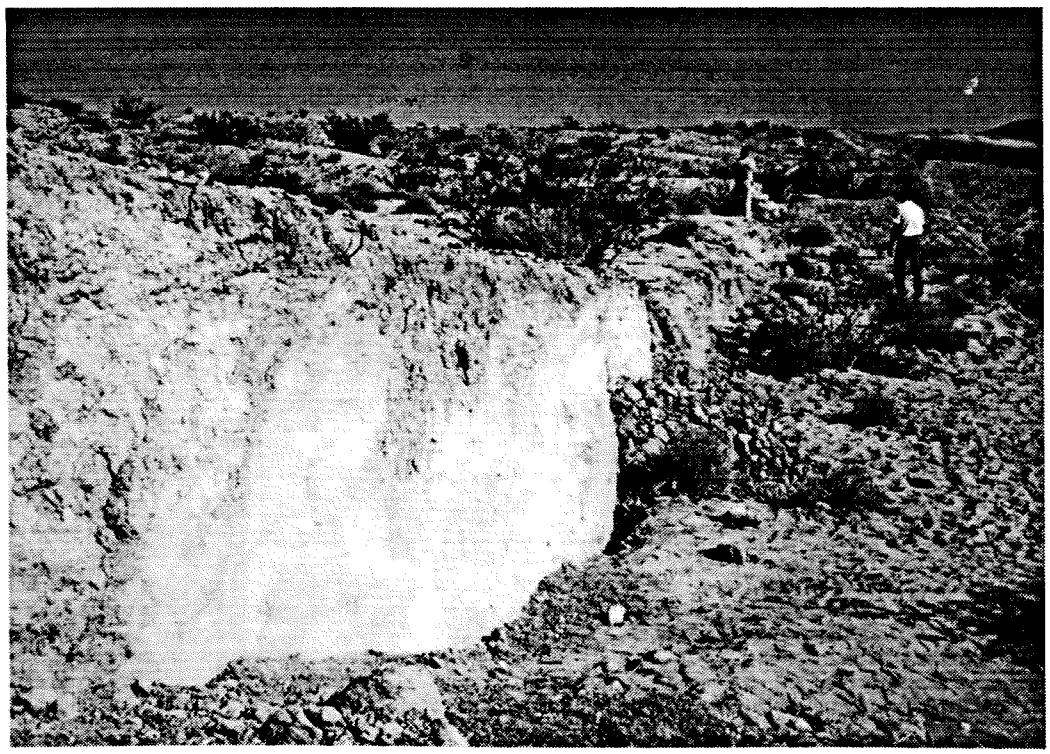

Figure 2.9 A Vertical Offset of About 6 Feet (Viewing in Northeast Direction).

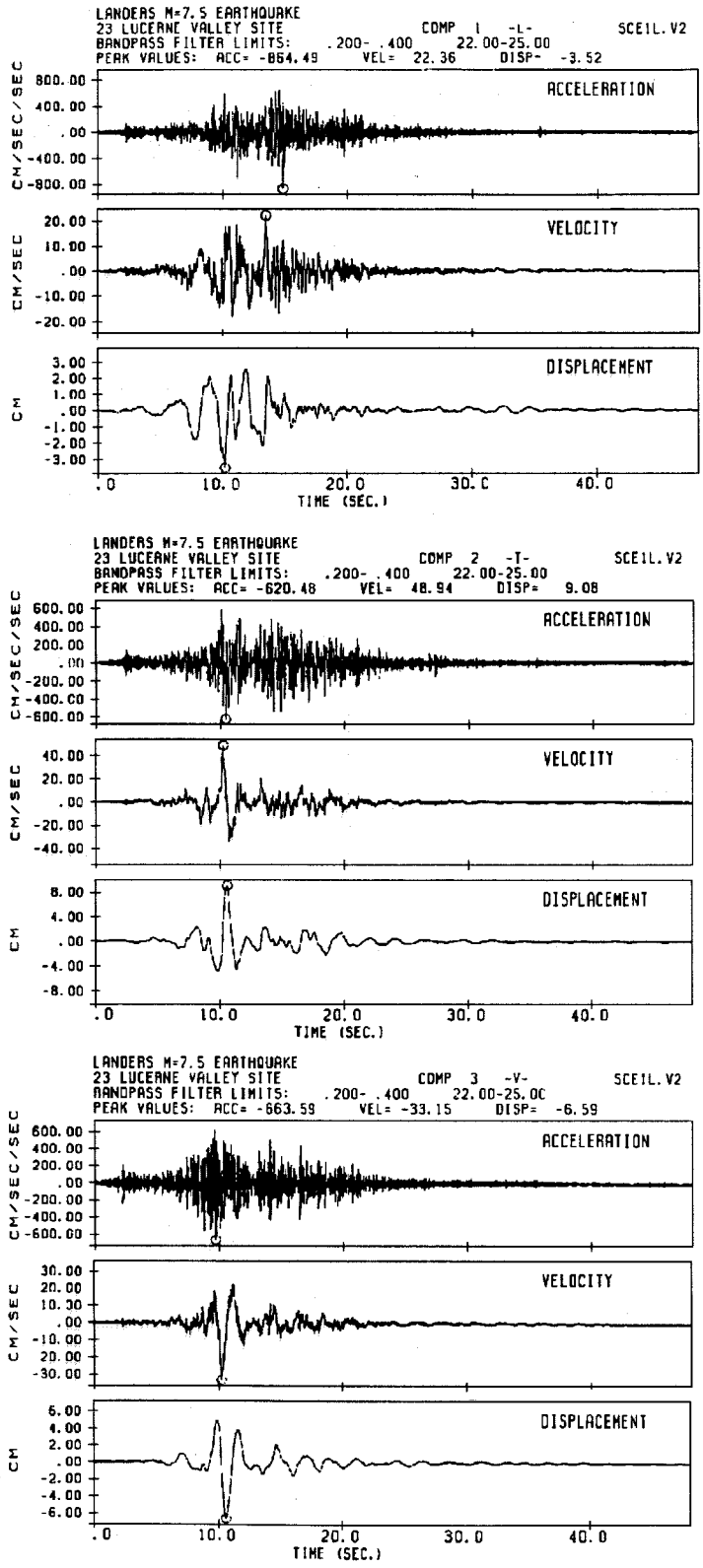

Figure 2.10 Processed Results of Lucerne Valley Record Using Conventional Data Processing Method with a Filter Band of 0.2 to 25 Hz.

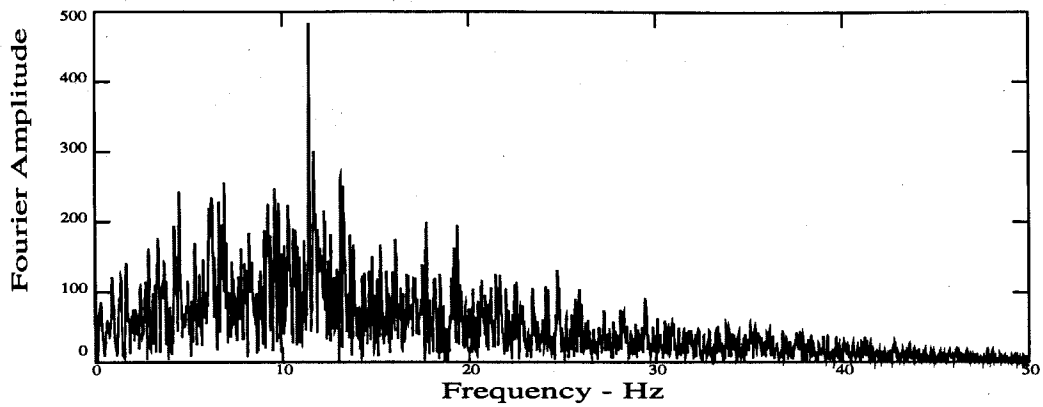

(a) Longitudinal

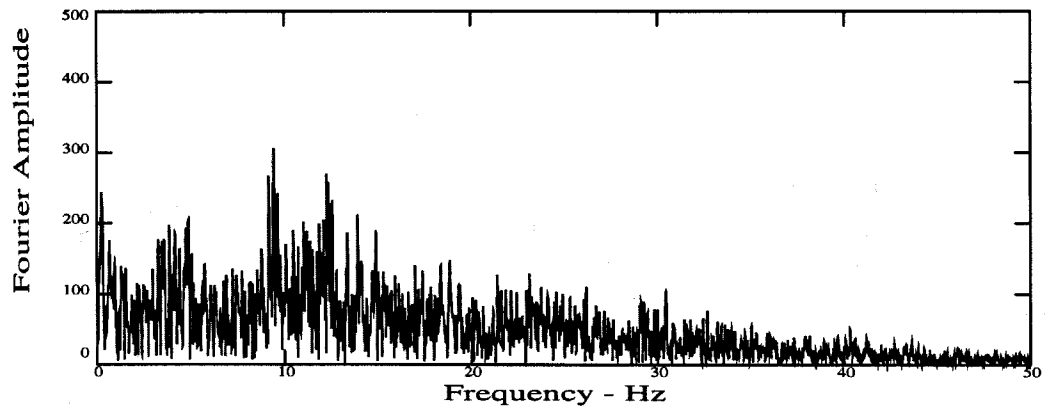

(b) Transverse

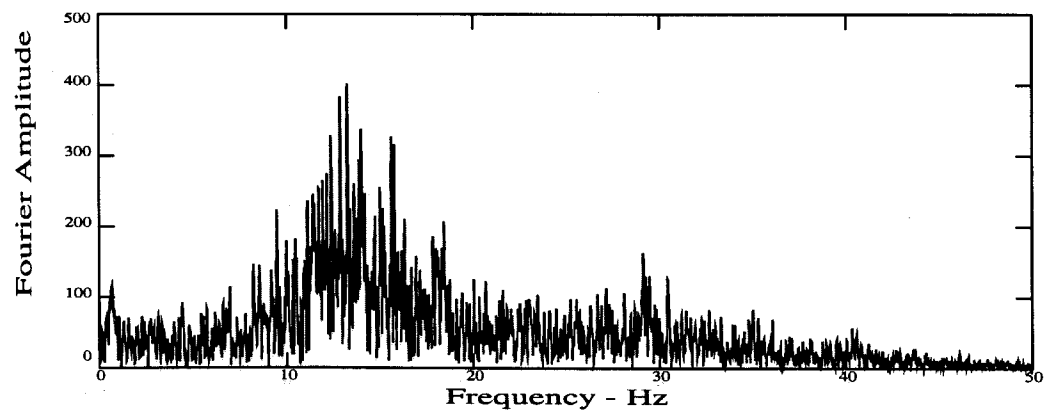

(c) Vertical

Figure 2.11 Fourier Spectra of the Three Components of the Uncorrected Lucerne Valley Record.

Chapter 3

The SMA-2/EMA Strong Motion Accelerograph

3.1 Strong Motion Accelerographs

Seismologists have traditionally been concerned more with small amplitude ground motions based on their global view of earthquakes. Engineers have been concerned more with local effects of large earthquakes which will possibly cause structural damage. The instruments which are designed for seismological studies are called seismometers. They are mainly used to record ground velocities and displacements. The instruments which are designed for engineering studies are called strong-motion accelerographs. They record accelerations. The investigation in this thesis is founded on engineering applications. The strong-motion accelerograph, especially the SMA-2/EMA strong-motion accelerograph, will be investigated in detail.

Development of the strong-motion accelerograph system is based on the need to understand ground motion and structural behavior in strong earthquakes, especially the earthquakes which cause structural damage. For the purpose of earthquake resistant design, and the study of structural response, engineers believe that it is important to obtain strong-motion data, and the instruments which are used to record these data need to be developed and understood.

Earthquake instrument development began in the late 1920's and early 1930's. At that time, the U.S. Coast and Geodetic Survey was responsible for the Strong Motion Program in the United States [13,14]. The first accelerograph was designed based on the principles of the Wood-Anderson type seismometer. It had a natural frequency of 10 Hz which was considered the frequency range of structural interest. At the same time it was realized that it would be difficult to obtain accurate information

from the accelerograph concerning long-period waves with periods greater than 10 seconds. For this purpose, a special long-period displacement meter was constructed.

Strong-motion accelerographs became commercially available in 1963. The first commercial accelerograph was the AR240. It had accelerometers with a natural frequency of 18 Hz and a horizontal starting pendulum. It recorded accelerations on 12-inch wide photographic paper. In 1966, under the direction of William Rihn, the RFT250 was designed with a simplified transducer and a compact inverted pendulum starter. Subsequently, the first analog tape recording accelerograph, the RMT280, was developed.

In 1969, Kinemetrics Inc. was founded as a manufacturer of strong motion accelerographs. A year later the SMA-1 accelerograph was designed and marketed by Kinemetrics. The SMA-1 instrument is an optical system with a vertical electrodynamic starter and it records earthquake acceleration on 70 mm film. It is still widely used around the world. In 1972, the SMA-1 instrument was modified to produce an electric output and appeared as the SMA-2 strong-motion accelerograph, an analog tape recording instrument, and the SMA-3 strong-motion accelerograph, a multichannel central analog tape recording accelerograph system. The tape recording instrument has two types of design; one has an electro-magnetic transducers (EMA) and the other has force-balance transducer (FBA). The nominal effective frequency range is from 0.1 Hz to 25 Hz for the EMA transducers and DC to 50 Hz for the FBA transducers. Soon after the development of the analog tape recording instrument, a digital instrument was invented. The digital instruments are constructed with FBA type transducers.

An analog instrument and a digital instrument are different in that the analog accelerograph records data in the form of an analog signal, while the digital accelerograph records data in a digital format [15,16]. Both systems have advantages and disadvantages. Digital instruments have a pre-event memory and wide dynamical range. Hence, the data processing procedure for data retrieved from these kinds of instruments is simpler and more reliable. But the digital instrument is more expensive because of its complexity. Analog instruments are of low cost but do not have a pre-event memory and their dynamic range is relatively limited.

The most popular accelerograph in use today is the SMA-1 instrument. There are also quite a few SMA-2 instruments in the field, especially in nuclear facilities. Relatively little study has been done on the SMA-2 strong-motion accelerograph, especially those having EMA type transducers. The response behavior over the entire frequency range of the EMA transducer was still not well understood at the time of this study. Since a very unique near-field record from Landers earthquake was recorded on this kind of instrument, it is very important to study the SMA-2 accelerograph and therefore to find a way to recover long-period information from the near-field earthquake motion.

3.2 Brief Description of the SMA-2 Strong-Motion Accelerograph

The appearance of the SMA-2 accelerograph is the same as the SMA-1. It is housed in a watertight aluminum case with dimensions 8 inches×8 inches×14 inches and has a total weight of 11.5 kg. The instrument remains in a standby condition until ground motion actuates the starter and turns on the power to operate the instrument. The SMA-2 is fully actuated in less than 0.1 second. It operates as long as the starter detects the earthquake, plus an additional 10 to 12 seconds after motion drops below the starter threshold, which is 0.01 g. During the earthquake, the ground motion is recorded as electronic signals on three channels according to the three translational directions: two horizontal directions and one vertical direction.

As mentioned above, there are two types of design for the SMA-2 accelerographs; an EMA transducer and FBA transducer. In this chapter, the characteristics and the dynamic response behavior of the EMA transducer are studied. For the force balance transducer, the reader is referred to [17,18] for a detailed analysis.

The EMA type transducer is a spring-mass system with a coil that moves in a magnetic field. The output voltage from the transducer is approximately proportional to the ground acceleration in the effective frequency response range. The full scale of the transducer response is 1 g and the nominal sensitivity is 2.5 volts/g. According to the manufacturer, the natural frequency of the spring-mass system is 25 Hz [19]. The transducers work with an analog tape recording system which records a signal on a four-track magnetic tape cassette.

The triaxial set of accelerometers of the SMA-2/EMA record longitudinal, transverse and vertical motion. This gives a full description of the ground motion at a particular location, under the assumption that the rotational ground motion is small and can be neglected. Each accelerometer has a coil which is supported by flexure springs. During the earthquake, the coil moves relative to the case in a magnetic field due to the inertia of the transducer mass. An electric current is then generated in the coil and the output voltage of the coil is proportional to the relative velocity of the transducer mass. After passing through an integration amplifier, the output voltage is then proportional to the relative displacement of the transducer mass. This spring-mass system plus a damping resistor and an integration circuit make up a second-order dynamic system. In the effective range of the frequency response of this transducer system, the ground acceleration is proportional to the relative displacement of the transducer mass and therefore proportional to the output voltage of the transducer system (see Section 3.3 for detail).

The output voltage from the three accelerometers passes through three integrators and then three Voltage Controlled Oscillators (VCO). At this time the analog voltage signals are converted into FM modulation signals and then recorded on three of the four tracks of the tape. Nominally a zero voltage is represented by a signal of 1000 Hz and ± 2.5 volts is represented by a signal of 1000 ± 500 Hz. The fourth track records the 1024 Hz signal which is used by the SMP-1 playback unit for tape speed compensation as well as for generation of timing marks.

The information recorded on the tape is retrieved by the SMP-1 playback unit. This unit demodulates the three FM acceleration signals and one reference signal. It also amplifies the 1024 Hz frequency modulation timing reference signal and divides it down to 2 Hz as a timing mark on the output of the chart recorder of the SMP-1. The demodulated signals are still analog signals. After tape error corrections, they are digitized by appropriate digitization equipment and retrieved by a Personal Computer. (Details regarding the recording and playback procedure are discussed in Section 4.3)

One of the important features of the instrument is its effective frequency response range. W.J. Rihn pointed out that for the SMA-2/EMA instrument "the frequency response is flat with respect to acceleration from the corner frequency of the integrator

(0.1 Hz) to the natural frequency of the spring-mass system (25 Hz)"[20]. Unfortunately, the instrument does not operate exactly in the way as it is designed. In 1972, D. E. Hudson and R. C. Dullien performed a test on the SMA-2/EMA instrument and concluded that "the response characteristics of the SMA-2/EMA appear to be very good in the frequency range 0.2 to 25 Hz," and that there was distortion in the components of SMA-2/EMA accelerograms for periods greater than 5 seconds [12]. In an attempt to recover information beyond 5 second periods, another test is conducted here for the SMA-2/EMA. In this chapter, the theoretical background of the EMA transducer design is carefully studied and a formulation is derived for the instrument correction. The test results discussed in Chapter 4 also show that the effective "flat" range of the frequency response of transducer is less than 0.2 to 25 Hz.

3.3 Theoretical Background of the Electro-Magnetic Transducer Design

The instrument correction in the standard CIT Vol II data procedure is based on the input and output relationship of a single-degree-of-freedom oscillator. A standard instrument correction algorithm is applied for most of the instruments with different transducer designs, since most of the transducers can be modeled as a SDOF system with different parameters. However, for the SMA-2/EMA instrument, the existing formulation can only be applied in a limited frequency range; for example, above 0.2 Hz. To perform the instrument correction for the SMA-2/EMA over the entire frequency range, a special instrument correction algorithm must be derived. In this section, the existing formulation and the modified formulation for the SMA-2/EMA instrument correction are discussed.

3.3.1 Existing Formulation

The EMA type transducer is a mass-spring system with a coil held by flexure springs in a magnetic field. This system was modeled by Hudson [21] as the second-order system described in Figure 3.1(a).

The voltage e_c generated by the coil-magnet system is

$$e_c = G\dot{x}_r \tag{3.1}$$

where G is a constant factor and $\dot{x}_r$ is the relative velocity of the transducer mass to the instrument case. And the electrodynamic force on the transducer mass will be

$$F_m = -Gi_c \tag{3.2}$$

where i_c is the current in the coil generated by the coil motion in the magnetic field. It can be seen from Figure 3.1(b) that

$$i_c = \frac{e_c}{R_c + R_d} \tag{3.3}$$

where R_d is a damping resistor and R_c is the coil resistance.

The output voltage from the EMA transducer, denoted as e_i, becomes

$$e_i = R_d i_c = \alpha \dot{x}_r \tag{3.4}$$

where $\alpha = \frac{R_d G}{R_c + R_d}$ is a constant factor.

Assume that x_a and x_g are the absolute displacement of the transducer mass and the actual ground displacement respectively, their relationship with the relative transducer mass displacement $x_r(t)$ is

$$x_a = x_r + x_g \tag{3.5}$$

During an earthquake, the inertia force of the transducer mass, $m\ddot{x}_a$, is in balance with the summation of the spring force, kx_r, the damping of mechanical system, $c\dot{x}_r$, and the electrodynamic force, F_m. That is,

$$\begin{aligned} m\ddot{x}_a &= -c\dot{x}_r - kx_r + F_m \\ &= -c\dot{x}_r - kx_r - Gi_c \end{aligned} \tag{3.6}$$

where c and k are mechanical damping and spring stiffness.

From Equation (3.1) and Equation (3.3)

$$i_c = \frac{G\dot{x}_r}{R_c + R_d} \tag{3.7}$$

Substituting Equation (3.5) and (3.7) into Equation (3.6) and performing a simple manipulation, the equation of motion of the transducer can be obtained as

$$m\ddot{x}_r + c\dot{x}_r + kx_r = -m\ddot{x}_g - \frac{G^2}{R_c + R_d}\dot{x}_r \tag{3.8}$$

or,

$$m\ddot{x}_r + \left[c + \frac{G^2}{R_c + R_d}\right]\dot{x}_r + kx_r = -m\ddot{x}_g \tag{3.9}$$

This can be written as

$$\ddot{x}_r + \left[2\omega_n\zeta + \frac{G^2}{m(R_c + R_d)}\right]\dot{x}_r + {\omega_n}^2 x_r = -\ddot{x}_g \tag{3.9a}$$

where $\omega_n = \sqrt{\frac{k}{m}}$ and $2\omega_n\zeta = \frac{c}{m}$ are the natural frequency and the damping ratio of the mechanical system. Since the electrodynamic damping is generally much larger than the mechanical system damping, the damping measured from the calibration is mainly electrical damping and the mechanical damping can be neglected.

Let

$$2\omega_n\zeta + \frac{G^2}{m(R_c + R_d)} = 2\omega_n\zeta_n \tag{3.10}$$

Then, Equation (3.9) can be written as

$$\ddot{x}_r + 2\omega_n\zeta_n\dot{x}_r + {\omega_n}^2 x_r = -\ddot{x}_g \tag{3.11}$$

where ζ_n is regarded as the damping ratio for the whole transducer system. Therefore, the transfer function has the form of a single-degree-of-freedom oscillation. The transfer function of the system will be

$$H(\omega) = \frac{1}{{\omega_n}^2 - \omega^2 + 2\omega_n\omega\zeta_n i} \tag{3.12}$$

The phase shift of the system can be expressed by:

$$\phi(\omega) = tan^{-1}\left[-\frac{2\omega_n\omega\zeta_n}{\omega_n^2 - \omega^2}\right] \tag{3.13}$$

The damping ratio ζ_n is set at approximately 0.6 which is indeed much larger than the mechanical damping. The natural frequency of the transducer, f_n, is designed to be approximately 25 Hz. Then, the transfer function will be expected to be nearly flat between 0 to 25Hz. Actually, the flat range is much smaller than 25

Hz. Figure 3.2 is a plot of the results from Equation (3.12) with different damping ratios of $\zeta = 0.5$, 0.6 and 0.7. When the frequency of the ground excitation is within this "flat" range, the ground acceleration will be approximately proportional to the relative displacement of the transducer mass. That is,

$$\ddot{x}_g \propto x_r \tag{3.14}$$

Since the EMA transducer is a velocity transducer, its output voltage is proportional to the relative velocity of the transducer. From Equation (3.4)

$$e_i = \alpha \dot{x}_r \tag{3.15}$$

To obtain an output signal which is proportional to the relative displacement of the transducer mass, (that is, proportional to the ground acceleration), an integrator is used in the electronic circuit. For an ideal integrator, the output voltage e_o is proportional to the relative displacement of the transducer mass:

$$e_o = \alpha x_r \tag{3.16}$$

The experimental results (see Chapter 4) show that the frequency response is very steep in the low frequency range from 0 Hz to 0.2 Hz, and the low frequency information will be seriously distorted after integration. This is caused primarily by leakage of the capacitor in the integration amplifier. When the ground motion contains mainly high frequency information (above 0.5 Hz), the leakage will not affect the recorded signal very much. But when the ground motion contains a significant amount of low frequency information (below 0.5 Hz), the above model can no longer be applied. It must be modified so that the instrument correction can recover long-period information from earthquake records. This is very important for the data processing of near-field earthquake accelerograms. The modified formulation for the SMA-2/EMA is presented in the following section.

3.3.2 Modified Formulation for the SMA-2/EMA Instrument

Since leakage exists in all capacitors, the circuit diagram for the amplifier should be considered as shown in Figure 3.3. Let e_i and e_o be the input and output voltage of the amplifier, R_i be the resistance of the circuit, C and R_f be the capacitance and

resistance of the amplifier respectively, then the relationship between the input and output of the integration amplifier will be

$$\frac{e_i}{R_i} + c\frac{de_o}{dt} + \frac{e_o}{R_f} = 0 \tag{3.17}$$

or

$$\dot{e}_o + \frac{1}{CR_f}e_o = -\frac{1}{CR_i}e_i \tag{3.18}$$

Substituting Equation (3.15) into Equation (3.18) gives

$$\dot{e}_o + \frac{1}{CR_f}e_o = -\frac{\alpha}{CR_i}\dot{x}_r \tag{3.19}$$

This differential equation represents the relationship between the relative displacement of the transducer mass and the output voltage of the transducer system, e_o. The transfer function of the integrator will be

$$H(\omega) = -\frac{\alpha}{CR_i}\frac{i\omega}{i\omega + \frac{1}{CR_f}} \tag{3.20}$$

Denote the corner frequency of the integrator as ω_{cr} or f_{cr}, which are defined as

$$\omega_{cr} = \frac{1}{CR_f}\,, \qquad f_{cr} = \frac{\omega_{cr}}{2\pi} \tag{3.21}$$

Then the Equation (3.20) can be written as

$$H(\omega) = -\frac{\alpha}{CR_i}\frac{i\omega}{i\omega + \omega_{cr}} \tag{3.22}$$

or,

$$H(f) = -\frac{\alpha}{CR_i}\frac{if}{if + f_{cr}} \tag{3.23}$$

Equation (3.23) shows that the amplifier is a high pass filter. Low frequency information (below f_{cr}) will be filtered out or seriously distorted. To recover the low frequency information, a new input-output relationship needs to be derived.

Consider the input of the system to be the ground acceleration $\ddot{x}_g$ and the output to be the measured voltage e_o. Denote $E_o(\omega)$ and $\ddot{X}_g(\omega)$ as the Fourier transforms of $e_o(t)$ and $\ddot{x}_g(t)$ respectively. Then, the transfer function of the entire system will be

$$H(\omega) = \frac{E_o(\omega)}{\ddot{X}_g(\omega)} \tag{3.24}$$

where

$$E_o(\omega) = \int e_o(t)e^{-i\omega t}dt \tag{3.25}$$

$$\ddot{X}_g(\omega) = \int \ddot{x}_g(t)e^{-i\omega t}dt \tag{3.26}$$

Applying a Fourier transform on Equations (3.11) and (3.19) leads to the following two equations

$$X_r(\omega)\left({\omega_n}^2 - \omega^2 + 2\omega_n\omega\zeta_n\right) = -\ddot{X}_g(\omega) \tag{3.27}$$

and,

$$E_o(\omega)\left(i\omega + \frac{1}{CR_f}\right) = -\frac{\alpha}{CR_i}i\omega X_r(\omega) \tag{3.28}$$

Eliminating $X_r(\omega)$ from Equations (3.27) and (3.28) gives

$$E_o(\omega) = \frac{\alpha i\omega/CR_i}{\left(i\omega + \frac{1}{CR_f}\right)\left({\omega_n}^2 - \omega^2 + 2\omega_n\omega\zeta_n i\right)}\ddot{X}_g(\omega) \tag{3.29}$$

Under the definition of Equation (3.24), the transfer function for the entire system will be

$$H(\omega) = \frac{\alpha i\omega/CR_i}{\left(i\omega + \frac{1}{CR_f}\right)\left({\omega_n}^2 - \omega^2 + 2\omega_n\omega\zeta_n i\right)} \tag{3.30}$$

The phase shift of the system is

$$\phi(\omega) = tan^{-1}\frac{\left[(\omega_n^2 - \omega^2) + 2\omega_n\omega_{cr}\zeta_n\right]\omega}{(\omega_n^2 - \omega^2)\omega_{cr} - 2\omega^2\omega_n\zeta_n} \tag{3.31}$$

Letting

$$a_0 = \frac{\alpha}{(2\pi)^2 CR_i} \tag{3.32}$$

and substituting $\omega = 2\pi f$, Equations (3.30) and (3.31) can alternatively be written as

$$H(f) = \frac{a_0 if}{\left(if + f_{cr}\right)\left({f_n}^2 - f^2 + 2f_n f\zeta_n i\right)} \tag{3.33}$$

and,

$$\phi(f) = tan^{-1}\frac{\left[(f_n^2 - f^2) + 2f_n f_{cr}\zeta_n\right]f}{(f_n^2 - f^2)f_{cr} - 2f^2 f_n\zeta_n} \tag{3.34}$$

where $a_0 = \frac{\alpha}{(2\pi)^2 CR_i}$ and $f_{cr} = \frac{1}{2\pi CR_f}$.

The inverse of f_{cr}, denoted by τ, is the *time constant* of the integration amplifier. Theoretically, if $\tau \to \infty$, the amplifier can be made into a perfect integrator. But in practice, such an amplifier cannot be built because the output of the circuit will wander off due to op-amp offsets and bias currents. Therefore, a large CR_f value will be chosen and the integrator will act as a high-pass filter for the relative displacement input of the transducer. The instrument correction should correct the distortion from the integrator in addition to the distortion from the transducer response.

3.4 Numerical Studies of the Electro-Magnetic Transducer

The characteristics of the EMA transducer are described by its transfer function. From Equation (3.33), it can be seen that the transfer function of the EMA transducer behaves like a filter. For example, take $f_{cr} = 0.1$, $f_n = 25$, $\zeta_n = 0.6$ and $a_0 = f_n^2$. Then, the transfer function $|H(f)|$ will have the shape shown in Figure 3.4 (the dotted line). Recorded accelerograms that have components beyond the frequency range of 0.2 to 25 Hz will be distorted by this type of transducer.

Figure 3.4 also gives another set of curves from Equation (3.33) with damping ratios of $\zeta_n = 0.5$ (solid line) and $\zeta_n = 0.7$ (sparse dotted line). All the other parameters are held constant. It seems that the damping ratio of $\zeta_n = 0.6$ gives the best transducer design among these three – it gives the broadest flat frequency range. Figure 3.5 shows the same results as Figure 3.4 on a logarithmic scale. This figure shows that the change of the damping ratio will hardly affect the low frequency part of the transfer function.

Figure 3.6 shows the results of Equation (3.33) with different corner frequencies while all the other parameters are held constant. It is obvious that the smaller the corner frequency the larger the flat frequency range will be. The results also show that the change of the corner frequency hardly affects the high frequency part of the transfer function.

Figure 3.7 shows the results of Equation (3.33) with different natural frequencies while all the other parameters are held constant. It can be seen, as we already know, that the larger the natural frequency, the broader will be the flat range of the transfer function. The variation of the natural frequency has only a slight effect on the low frequency part of the transfer function.

The above results indicate that the characteristics of the transducer are determined by the the parameters of its transfer function. The wise selection of these parameters can give the optimal design of the transducer. The goal of the optimal design of the transducer is to obtain a transducer which is capable of working in a widest frequency range with a minimum signal distortion. The next section discusses the effective frequency range of the EMA transducer.

3.5 Optimal Design of the Electro-Magnetic Transducer

As shown in Section 3.4, the effective frequency range of a transducer is controlled by the structure of the transducer and the parameters, such as corner frequency, natural frequency, and electronic damping ratio. To obtain the widest effective frequency range, the corner frequency should be as small as possible, while the natural frequency should be as large as possible. For certain values of natural frequency and corner frequency, the damping ratio can be chosen such that the transducer can have the widest effective frequency range with a certain acceptable error.

Since the transfer function cannot be exactly flat, a certain acceptable range should be defined. Assume that the transfer function can be considered as "flat" when the deviation from the absolute value of the transfer function is not more than ϵ. Then the optimal value of the damping ratio, which is error dependent, should be found so that the transfer function has the maximum effective range. This can be done as indicated below.

Based on the previous numerical analysis, the variation of the corner frequency hardly affects the high frequency part of the transfer function, and the variation of the natural frequency and the damping ratio has almost no effect on the low frequency part of the transfer function. Hence, the analysis here can be completed by two simple steps: 1) determine the effective low frequency range by studying the transfer function of the integrator 2) determine the effective high frequency range by studying the transfer function of the single-degree-of-freedom oscillator. That is, find the frequency range which satisfies the following two inequalities:

$$\left|1 - \left|H_1(f)\right|\right| \leq \epsilon_1 \tag{3.35}$$

$$\left|1 - \left|H_2(f)\right|\right| \leq \epsilon_2 \tag{3.36}$$

where $H(f) = H_1(f)H_2(f)$ and

$$|H_1(f)| = \left|\frac{if}{if + f_{cr}}\right| \tag{3.37}$$

$$|H_2(f)| = \left|\frac{1}{1 - f_1^2 + 2i\zeta_n f_1}\right| \tag{3.38}$$

When inequalities of Equations (3.35) and (3.36) are satisfied, it can be shown that the following inequality is satisfied. That is

$$\left|1 - \left|H(f)\right|\right| \leq \epsilon_1 + \epsilon_2 = \epsilon \tag{3.39}$$

With the substitution of Equations (3.37) and (3.38), Equation (3.35) and (3.36) can be written as

$$\left|1 - \frac{f}{\sqrt{f^2 + f_{cr}^2}}\right| \leq \epsilon_1 \tag{3.40}$$

$$\left|1 - \frac{1}{\sqrt{(1 - f_1^2)^2 + 4\zeta_n^2 f_1^2}}\right| \leq \epsilon_2 \tag{3.41}$$

where $f_1 = f/f_n$.

The solution of Equation (3.40) gives

$$f \geq \gamma f_{cr} \tag{3.42}$$

where $\gamma = \dfrac{1 - \epsilon_1}{\sqrt{\epsilon_1(2 - \epsilon_1)}}$.

The solution of Equation (3.41) gives

$$f_1^2 \leq (1 - 2\zeta_n^2) + \sqrt{(1 - 2\zeta_n^2)^2 + a} \tag{3.43}$$

and,

$$f_1^2 \geq (1 - 2\zeta_n^2) + \sqrt{(1 - 2\zeta_n^2)^2 - b} \tag{3.44}$$

or

$$f_1^2 \leq (1 - 2\zeta_n^2) - \sqrt{(1 - 2\zeta_n^2)^2 - b} \tag{3.45}$$

where $a = \frac{\epsilon_2(2-\epsilon_2)}{(1-\epsilon_2)^2}$, $b = \frac{\epsilon_2(2+\epsilon_2)}{(1+\epsilon_2)^2}$.

The relationships between f_1^2 and ζ_n which satisfy the above inequalities can be described by the Figure 3.8. The shaded area is the solution of the two inequalities of Equation (3.40) and (3.41). The optimal transducer design is then to select a damping ratio by $\zeta_n = \sqrt{\frac{1-\sqrt{b}}{2}}$ with error of $\epsilon_1 + \epsilon_2$ to obtain the effective frequency range by

$$\gamma f_{cr} \leq f \leq \sqrt{\sqrt{b} + \sqrt{a+b}}\, f_n \tag{3.46}$$

Take $\epsilon_1 = \epsilon_2 = 2.5\%$, then the damping ratio for optimal design is $\zeta_n = 0.62$ and the effective frequency range of the transducer will be:

$$4.4 f_{cr} \leq f \leq 0.73 f_n \tag{3.47}$$

When $f_{cr} = 0.1$ and $f_n = 25$ Hz, Equation (3.47) becomes

$$0.44\ Hz \leq f \leq 18.25\ Hz \tag{3.48}$$

A similar evaluation can be carried out for the other cases. For example, take $\epsilon_1 = \epsilon_2 = 5\%$, then the effective frequency range of the transducer and the damping ratio for optimal design will be

$$3 f_{cr} \leq f \leq 0.87 f_n, \quad with \ \ \zeta_n = 0.59 \tag{3.49}$$

if $\epsilon_1 = \epsilon_2 = 1\%$, then

$$7 f_{cr} \leq f \leq 0.58 f_n, \quad with \ \ \zeta_n = 0.66 \tag{3.50}$$

Similarly, for $f_{cr} = 0.1$ and $f_n = 25$ Hz, Equation (3.49) and (3.50) become:

$$0.3\ Hz \leq f \leq 21.7\ Hz, \quad with \ \ \zeta_n = 0.59 \tag{3.51}$$

and,

$$0.7\ Hz \leq f \leq 14.5\ Hz, \quad with \ \ \zeta_n = 0.66 \tag{3.52}$$

So, if the transducer is designed to have the parameters of $f_{cr} = 0.1$, $f_n = 25$ Hz and $\zeta = 0.62$, the errors involved in the dynamic response of the transducer between

the frequency range of 0.44 Hz to 18.25 Hz will be controlled within 5%. Similar interpretations can be drawn for the other two cases. For the same corner frequency and the natural frequency, the transducer can be designed to control the response error within 2% in the frequency range of 0.7 Hz to 14.5 Hz by selecting $\zeta_n = 0.66$, or within 10% in the frequency range of 0.21 Hz to 27.5 Hz by selecting $\zeta_n = 0.59$.

3.6 Instrument Correction

The recorded acceleration is not the same as the real input acceleration because of the limitation from the transducer design. To recover a real acceleration record, an instrument correction needs to be performed on the recorded data.

Theoretically, the instrument correction for the records can be performed in both frequency domain and time domain. The basic procedure for frequency domain analysis and time domain analysis can be described in the following.

3.6.1 Frequency Domain Analysis

If the ground motion and the measured output of the transducer are $\ddot{x}_g(t)$ and $e_o(t)$, then the Fourier transforms of these two quantities will be $\ddot{X}_g(\omega)$ and $E_o(\omega)$. Then

$$E_o(\omega) = H(\omega)\ddot{X}_g(\omega) \tag{3.53}$$

where $H(\omega)$ is represented by Equation (3.33). The transfer function $H(\omega)$ is determined by the system parameters. Since $E_o(\omega)$ can be obtained from the Fourier transform of the recorded data, the real ground motion $\ddot{x}_g(t)$ can be obtained by the inverse Fourier transform of $\ddot{X}_g(\omega)$, i.e.,

$$\ddot{x}_g(t) = \int \ddot{X}_g(\omega)e^{i\omega t}d\omega = \int \frac{E_o(\omega)}{H(\omega)}e^{i\omega t}d\omega \tag{3.54}$$

Notice that singularity occurs at $\omega = 0$ since $H(\omega)\big|_{\omega=0} = 0$. This causes difficulties in working out the precise result by a frequency analysis. To make the analysis simpler, a time domain analysis is preferred.

3.6.2 Time Domain Analysis

Time domain analysis is based on the derivation of the relationship of input $\ddot{x}_g(t)$ and output $e_o(t)$ in the time domain. From Equation (3.19), the relative velocity of

the transducer mass $\dot{x}_r(t)$ can be obtained as a function of the output voltage $e_o(t)$ as

$$\dot{x}_r(t) = -\frac{CR_i}{\alpha}\left(\dot{e}_o(t) + \frac{1}{CR_f}e_o(t)\right) \tag{3.55}$$

After integration and differentiation, the relative displacement $x_r(t)$ and the acceleration $\ddot{x}_r(t)$ of the transducer mass can be obtained from the Equation (3.55) as

$$x_r(t) = -\frac{CR_i}{\alpha}\left(e_o(t) + \frac{1}{CR_f}\int_0^t e_o(t)dt\right) \tag{3.56}$$

$$\ddot{x}_r(t) = -\frac{CR_i}{\alpha}\left(\ddot{e}_o(t) + \frac{1}{CR_f}\dot{e}_o(t)\right) \tag{3.57}$$

Substituting Equations (3.55), (3.56) and (3.57) into (3.11) gives

$$\frac{CR_i}{\alpha}\left[\ddot{e}_o(t) + \left(\frac{1}{CR_f} + 2\omega_n\zeta_n\right)\dot{e}_o(t) + \left(\frac{2\omega_n\zeta_n}{CR_f} + \omega_n^2\right)e_o(t) + \frac{\omega_n^2}{CR_f}\int_0^t e_o(t)dt\right] = \ddot{x}_g(t) \tag{3.58}$$

This equation can be used to perform instrument correction for the SMA-2/EMA. Substituting Equation (3.21) and (3.32) into Equation (3.38), the instrument correction formula can be alternatively written as

$$\ddot{e}_o(t) + (\omega_{cr} + 2\omega_n\zeta_n)\dot{e}_o(t) + \omega_n(2\omega_{cr}\zeta_n + \omega_n)e_o(t) + \omega_{cr}\omega_n^2\int_0^t e_o(t)dt = a_0(2\pi)^2\ddot{x}_g(t) \tag{3.59}$$

where $\ddot{x}_g(t)$ is the input ground acceleration, $e_o(t)$ is the output voltage of the transducer, and ω_n, ζ_n, ω_{cr} and a_0 are the natural frequency, damping ratio, corner frequency and sensitivity of the transducer respectively.

To investigate the distortions caused by the transducer in different frequency response ranges, a harmonic function is employed to test Equation (3.58) or (3.59). For simplicity, a harmonic function $e_o(t) = sin(2\pi f_1 t)$ is chosen and $\ddot{x}_g(t)$ is calculated for different values of f_1. Assume that $a_0 = f_n^2$, $f_{cr} = 0.1$, $\zeta_n = 0.6$ and $f_n = 25$ Hz. The input and output with frequencies of 0.1 Hz, 0.2 Hz, 0.5 Hz, 1 Hz, 5 Hz, 10 Hz, 20 Hz and 25 Hz are considered and the results are shown in Figure 3.9 and 3.10. In the figures, the solid lines represent the input signal $\ddot{x}_g(t)$ and the dotted lines represent the output signal $e_o(t)$. The results show that for the excitation frequencies of 0.5 Hz and 1 Hz, there is little distortion on the transducer response. For the excitation frequencies of 10 Hz, 15 Hz and 20 Hz, little amplitude distortion occurs

but the phase distortion is significant. For the excitation frequencies of 0.1 Hz, 0.2 Hz and 25 Hz, the transducer applies a large distortion to both of the amplitude and the phase shift of the responses.

Since the instrument distortions are significant on both the low and high frequency components, an instrument correction should be performed on the recorded data. This correction can be performed by employing the Equation (3.58) or (3.59). The parameters a_0, f_{cr}, f_n and ζ_n in the equation are determined by the calibration results. The detailed procedure for the dynamic test of the SMA-2/EMA and determination of the system parameters are discussed in Chapter 4.

3.7 Summary and Conclusions

In this chapter, a modified instrument correction scheme is derived and the characteristics of the transfer function of the EMA transducer are studied. An optimal design method is also suggested for the EMA transducer by an appropriate selection of the damping ratio of the transducer. Several conclusions which can be drawn from the analysis are:

(1). Unlike other types of transducers, the EMA transducer will filter out the low frequency information. This causes large distortions of the low frequency components from the recorded data. A special instrument correction scheme needs to be derived for the SMA-2/EMA instrument.

(2). Besides the natural frequency, damping ratio and sensitivity of the instrument, an additional parameter of the corner frequency of the integrator must also be specified in the instrument correction.

(3). The optimal design of the EMA transducer can be accomplished by selection of the damping ratio for the EMA transducer. With certain acceptable deviations from the response, the damping ratio can be selected to give the largest effective frequency range.

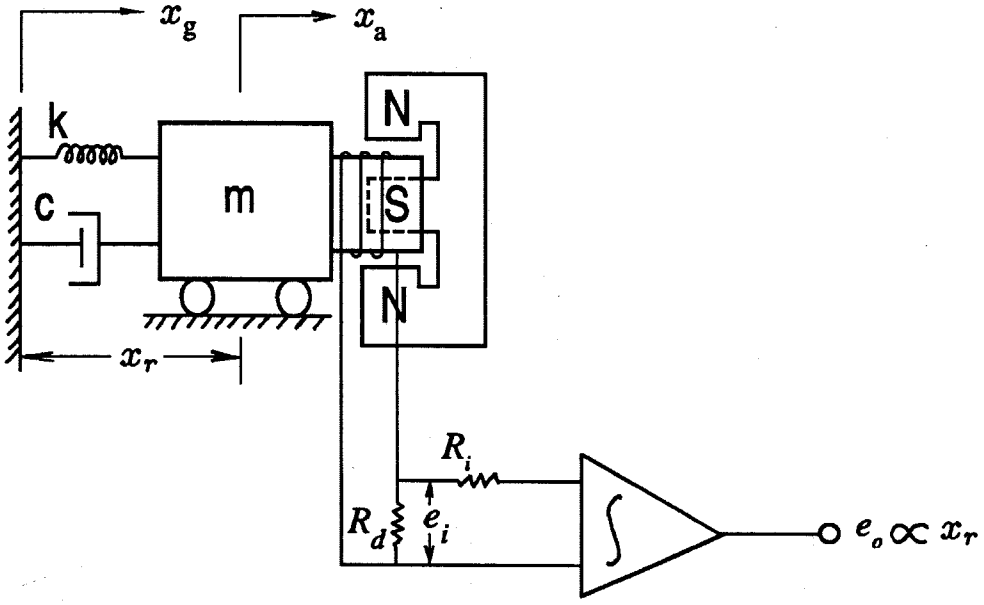

(a)

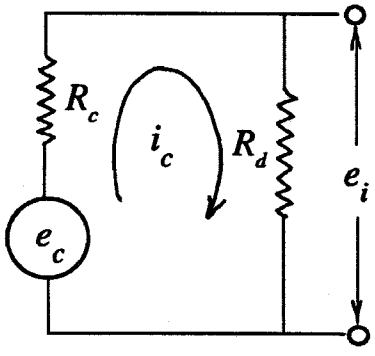

$$e_c - R_c i_c - R_d i_c = 0$$

$$i_c = \frac{e_c}{R_c + R_d}$$

$$e_o = R_d i_c = \frac{R_d G}{R_c + R_d} \dot{x}_r$$

(b)

Figure 3.1 Schematic Diagram of the Electro-Magnetic Transducer Design without Considering Leakage of the Amplifier.

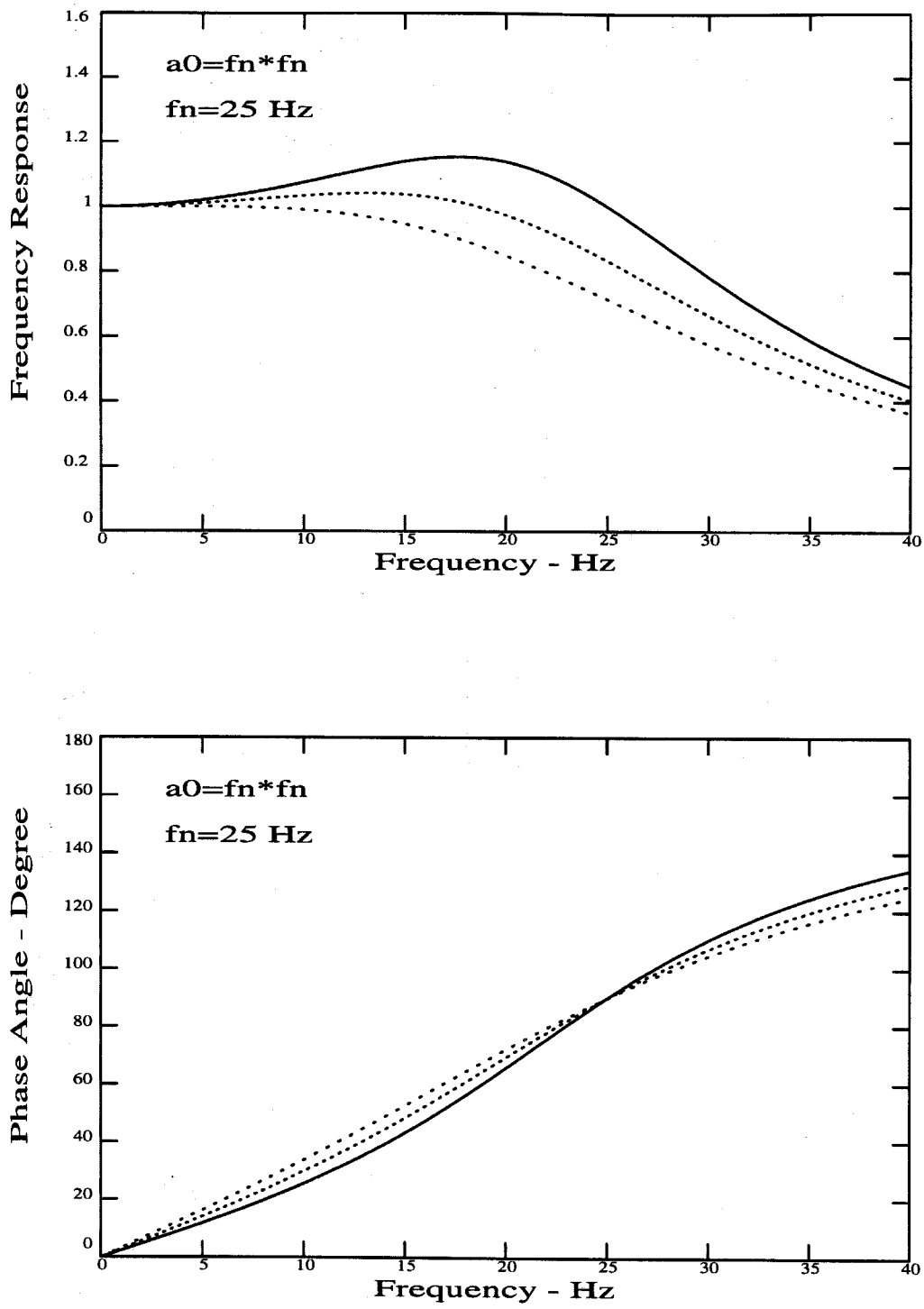

Figure 3.2 Transfer Function and Phase Shift of the EMA Transducer without Considering the Corner Frequency (in linear scale). Plots are for $f_n = 25$ Hz, $a_0 = f_n^2$, and $\zeta_n = 0.5, 0.6, 0.7$.
—— $\zeta_n = 0.5$, $\cdots\cdots$ $\zeta_n = 0.6$, $\cdot\ \cdot\ \cdot\ \cdot$ $\zeta_n = 0.7$.

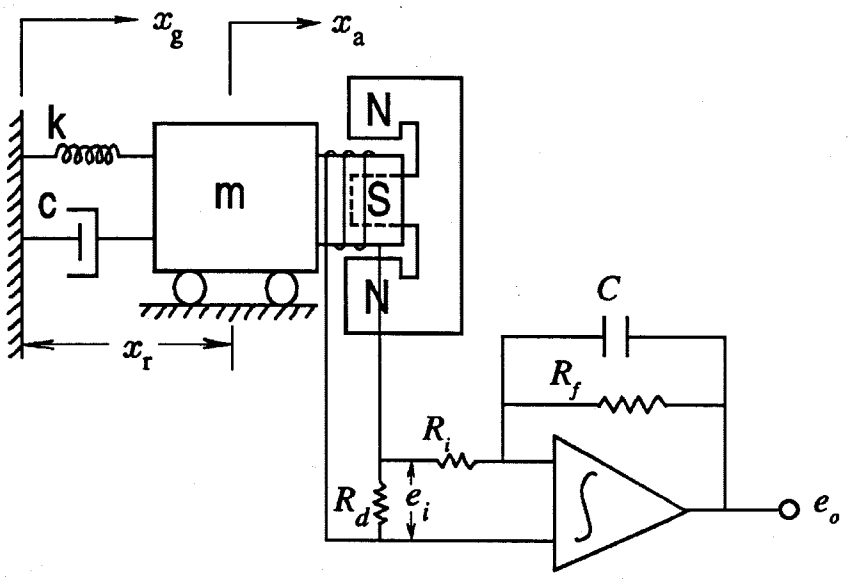

Transfer Function:

$$H(f) = \frac{a_0 if}{(if + f_{cr})(f_n{}^2 - f^2 + 2f_n f\zeta_n i)}$$

$a_0 = \frac{\alpha}{(2\pi)^2 C R_i}$

$f_{cr} = \frac{1}{2\pi C R_f}$ – Corner Frequency

f_n – Natural Frequency

ζ_n– Damping Ratio

Figure 3.3 Schematic Diagram of the EMA Transducer Design Considering the Leakage of the Amplifier and Transfer Function of the System.

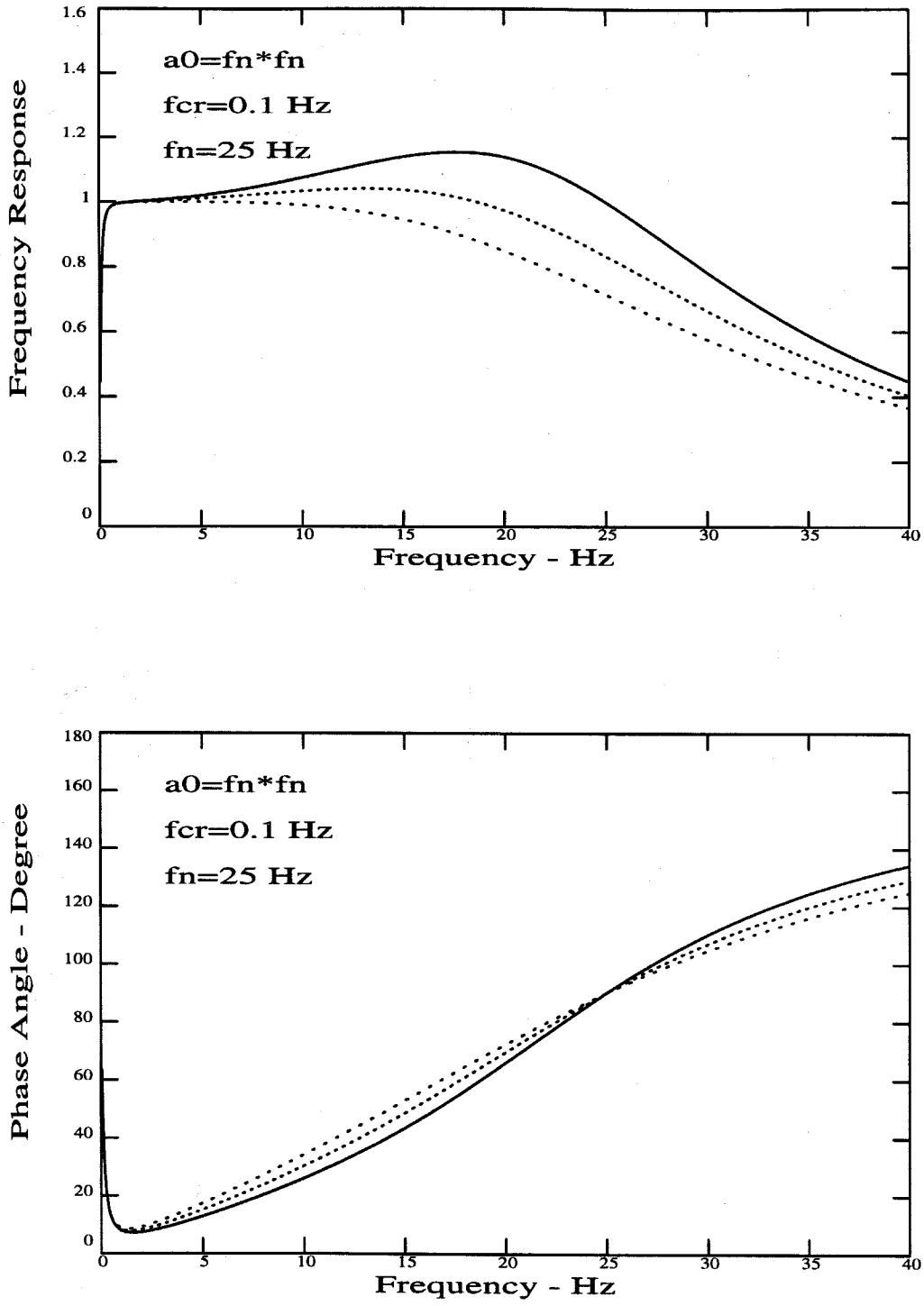

Figure 3.4 Transfer Function and Phase Shift of the EMA Transducer Considering the Corner Frequency (in linear scale). Plots are for f_{cr}=0.1 Hz, f_n = 25 Hz, $a_0 = f_n^2$, and $\zeta_n = 0.5, 0.6, 0.7$.
—— $\zeta_n = 0.5$, $\cdots\cdots$ $\zeta_n = 0.6$, $\cdot\ \cdot\ \cdot\ \cdot$ $\zeta_n = 0.7$.

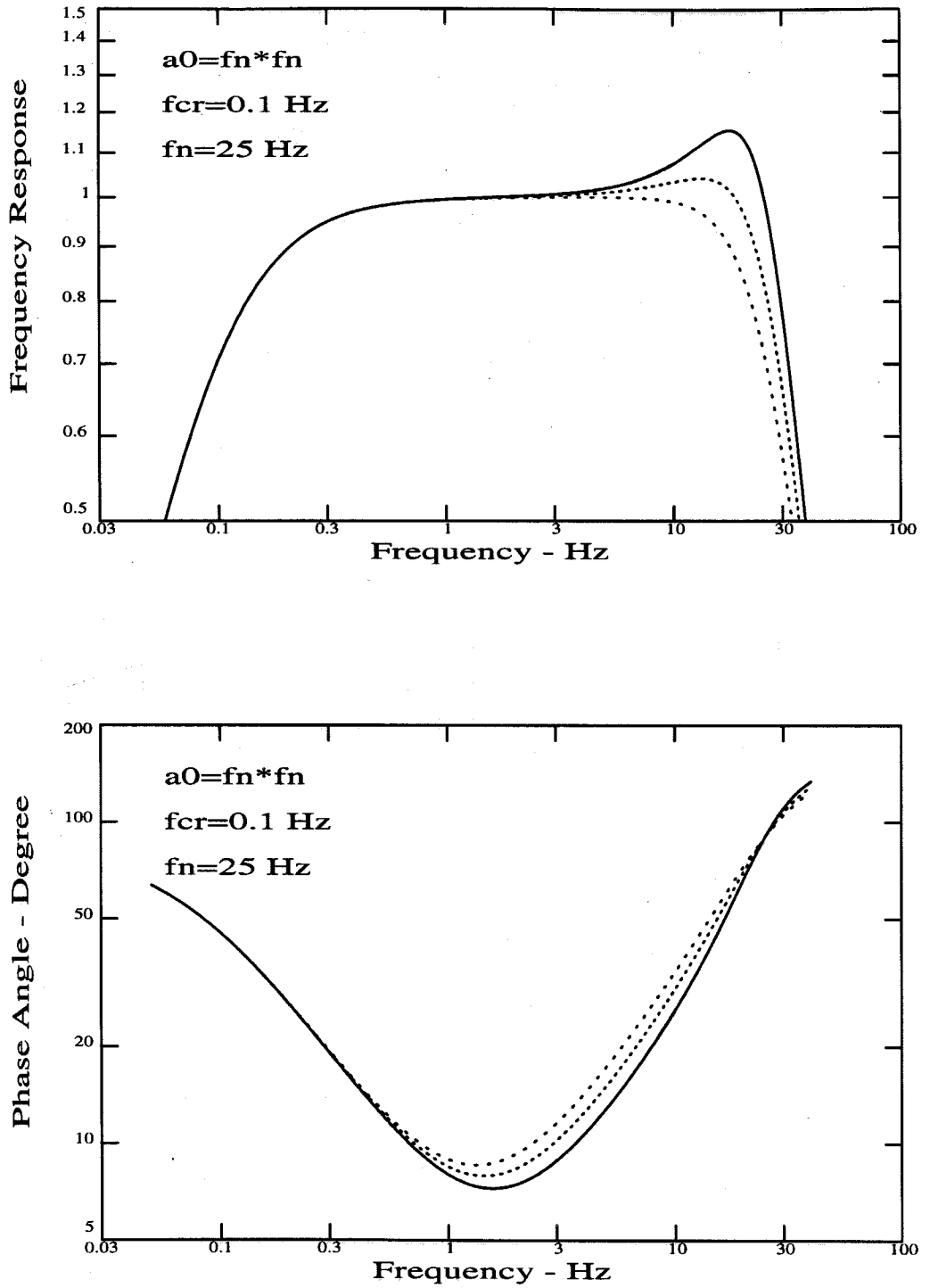

Figure 3.5 Transfer Function and Phase Shift of the EMA Transducer Considering Corner Frequency (in Logarithmic Scale). Plots are for f_{cr}=0.1 Hz, f_n = 25 Hz, $a_0 = f_n^2$, and $\zeta_n = 0.5, 0.6, 0.7$.
—— $\zeta_n = 0.5$, $\cdots\cdots$ $\zeta_n = 0.6$, $\cdot\ \cdot\ \cdot\ \cdot$ $\zeta_n = 0.7$.

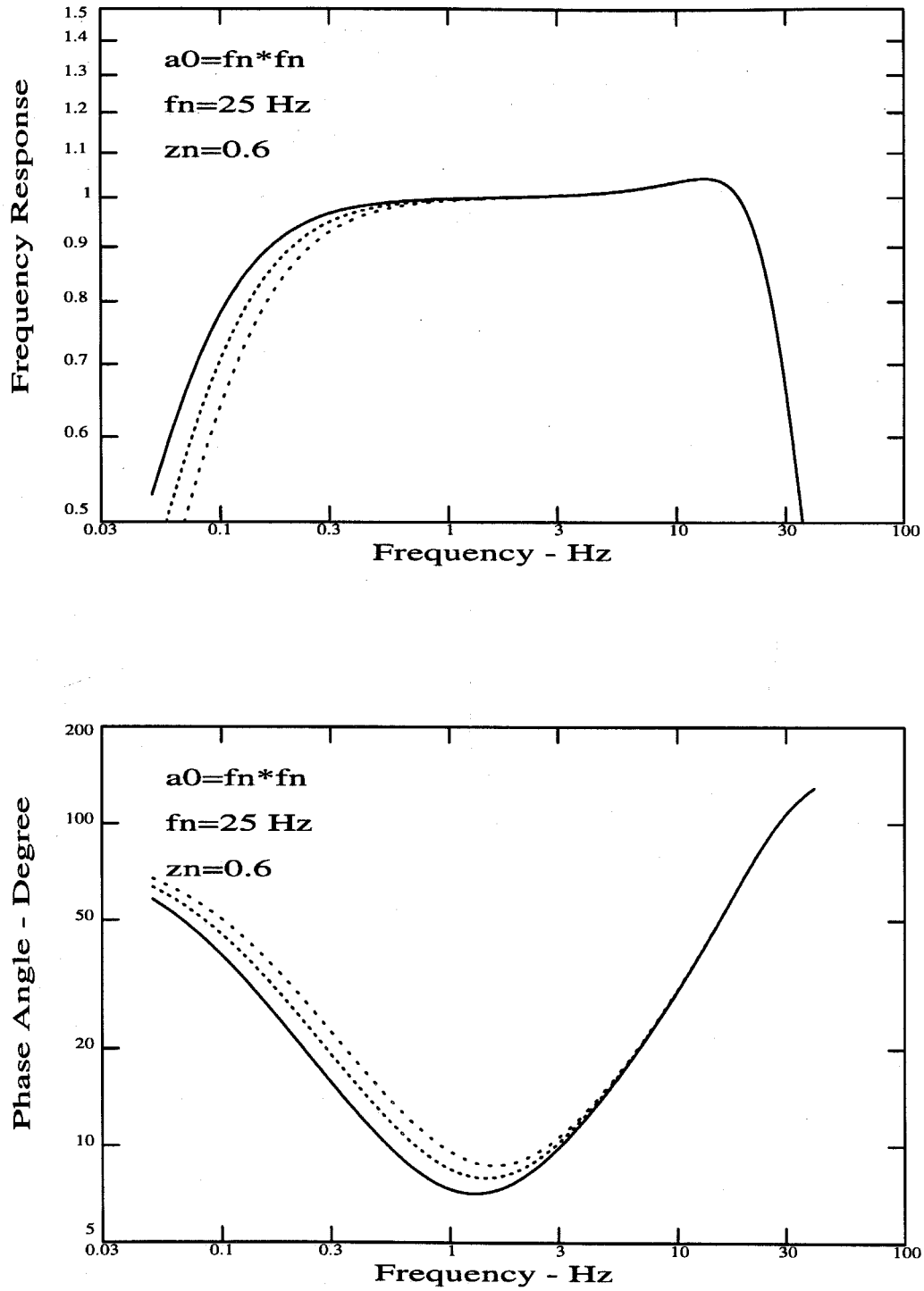

Figure 3.6 Transfer Function and Phase Shift of the EMA Transducer Considering the Corner Frequency (in linear scale). Plots are for $f_n = 25$ Hz, $\zeta_n = 0.6$, $a_0 = f_n^2$, and $f_{cr} = 0.08, 0.1, 0.12$ Hz.
—— $f_{cr} = 0.08$ Hz, $\cdots\cdots$ $f_{cr} = 0.1$ Hz, $\cdot\ \cdot\ \cdot\ \cdot$ $f_{cr} = 0.12$ Hz.

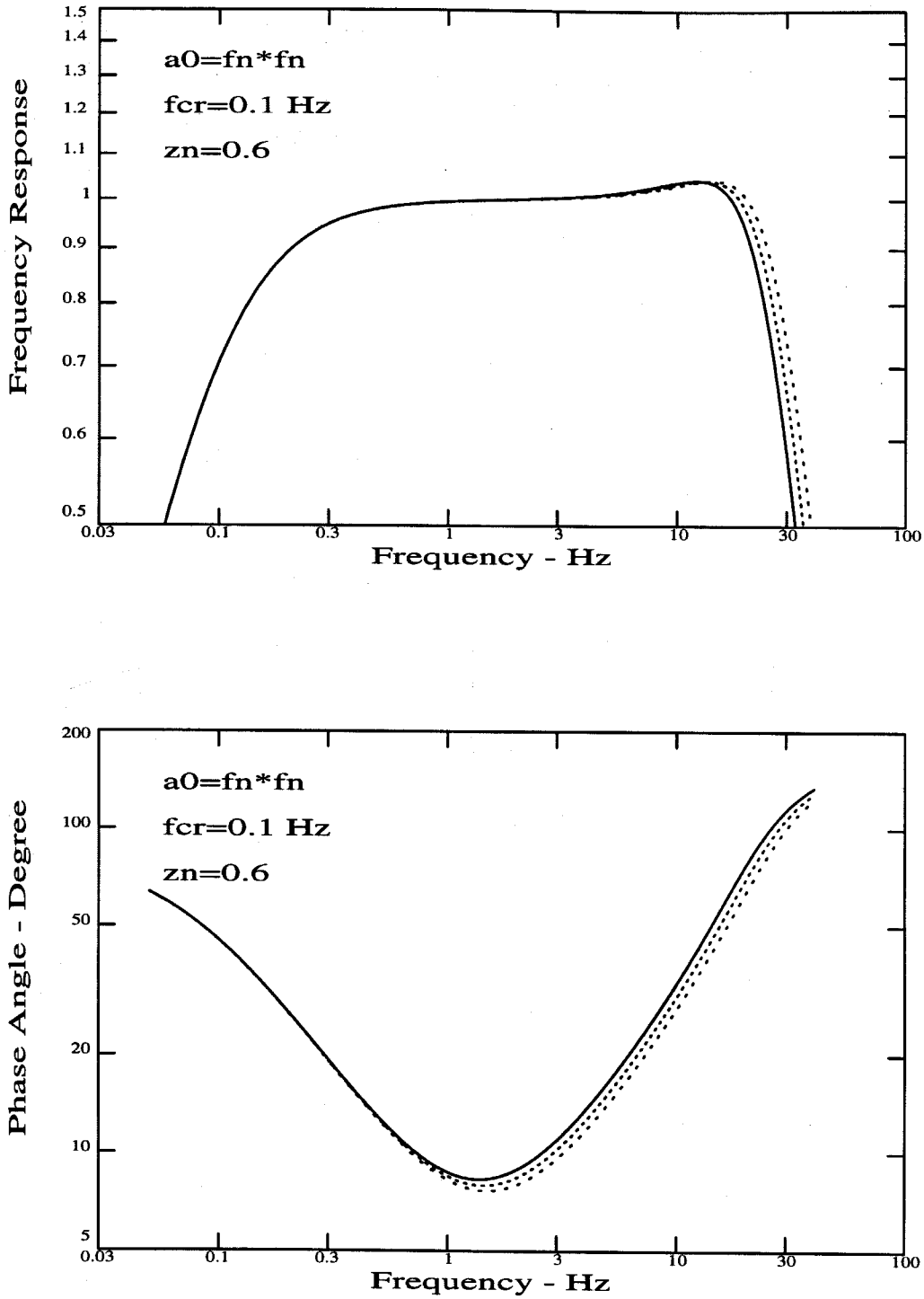

Figure 3.7 Transfer Function and Phase Shift of the EMA Transducer Considering the Corner Frequency (in linear scale). Plots are for $f_{cr} = 0.1$ Hz, $\zeta_n = 0.6$, $a_0 = f_n^2$, and $f_n = 23, 25, 27$ Hz.
—— $f_n = 23$ Hz, $\cdots\cdots$ $f_n = 25$ Hz, $\cdot\ \cdot\ \cdot\ \cdot$ $f_n = 27$ Hz.

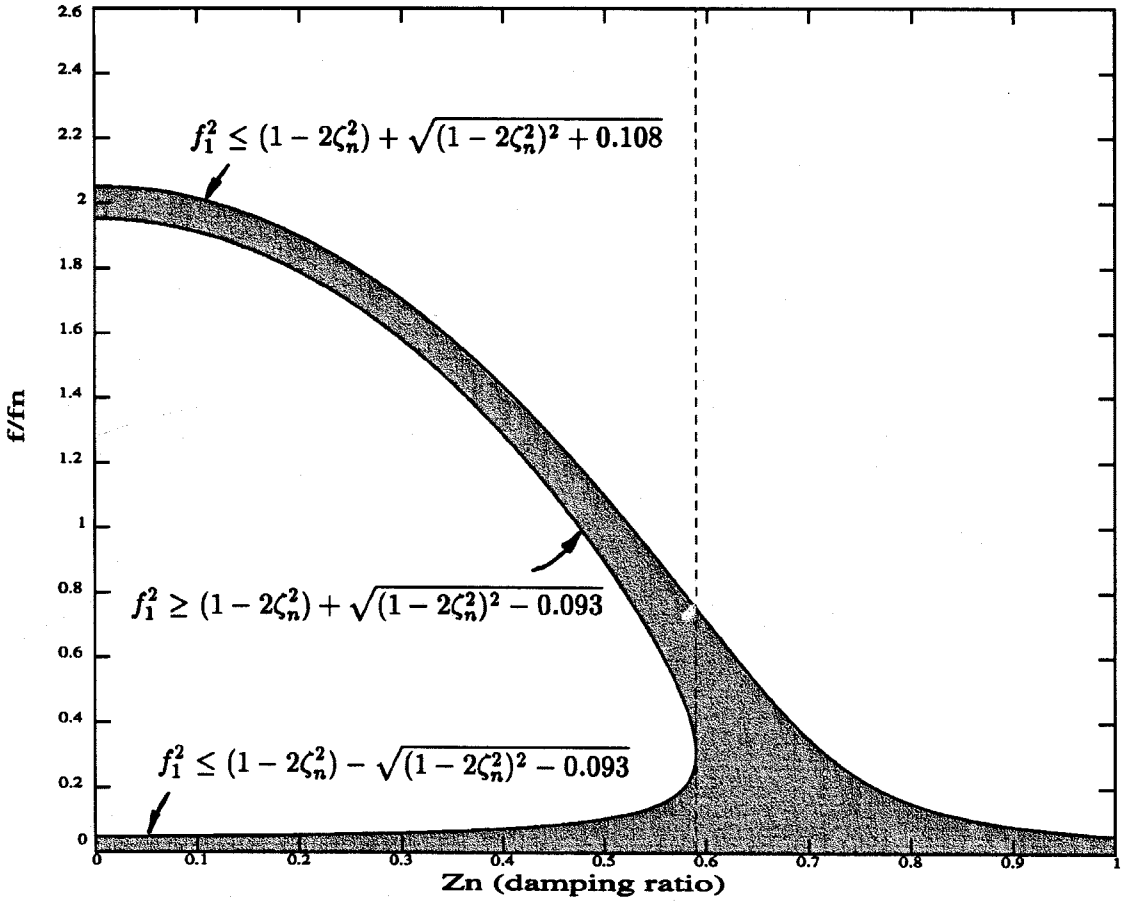

Figure 3.8 Optimal Design of EMA Transducer with Error Controlled within 5%.

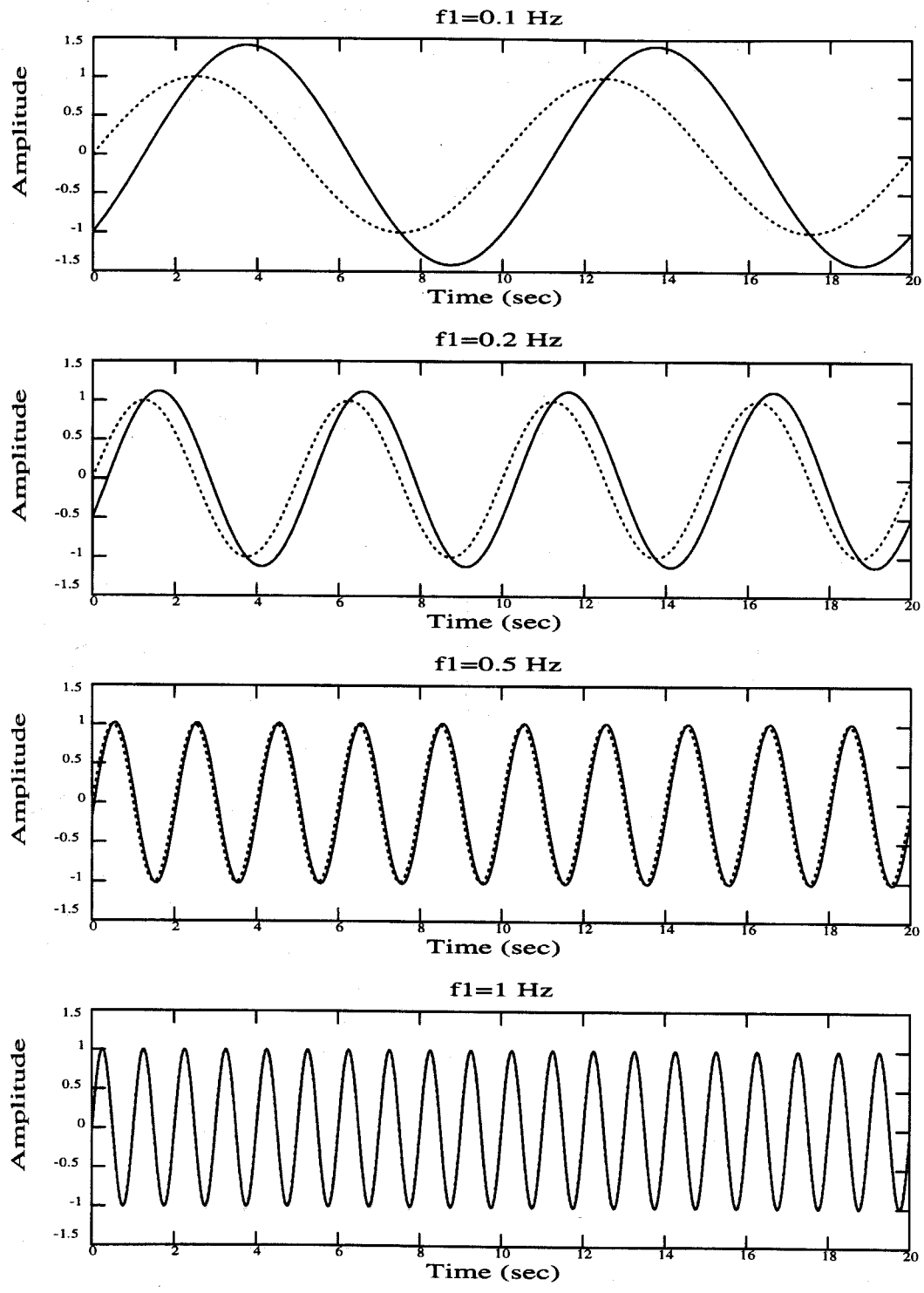

Figure 3.9 Harmonic Input and Output Signal of the EMA Transducer for Input Frequencies of $f_1 = 0.1, 0.2, 0.5, 1$ Hz.
$a_0 = f_n^2$, $\zeta_n = 0.6$, $f_n = 25$ Hz, —— Input, ····· Output.

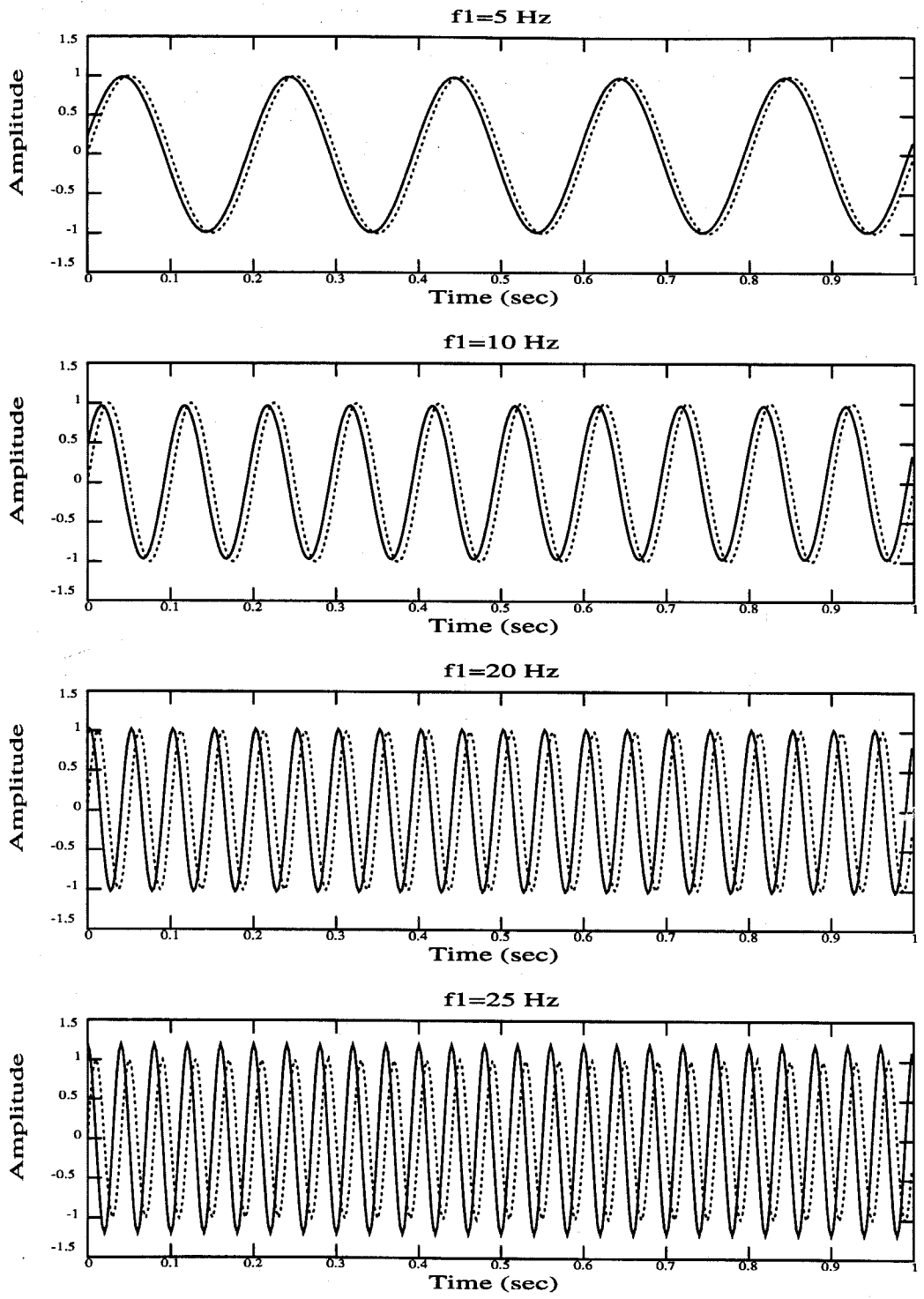

Figure 3.10 Harmonic Input and Output Signal of the EMA Transducer for Input Frequencies of $f_1 = 5, 10, 20, 25$ Hz.
$a_0 = f_n^2$, $\zeta_n = 0.6$, $f_n = 25$ Hz, —— Input, ····· Output.

Chapter 4

Calibration of the SMA-2/EMA Strong-Motion Accelerograph

4.1 Introduction

The purpose of the instrument calibration is to identify the characteristics of the Kinemetrics SMA-2/EMA instrument and therefore to be able to perform the instrument correction on the earthquake data which are recorded by this instrument. The shake table tests here were performed on two horizontal transducers of the Lucerne Valley SMA-2/EMA instrument. A digital instrument, an SSA-1, was used as a reference measurement. After the test, the test results are analysed and the properties of the EMA transducer such as natural frequency, electronic damping ratio, sensitivity and time constant (corner frequency) of the integrator are determined.

In this chapter, the details of the experimental setup, test procedure, noise test, and the simulation of a near-field ground motion are described.

4.2 Experimental Setup

The test was conducted at the Earthquake Engineering Research Laboratory of the California Institute of Technology. The equipment involved in the test was a shake table, control panel, chart recorder and personal computer. The other instruments used for the test of the SMA-2/EMA were an SSA-1, FBA-11, SSR-1 and SMP-1. Figure 4.1 is the diagram describing the whole test system.

4.2.1 Shake Table

The shake table used in this test was an MTS hydraulic dynamic controlled shake table. The table has dimensions of 44 inches×36 inches and has a maximum peak to peak displacement of 6 inches. The effective frequency range is between 0.5 to 200 Hz.

The dynamic response of the shake table can be controlled by either acceleration-based motion or displacement-based motion. Acceleration-based motion means that the acceleration of the shake table is kept at a nearly constant level when varying the frequency of the shake table motion. As a result, the displacement of the shake table will be inversely proportional to the square of the frequency. Displacement-based motion means that the displacement level of the shake table is kept approximately at a constant level when varying the frequencies of the shake table motion. As a result, the acceleration of the shake table will be proportional to the square of the frequency. In this test, displacement-based motion was chosen to perform the low frequency test and acceleration-based motion was chosen to perform the high frequency test.

4.2.2 Control System

The control system includes a MTS Model 439.11 Dynamic Response Controller, a MTS Model 436 Control Unit and a Function (or Noise) Generator. The Control Panel controls the fluid from a hydraulic power supply to a piston under the shake table through a service manifold. The service manifold gives a pressure to the shake table and generates a motion at a required acceleration (or displacement).

A Function Generator connected to the control unit can generate a sine wave, square wave, or triangular wave form as needed. A noise generator is used to generate Gaussian Noise at a certain frequency range, for example, from 5 to 50000 Hz.

4.2.3 Chart Recorder

A chart recorder was used to record the voltage output as an analog signal on a paper strip. In this test, a two channel recorder which was connected to the SMA-2/EMA instrument and FBA-11 accelerometer was used to obtain an immediate output from the shake table and the SMA-2/EMA. It was used as a visual reference during the test to ensure that the test was under control and that the information recorded on the SMA-2/EMA was correct.

4.2.4 The SSA-1 Solid State Recorder

The Kinemetrics SSA-1 is a self-contained three channel digital instrument. It has force-balance type transducers. The data recorded is stored in a PC RAM until later retrieval by the user. In this test, an Intel486 personal computer was connected to the SSA-1 through an RC-232C interface. The PC was used to control the trigger and recording of the SSA-1. By means of SSA-1 support software, the output of the SSA-1 can be retrieved immediately and stored directly on the hard disk of the PC.

The effective frequency response range of the SSA-1 is DC to 50 Hz. The full scale of the SSA-1 response can be set at $\frac{1}{4}$ g, $\frac{1}{2}$ g, 1 g and 2 g. The output voltage of the transducer is 2.5 volts for full-scale input acceleration. In this test, a full-scale range of 2 g was chosen for the SSA-1.

4.2.5 The SMP-1 Playback System

The playback unit used in this test is the Kinemetrics SMP-1. It is a magnetic tape playback system designed for use with the SMA-2 or SMA-3 instrument which have magnetic tape recording systems. In this test, the playback system also included a Data Compensator, which is used for amplitude compensation; and a Frequency Divider (divide 1024 Hz to 512 Hz, 256 Hz, 128 Hz or 64 Hz according to the user's need) which is used for time-base compensation. The SMP-1 playback unit will play back four channels of information recorded on the cassette: 3 signal channels and one timing channel. It contains a tape transport, a four-track cassette head, 4 preamplifiers, 4 pulse averaging demodulators and a chart recorder.

The details of the playback procedure are described in Section 4.3.2.

4.2.6 The SSR-1 Solid State Recorder

The Kinemetrics SSR-1 Solid State Recorder is a data acquisition system. It has 3 channels and is expandable up to 6 channels. It can be used for rapid access to the data in the field. In this test, a SSR-1 instrument was used as a data acquisition system to digitize the analog signal from the SMP-1 magnetic playback unit in the laboratory. The three-channel option was chosen in this test since the SMA-2/EMA records three channels of data.

4.2.7 The FBA-11 Accelerometer

The Kinemetrics FBA-11 is a force balance transducer with a frequency bandwidth of DC to 50 Hz. It was bolted on the shake table along with the SMA-2/EMA and SSA-1 instruments and connected to the chart recorder for immediate observation of the shake table output during the test.

4.3 Recording and Playback Procedures

During an earthquake, the ground acceleration is recorded as a frequency modulated (FM) analog signal on a magnetic tape cassette in the SMA-2/EMA. The signal is demodulated by the SMP-1 playback unit and digitized by a data acquisition system such as the SSR-1. By means of a personal computer, the digital-formatted data can then be retrieved and used for engineering study after data processing.

Before digitization, Amplitude Compensation and Time Base Compensation are performed on the playback signal by a Data Compensator and Frequency Divider [22]. Figure 4.2 is a flow chart describing the global view of the recording and playback procedure.

4.3.1 Recording Procedure for the SMA-2/EMA Accelerograph

As mentioned in Section 3.2, the output voltage of the transducers represents the ground acceleration as an analog signal. It is an amplitude modulated (AM) signal which is converted to a frequency modulation (FM) signal through a voltage-controlled oscillator (VCO). The FM signal is "written" on a four-track magnetic tape cassette. The recording deck of the SMA-2 records three signals from the output voltages of the three transducers and one reference signal from a 1024 Hz oscillator. This 1024 Hz oscillator is independent of the other three VCOs. It is used for tape speed correction and also for control of the digitization interval. The VCO will convert a zero volt input into a 1000 Hz signal and a ± 2.5 volt input into a 1000 ± 500 Hz signal. The details of the recording procedure are described on the left side of Figure 4.3.

In practice, the central frequency of 1000 Hz may slightly fluctuate and subsequently causes a baseline shift in the final retrieved data. This type of error can be

corrected by a baseline correction. The whole data processing procedure is discussed later in Chapter 5 and will not be considered at this stage of instrument correction.

4.3.2 Playback Procedure for the SMP-1 Playback System

A four-track head in the SMP-1 is used to playback the FM signals from the recorded cassette tape. After preamplification, the FM signals from 4 channels are demodulated into AM signals. The signals from channels 1, 2 and 3 represent the output of the longitudinal, transverse and vertical information recorded by the the SMA-2/EMA respectively. Channel 4 carries the timing signal from the 1024 Hz oscillator in the SMA-2/EMA. After demodulation, the signal from channel 4 is separated into two from the SMP-1 playback unit (Figure 4.3). One is demodulated AM timing signal, the other remains as an 1024 Hz FM signal which is amplified but not demodulated. It appears as the output of channel 5 from the SMP-1 playback unit. The signals from channel 1, 2, 3, and 4 go to the Data Compensator, while the signal form channel 5 goes to the Frequency Divider. The demodulators will convert the 1000 Hz FM Signal into the zero volts signal and the 1000 ± 500 Hz signals into ± 2.5 volts signals, which is the inverse procedure of the VCO's. Similarly, a central frequency of 1000 Hz may not be exactly converted into a zero volt signal. This will cause a baseline shift in earthquake records, which must be corrected by the data processing procedure which is discussed in Chapter 5.

Some other errors will also occur after playback. The data will contain two types of tape speed errors. One is a change in apparent amplitude due to unwanted tape speed changes. It is corrected by the Data Compensator by subtracting channel 4 signal from the signals of channel 1, 2, and 3. Correction of this error is called "Amplitude Compensation." The other is a change in apparent length of an earthquake record due to different tape speeds during recording and playback. It is corrected in digitization through use of channel 5 signal as a time base. The correction of this error is called "Time Base Compensation." The details of the tape speed compensation are discussed in the next section.

4.3.3 Tape Speed Compensations

Since the tape speed errors will occur during the recording and playback procedure, two tape speed error compensations need to be performed. In this test, a Data Compensator and a Frequency Divider are used to perform those corrections.

A Data Compensator is used to perform the Amplitude Compensation. It corrects the error in the signal caused by changes in the tape speed during recording and playback. The motor drives of the recorder and playback unit may not run smoothly because of friction in the mechanical system. Since channel 4 records a fixed frequency of 1024 Hz without being involved in any ground motion information, it should be played back as zero volt signal under ideal conditions. But in reality, it records a fluctuating signal caused by variation of the tape speed. Meanwhile, the other three channels which record ground motion contain the same fluctuations. By means of the Data Compensator, the three transducer output signals are amplitude compensated by subtraction of channel 4 from channels 1, 2, and 3.

A Frequency Divider is used to perform Time Base Compensation, it corrects the tape speed error which is associated with the difference between the total time length of recording and playback. The FM signal from channel 5 of the SMP-1 is 1024 Hz plus or minus the tape speed error. In this test, the FM signal is divided by four to obtain a signal of 256 Hz $\pm deviation$ to be used as the timing signal for the digital conversion time interval. The reasons for the division are twofold: 1) to reduce the volume of the data so that the SSR-1 can accept the signal and process the data for three or four channels simultaneously, and 2) a sample rate of 256 samples per second contains enough frequency information within the frequency range of interest. A signal with a sample rate of 256 per second will contain the frequencies from 0 to 128 Hz without aliasing. The dominant frequencies of most earthquakes are within this frequency range. Moreover, dividing the 1024 Hz to 256 Hz reduces the data volume by 75% and saves tremendous disk space on the PC. At the same time of the dividing process, time base compensation is performed. The 1024 Hz signal is also divided into a 2 Hz signal as a timing mark for the chart record output of the SMP-1 unit.

4.3.4 Digitization

After tape speed error corrections, the output from channels 1, 2 and 3 of the Data Compensator are still analog signals. In this test, a SSR-1 Solid State Recorder data acquisition system and a PC were used to digitize and store the data. The SSR-1 contains an analog to digital convertor. The 3-channel option was chosen for this data acquisition system. By connecting the SSR-1 to the PC with an RS-232C

interface, and executing the SSR-1 support software, the digitized accelerations were retrieved and stored on the hard disk of the PC. The SSR-1 support software includes QuickTalk communication software and QuickLook display software. This software was provided by Kinemetrics.

4.3.5 Summary

Although tape speed errors have been corrected by the Data Compensator and Frequency Divider, some systematic errors still exist. These include 1) a baseline shift caused by the shift of the central frequency of the VCO, 2) the sensitivity deviation of the transducers, 3) deviation from the 1024 Hz timing signal, and 4) the deviation of the overall frequency response from flat. The imperfection of the transducer frequency response is indicated as a mechanical system error. It can be recovered by Equation (3.33) based on the test results. The other errors are "electronic" errors. Some of these electronic errors can be corrected by Equation (3.33) and the others can be corrected by a linear scaling factor γ which is calculated from the sensitivities of the instruments such as the SMA-2/EMA, SMP-1 and SSA-1. This factor will be discussed later in Section 4.5. Its nominal value is 1 g per 2.5 volts. The following sections discuss the procedures and results of the tests for instrument correction purposes.

4.4 Instrument Test

The tests conducted were: 1) a tilt test of the SSA-1, 2) a frequency response test of the SMA-2/EMA, 3) a noise test of the SSA-1 and SMA-2/EMA, and 4) a simulation of near-field ground motion.

The purpose of the tilt test of the SSA-1 is to obtain the sensitivities of its two horizontal transducers. By using the SSA-1 as a "standard" recording of the shake table motion, the sensitivities of the EMA can be calculated from the dynamic test results based on the output of the FBA (Force Balance Accelerograph) transducers of the SSA-1.

The transfer function test for the SMA-2/EMA is the most important part of the test. As mentioned earlier, the purpose of the test is to identify the characteristic parameters of the SMA-2/EMA such as natural frequency, electronic damping ratio,

corner frequency of the transducer amplifier and sensitivity. These parameters play an important role in instrument correction of earthquake records.

The noise test gives the output noise level of the instruments. It will also give an estimation of how much contamination of high frequency noises are involved in earthquake records. The signal-to-noise ratio has been frequently employed to determine a frequency band for filtering the earthquake data [23,24,25,26]. But this approach is not employed in this study.

The purpose of simulating near-field accelerograms is to use these records to verify the new data processing procedure which is discussed in Chapter 5. Since the simulation is conducted in the laboratory, the displacement of the instrument can be measured and used for later comparison with the displacement time history calculated by the new data processing scheme.

4.4.1 Static Tilt Test of the SSA-1 Instrument

The SSA-1 has a force-balance type of transducer, the sensitivity of the transducer can be determined by a static tilt test in the earth's gravitational field. In this test, the SSA-1 instrument was bolted to a table which can be tilted through different angles. A tilt test was performed on the SSA-1 from $-90°$ to $90°$. The results for both longitudinal and transverse transducers of the SSA-1 are listed in Table 4.1. These results are shown in Figure 4.4. The nominal sensitivity is 1.25 volt/g. In the figure, the solid boxes represent the test results and the solid line represents the results calculated from the nominal sensitivity. The results show that the SSA-1 performs with a very good linearity.

The true sensitivities of the longitudinal and transverse transducers can be calculated from the results in Table 4.1. By applying the least mean square method to fit those data to a straight line $a + bx$, the baseline shift a and the slope b of the straight line can be obtained. The results of a and b for horizontal transducer tests are listed in Table 4.2. The sensitivity of SSA-1, denoted by ϵ_1, can be calculated from $\epsilon_1 = 2.5b$. The sensitivities of the longitudinal and transverse transducers are obtained to be 1.245 volt/g and 1.237 volt/g respectively. These values are also listed in Table 4.2.

The results in Table 4.2 show that the sensitivity of the longitudinal transducer of the SSA-1 is very close to the nominal value, with the difference of only 0.4%. The sensitivity of the transverse transducer of the SSA-1 differs from the nominal value by 1.0% which is also very small. In the following test, the longitudinal transducer of the SSA-1 is used as the reference recording for the shake table motion.

4.4.2 Transfer Function Test of the SMA-2/EMA Instrument

The transfer function test of the SMA-2/EMA is the main and most important part of the test. The transfer function provides the frequency response of the dynamic system.

The transfer function is obtained by recording the amplitude of the instrument response under harmonic excitation at selected frequencies. The experimental data can be used to verify the theoretical model of the transducer system. The parameters of the system can be obtained by the curve fitting method. The details of the test procedure and data analysis of the results are discussed below.

4.4.2.1 Brief Description of the Test

The responses of the SMA-2/EMA were tested in the frequency range from 0.1 Hz to 40 Hz. Seventeen different frequencies between this range were chosen in the test. A steady-state harmonic motion was performed by the shake table for each frequency. Since the "flat" frequency range of SSA-1 is DC to 50 Hz (according to the manufacturer), which is much greater than that of the SMA-2/EMA, the SSA-1 was used as a standard measurement of the shake table response.

The test frequencies were chosen to be 40, 35, 30, 25, 23, 20, 15, 10, 5, 2, 1, 0.8, 0.5, 0.4, 0.3, 0.2, 0.1 Hz. As mentioned in Section 4.1.1, because of the limitation of the shake table, the high frequency shaking was performed using acceleration control while the low frequency shaking was performed using displacement control. In this test, the harmonic motions at the frequencies from 0.1 to 0.5 Hz were performed using displacement control with the displacement level fixed at approximately 5.5 inch peak-to-peak. The sinusoidal motions at frequencies from 0.8 to 15 Hz were performed using acceleration control with a constant shake table acceleration of 0.1 g. The motions at frequencies from 20 to 40 Hz were also performed using acceleration control

with a shake table acceleration of 0.5 g. The SSA-1 and SMA-2/EMA instrument were bolted directly to the shake table as shown in Figure 4.1.

Since the SMP-1 playback system was not available at Caltech, and hence the data retrieval was performed at Kinemetrics, the SMA-2/EMA records could not be viewed during or right after each shake table test. To be able to observe the dynamic response of the SMA-2/EMA during the test, a chart recorder was connected to the SMA-2/EMA. The SMA-2/EMA was manually triggered during the test.

An FBA-11 accelerometer was also bolted to the shake table and used to set the acceleration level of the shake table during the test.

4.4.2.2 Test Data Analysis and Results

After the shake table tests, the data from both the SSA-1 and SMA-2/EMA were retrieved and analysed. By taking the ratio of the steady-state response of the SMA-2/EMA and SSA-1 at every tested frequency, the frequency responses of the SMA-2/EMA at those frequencies were obtained.

Unfortunately, tremendous high frequency noises were present in the low frequency shaking tests. These noises made it difficult to accurately measure the amplitude of a sinusoidal wave. One method of compensating for these noises is to filter out the high frequency noises to obtain a smooth "pure" sinusoidal wave of a steady-state response.

A second method is to perform a Fourier transform on every steady-state response and take the ratios of peak values at the test frequencies. This method was not very successful since the sample rates generated from the different data retrieval systems are different. The sample rate for the data retrieved from the SSA-1 was 200 per second while the sample rate for the data retrieved from the SMA-2/EMA was 256 per second.

A third method is to use a noise generator to generate a broad-band frequency shaking. The ratio of the Fourier spectra of the SMA-2/EMA and SSA-1 should give the transfer function of the SMA-2/EMA system. In practice, because of the deviation of the random data, a very large number of samples must be generated in order to obtain satisfactory statistical results.

A fourth method is to curve fit the recorded response data to a harmonic function. The target function chosen will have the form of

$$f(t) = a\ cos(2\pi f_0 t) + b\ sin(2\pi f_0 t) + c$$

where $f(t)$ represents the sinusoidal wave function, f_0 is the test frequency of the shake table motion, and a, b and c are the parameters to be determined by the least-mean-square fit method. The amplitude of the signal will be computed as $A = \sqrt{a^2 + b^2}$ while the probable baseline shift will be evaluated by c.

Herein, the fourth method is adopted to do the analysis. The curve fitting procedure basically filters out the high frequency noise in the signal. There is also low frequency noise which caused fluctuation of the baseline and the amplitude. To obtain the best result, a statistical analysis was applied. From every frequency response, ten segments of the sinusoidal waves were taken, each segment having four to six cycles. The curve fitting was applied to each of the ten segments to obtain 10 steady-state response amplitudes for each test frequency.

The average results for these ten samples of frequency response are calculated and are listed in Table 4.3. These are experimental data of the transfer function for the SMA-2/EMA at discrete values of frequency.

The model parameters of the SMA-2/EMA were determined by curve fitting the test data from all the ten samples to the Equation (3.33). An iterative scheme was employed to obtain the characteristic parameters of the EMA and the results are listed in Table 4.4. Since the test of the vertical transducer was not possible with the available test equipment, the parameters for the vertical transducer were taken to be the average of the parameters for the longitudinal and transverse transducers.

With the parameters shown in Table 4.4, the transfer function of the SMA-2/EMA can be calculated as a continuous function of frequency using Equation (3.33). Figures 4.5(a) and (b) show the frequency responses represented by both the test results and Equation (3.33) for the two horizontal transducers of the SMA-2/EMA. The cross symbols are the test results for ten samples. The dotted line represents the average of ten test samples. The solid line represents the result of theoretical formula from Equation (3.33).

The plots of Figure 4.5(a) and (b) show good agreement between the test results and the theoretical formula results. They also show that the dynamic response of the electromagnetic transducer "filters out" significant low frequency and high frequency information. The response is fairly flat only between 0.5 Hz and 10 Hz. The frequency response drops off below 0.5 Hz and is about 70% of the full response at the 0.1 Hz. The transfer function has a small hump between 15 and 23 Hz and drops off again after 23 Hz. This implies that the data recorded on the SMA-2/EMA will be under-represented in the low frequency range (below 0.5 Hz) as well as in the high frequency range (above 23 Hz), and will be over-represented by a small amount in the frequency range from 15 to 23 Hz.

Determination of the characteristic parameters of the SMA-2/EMA instrument provides not only the response amplitude of the instrument but also phase delay information. Figure 4.6(a) shows the the transfer function and the phase angle in logarithmic scale versus the frequency for the three transducers of the SMA-2/EMA instrument. The solid line represents the longitudinal transducer response, the dotted line represents the transverse transducer response, and the dashed line represents the vertical transducer response which is the average of the other two. Figure 4.6(b) shows the same response plots as in Figure 4.6(a) but in linear scale. The curves are computed using the Equation (3.33) and Equation (3.34) with the experimentally determined parameters. Considerable input-output phase shift (phase distortion) is observed.

From Figure 4.6, it can be seen that the longitudinal and the transverse transducer responses are very close to each other, so that to take their average as a vertical transducer response is reasonable. The phase angle plot shows that the phase distortion occurs in both the low and high frequency range. Ideally, the phase angle would be a linear function of frequency. This is approximated only in the mid-frequency range of the system.

The natural frequency f_n, damping ratio ζ_n and time constant of the amplifier CR_f are given in the Table 4.4. The a_0 values are directly related to the sensitivities of the instrument. Calculation of the sensitivities of the SMA-2/EMA is discussed in Section 4.5.

4.4.3 Noise Test

Laboratory noise signals were recorded for the SSA-1/FBA, the SMA-2/EMA transducers and the SMA-2/EMA with SMP-1 playback system. Figure 4.7 shows the typical noise signals recorded in a quiet environment for those three systems. Figure 4.8 is the Fourier spectra of the noise signals of Figure 4.7. It can be seen that the noise of the SSA-1 is very small while the noise from the SMA-2/EMA with SMP-1 playback system is relatively larger. It can also be noticed that the high frequency noise mostly comes from the recording and playback system. The high frequency noise from the SMA-2/EMA transducers is about the same magnitude as that of the SSA-1/FBA. The low frequency noise of the SMA-2/EMA transducers are of the same magnitude as that of the SMA-2/SMP-1 system which is about 100 times the magnitude of that of the SSA-1.

Any data recorded on the SMA-2/EMA instrument will be contaminated by the noise. If the magnitude of the noise is bigger than that of the signal, the signal information will be lost. In standard CIT "Vol. II" data processing procedures, the noise correction to the signal is to apply a filter to the signal with cut-off frequency f_c and roll-off termination frequency f_t. The f_c and f_t values are determined by the intersection of the response spectrum and the noise spectrum. That means the signal-to-noise ratio should be greater than one. For purpose of convenience, Fourier spectra are sometimes employed to determine the signal-to-noise ratio since Fourier spectra are very close to the relative velocity response spectra of a undamped oscillator. In general, the relative velocity spectra is always greater than the Fourier spectra. Studies [27,28] have shown that for any earthquake of magnitude greater than $M = 4.5$, the ground motion near the epicenter can be distinguished from background noise over the whole frequency spectrum of engineering significance. And, for an earthquake with $M = 6.5$, the Fourier spectra of the ground motion will be above the noise spectra over the entire frequency range when the station site is away beyond 100 Km.

For the Landers earthquake, since the geological location of the Lucerne Valley station is about 1.2 miles away from the fault and 26 miles (42 Km) away from the epicenter, the ground motion will be above the noise level for the whole frequency range of interest. Figure 4.9 gives a plot of response spectra of the noise and the ground motion for three components of the Lucerne Valley record. The plot shows

that the earthquake spectra and the noise spectra have no intersections in the frequency range of interest and the signal-to-noise ratio is generally greater than 4 or 5. It can be concluded that for near-field ground motion of a moderate to large earthquake, the noise contaminations can usually be neglected.

4.4.4 Simulation of Near-Field Earthquake Accelerograms

For purposes of this study, twelve different near-field earthquake accelerograms were simulated. The simulation was performed by manually sliding the SMA-2/EMA instrument along a flat surface on the ground. A 2 inches×2 inches metal extrusion was bolted to the floor to make a straight surface for the SMA-2/EMA to slide against. It should be pointed out that the simulation could not be conducted on the shake table because of the limitation of the shake table displacement. As indicated, the maximum peak-to-peak displacement of the shake table is 6 inches.

To simulate a near-field ground motion from a strike-slip fault earthquake (for example, Landers earthquake) as realistically as possible, the instrument was given a pulse-like motion of approximately 4 to 5 seconds duration and a maximum displacement of approximately 6 feet. Three types of ground motion as in Figure 4.10(a)(b)(c) were simulated. Type 1 ground motion was generated by moving the instrument 6 feet in a positive direction, moving it back 3 feet in a negative direction, and then stopping. Type 2 ground motion was generated by moving the instrument 6 feet in the positive direction of the transducer and then stopping. Type 3 ground motion was generated by moving the instrument 6 feet in the positive direction without stopping, moving it back to the original position, and stopping. The total duration for each of these three types of "ground motion" was 5 to 6 seconds.

Of the twelve manually generated earthquakes, nine were recorded by the longitudinal transducer and three were recorded by the transverse transducer. The accelerograms of the twelve simulated earthquakes are numbered from #1 to #12 in Figure 4.11. Records #1 to #3 are expected to have the displacement time history as in Figure 4.10(a), records #4 to #6 are expected to have the displacement time history as in Figure 4.10(b), and records #7 to #9 are expected to have the displacement time history as in Figure 4.10(c). These nine records were recorded by the longitudinal transducer. Records #10 to #12 were recorded by the transverse transducer. They represent Type One ground motion.

As mentioned earlier, the purpose of generating simulated near-field ground motions for the SMA-2/EMA is to use the resulting records to test the reliability of the data processing scheme. If the data processing scheme can recover long-period information from the simulated earthquakes and the resulting displacements are consistent with the measured displacements, the calibration and data processing procedure will be considered successful. The application of the data processing procedure on those simulated records is discussed in Chapter 5.

4.5 Sensitivity Error Correction

In this test, the data retrieved were based on the nominal sensitivities of the instruments. In practice, the deviations of the instrument sensitivities will introduce errors in recorded earthquake data. So, correction of these errors needs to be performed during data processing. For simplicity, the correction of the sensitivity deviations was carried out by scaling a constant factor γ on the final processed record, where γ represents the total sensitivity error corrections combined from all the instruments involved in data recording and playback. It can be shown by Equation (3.59) that the instrument correction filter is a linear operator.

4.5.1 Sensitivity Error Correction for the SSA-1 Instrument

The instrument correction performed by Equation (3.59) actually gives the output of the SSA-1, since the SSA-1 is used as a reference to determine the instrument parameters. The motion of the shake table should be given by:

$$\left[\ddot{x}_g(t)\right]_{shake\ table} = \left[\ddot{x}_g(t)\right]_{SSA-1\ output} \times \frac{1.25}{\epsilon_1} \tag{4.1}$$

where ϵ_1 is the sensitivity of the SSA-1 instrument. Its value can be obtained from the tilt test results of the SSA-1. The ϵ_1 values for the two horizontal transducers are listed in Table 4.2. The value 1.25 is the nominal sensitivity of the SSA-1. As mentioned in Section 4.4.1, only the longitudinal transducer of the SSA-1/FBA is employed to record the "standard" table motion when testing the SMA-2/EMA in both horizontal directions. Therefore, only the value $\epsilon_1 = 1.246$ in Table 4.2 is used for sensitivity error correction and the correction factor is $\alpha_1 = \frac{1.25}{\epsilon_1}$.

4.5.2 Sensitivity Error Correction for the SMA-2/EMA Instrument

To evaluate the sensitivities of the EMA transducers from the test, the following relationship is adopted:

$$\epsilon_2 = 2H(\bar{f})\epsilon_1 \quad \bar{f} = 4Hz \tag{4.2}$$

where ϵ_1 is the sensitivity of the SSA-1/FBA instrument and ϵ_2 is the sensitivity of the SMA-2/EMA instrument in this test. $H(f)$ is the transfer function represented by Equation (3.33). The value of $H(\bar{f})$ is the frequency response at $f = \bar{f}$ Hz, and $\bar{f} = 4$ Hz is recommended by the manufacturer for performing the sensitivity calibration.

By simple calculation, the sensitivities for both the longitudinal and transverse transducers of the SMA-2/EMA can be obtained and the results are listed in Table 4.5, where the sensitivity for the vertical transducer is calculated from the average sensitivity values of the longitudinal and transverse transducers.

The Kinemetrics calibrated sensitivity values for the three transducers of the SMA-2/EMA are also listed in Table 4.5. It should be pointed out that before the time of the test and after the Landers earthquake, Kinemetrics did a recalibration on the SMA-2/EMA. Therefore, an appropriate adjustment needs to be performed on the instrument corrected results. In Table 4.5, ϵ_a represents the sensitivity of the SMA-2/EMA after the Kinemetrics' recalibration while the ϵ_b represents the sensitivity before the Kinemetrics' recalibration. The laboratory test of the SMA-2/EMA was performed after the Kinemetrics' recalibration and hence the characteristic parameters obtained are based on the sensitivity ϵ_a. So a correction factor of $\alpha_2 = \frac{\epsilon_a}{\epsilon_b}$ needs to apply to the Lucerne Valley record in order to obtain the data which are adjusted to the instrument condition during the Landers earthquake.

4.5.3 Sensitivity Error Correction for the SMP-1 Playback System

A correction based on sensitivities of the playback unit also needs to be considered since the Landers earthquake data were retrieved by a different SMP-1 playback unit than that used in this test. As described in Section 4.2, the frequency signals recorded on the tape will be demodulated by the playback board during the playback procedure. Under ideal conditions, a 1000 frequency signal will be played back as a zero volt analog signal and a 1000 ± 500 Hz frequency signal will be played back

as a ± 2.5 volt analog signal. In reality, deviations were possibly involved. Table 4.6 gives two sets of sensitivities for two different playback units [29,30]. One set of sensitivities was used for the Lucerne Valley record and the other was used for the test data. According to the information from Kinemetrics, the Lucerne Valley record was played back on the SMP-1 unit with serial number 136 and the test data were played back on the SMP-1 unit with serial number 259. Ignoring the slight nonlinearity, the average values of the full scale output of these two SMP-1 (provided by Kinemetrics) are calculated and the results are listed in Table 4.6 with the notation of $\bar{v}$ (volts). Then, the adjustment of the sensitivities of the playback unit for the Lucerne record is a scaling of the earthquake accelerogram by a factor of α_3. The scaling factors for three components are calculated in Table 4.7 by $\alpha_3 = \frac{\bar{v}_T}{\bar{v}_L}$, where $\bar{v}_T$ represent the sensitivity of the SMP-1 which was used for the test and $\bar{v}_L$ represents the sensitivity of the SMP-1 which was used for correcting the Lucerne Valley record.

4.5.4 Summary of the Sensitivity Error Corrections

The total sensitivity error correction for the Lucerne Valley record is a scaling of the data by a factor of $\gamma = \alpha_1\alpha_2\alpha_3$. Since the whole data processing procedure is assumed to be linear, this factor γ can be applied to the final processed record. The γ values for the three channels are calculated and listed in the Table 4.8.

The results show that the differences between the earthquake data as corrected and uncorrected for sensitivity errors are not very significant. The differences for the longitudinal, transverse and vertical components are 2.27%, 2.36% and 6.9% respectively. The difference from the vertical component is relatively larger than those from the two horizontal components mainly because the sensitivity of the vertical transducer is beyond the normal allowable range. Normally the sensitivity of the instrument in operation must be between 2.35 and 2.55 VDC [31]. So in most of the cases, the difference between the sensitivity error corrected earthquake data and the uncorrected data is expected to be small if the instrument in the field is calibrated regularly. Therefore, when the sensitivity information of the instrument is unknown, neglecting of the sensitivity error correction during the data processing is acceptable.

4.6 Summary and Conclusions

In summary, this chapter gives a full description of the laboratory test of the SMA-2/EMA instrument. The transfer function test of the SMA-2/EMA at seventeen frequencies from 0.1 to 40 Hz gave the experimental data of the transfer function for two horizontal transducers. By the least-mean-square fit of the test data to Equation (3.33), the characteristic parameters of the SMA-2/EMA instrument were obtained. With those important parameters, the instrument correction can be successfully performed by the application of Equation (3.59) with a proper sensitivity error correction.

The following conclusions can be obtained from the test of the SMA-2/EMA instrument:

(1). The frequency response behavior of the SMA-2/EMA can be viewed as a band-pass filter. It will filter out ground motion with frequency contents below 0.5 Hz and above 23 Hz. Therefore, instrument correction will be very important for near-field earthquake accelerograms because much of the near-field earthquake ground motion contains a significant amount of low frequency energy with frequencies below 0.5 Hz. The large amplitude low frequency content in the near-field ground motion could be very destructive to the long-period structures.

(2). The test results of the frequency response of the SMA-2/EMA show good agreement with the theoretical formulation of its transfer function, which means that the modeling of the EMA dynamic system is very close to reality.

(3). The noise test shows that for a near-field ground motion like the Lucerne Valley record from the Landers earthquake, the signal-to-noise ratio is large enough to distinguish the signal from the noise. Hence, the high frequency errors will not have an important affect on the signal. In other words, high frequency filtering can be neglected in processing near-field earthquake records. While the correction of the low frequency error, which is the cause of the large baseline shift, is very important. This correction will be discussed in detail in Chapter 5.

(4). Neglecting the sensitivity error will be acceptable in the data processing procedure if the instrument is calibrated regularly. The error caused by sensitivity deviation can be normally controlled under 5%.

(5). The tilt test results for the SSA-1 show that the FBA performs with good linearity. It can be used as a standard measurement of the shake table when performing the dynamic test on other instruments.

90°			−90°		
Grav(g)	% 2.5v(L)	% 2.5v(T)	Grav(g)	% 2.5v(L)	% 2.5v(T)
0.00	0.0034	-0.0048	-0.00	0.0034	-0.0048
0.05	0.0278	0.0190	-0.05	-0.0209	-0.0288
0.10	0.0541	0.0414	-0.10	-0.0458	-0.0541
0.15	0.0791	0.0688	-0.15	-0.0708	-0.0781
0.20	0.1040	0.0932	-0.20	-0.0957	-0.1035
0.25	0.1289	0.1186	-0.25	-0.1206	-0.1284
0.30	0.1452	0.1430	-0.30	-0.1455	-0.1538
0.35	0.1787	0.1684	-0.35	-0.1704	-0.1777
0.40	0.2036	0.1923	-0.40	-0.1948	-0.2026
0.45	0.2275	0.2172	-0.45	-0.2192	-0.2266
0.50	0.2534	0.2421	-0.50	-0.2441	-0.2514
0.55	0.2788	0.2670	-0.55	-0.2695	-0.2768
0.60	0.3032	0.2919	-0.60	-0.2929	-0.3007
0.65	0.3286	0.3168	-0.65	-0.3183	-0.3261
0.70	0.3540	0.3413	-0.70	-0.3437	-0.3510
0.75	0.3789	0.3662	-0.75	-0.3681	-0.3754
0.80	0.4042	0.3916	-0.80	-0.3930	-0.4008
0.85	0.4287	0.4165	-0.85	-0.4179	-0.4257
0.90	0.4541	0.4409	-0.90	-0.4433	-0.4506
0.95	0.4790	0.4663	-0.95	-0.4682	-0.4750
1.00	0.5039	0.4907	-1.00	-0.4931	-0.5000

Table 4.1 Tilt Test for Longitudinal and Transverse Transducers from −90° to 90°

Transdecer	a	b	$\epsilon_1(v/g)$	nominal	error
Longitudinal	0.0045	0.4980	1.246	1.25	0.4%
Transverse	-0.0048	0.4948	1.237	1.25	1.0%

Table 4.2 Sensitivities of the SSA-1/FBA for the Two Horizontal Transducers and Their Errors in Compared with the Nominal Values

Freg(hz)	Amp (Longitudinal)	Amp (Transverse)
0.1	0.6394	0.7049
0.2	0.8679	0.8608
0.3	0.9470	0.9303
0.4	0.9650	0.9534
0.5	0.9786	0.9607
0.8	0.9915	0.9911
1.0	1.0035	0.9927
2.0	1.0055	0.9975
5.0	1.0162	1.0094
10.0	1.0533	1.0389
15.0	1.0890	1.0609
20.0	1.0729	1.0469
23.0	1.0211	1.0046
25.0	0.9726	0.9602
30.0	0.8232	0.8361
35.0	0.6738	0.6984
40.0	0.5312	0.5546

Table 4.3 Average of Frequency Response of the Ten Test Samples

Transducer	f_n	ζ_n	CR_f	$a_0 = \frac{\alpha}{CR_i(2\pi)^2}$
Longitudinal	28.07	0.57	1.32	795
Transverse	29.35	0.58	1.46	857
Vertical	28.71	0.575	1.39	826

Table 4.4 Characteristic Parameters of the SMA-2/EMA Instrument

Transducer	$H(4)$	ϵ_1	ϵ_2	ϵ_a	ϵ_b	$\alpha_2 = \frac{\epsilon_a}{\epsilon_b}$
Longitudinal	1.0156	1.245	2.5288	2.495	2.555	0.9765
Transverse	1.0004	-	2.4910	2.466	2.416	1.0207
Vertical	1.008	-	2.5099	2.505	2.347	1.0673

Table 4.5 Sensitivities and its Error Correction Factors for the SSA-1 and SMA-2/EMA

	SMP-1 (Landers Earthquake)			*SMP*-1 (Test)		
Frequency	L	T	V	L	T	V
$v^{\circ} = 1000$ Hz	-0.004	-0.008	0.002	0.0002	0.0009	0.0005
$v^{-} = 500$ Hz	-2.520	-2.531	-2.552	-2.510	-2.512	-2.510
$v^{+} = 1500$ Hz	2.491	2.473	2.455	2.490	2.491	2.490
$\bar{v} = \frac{v^{+}-v^{-}}{2}$	2.5055	2.502	2.5035	2.500	2.5015	2.500

Table 4.6 Sensitivities for Longitudinal (L), Transverse (T) and Vertical (V) Components of the SMP-1 Playback Unit

Components	$\bar{v}_L$	$\bar{v}_T$	$\alpha_3 = \frac{\bar{v}_T}{\bar{v}_L}$
Longitudinal	2.5055	2.500	0.9978
Transverse	2.5025	2.5015	0.9998
Vertical	2.5035	2.500	0.9986

Table 4.7 Sensitivity Error Correction Factors for the SMP-1

Components	α_1	α_2	α_3	γ	error
Longitudinal	1.0030	0.9765	0.9978	0.9773	2.27%
Transverse	1.0030	1.0207	0.9998	1.0236	2.36%
Vertical	1.0030	1.0673	0.9986	1.069	6.9%

Table 4.8 Total Sensitivity Error Correction Factor γ for the Three Transducers of the SMA-2/EMA

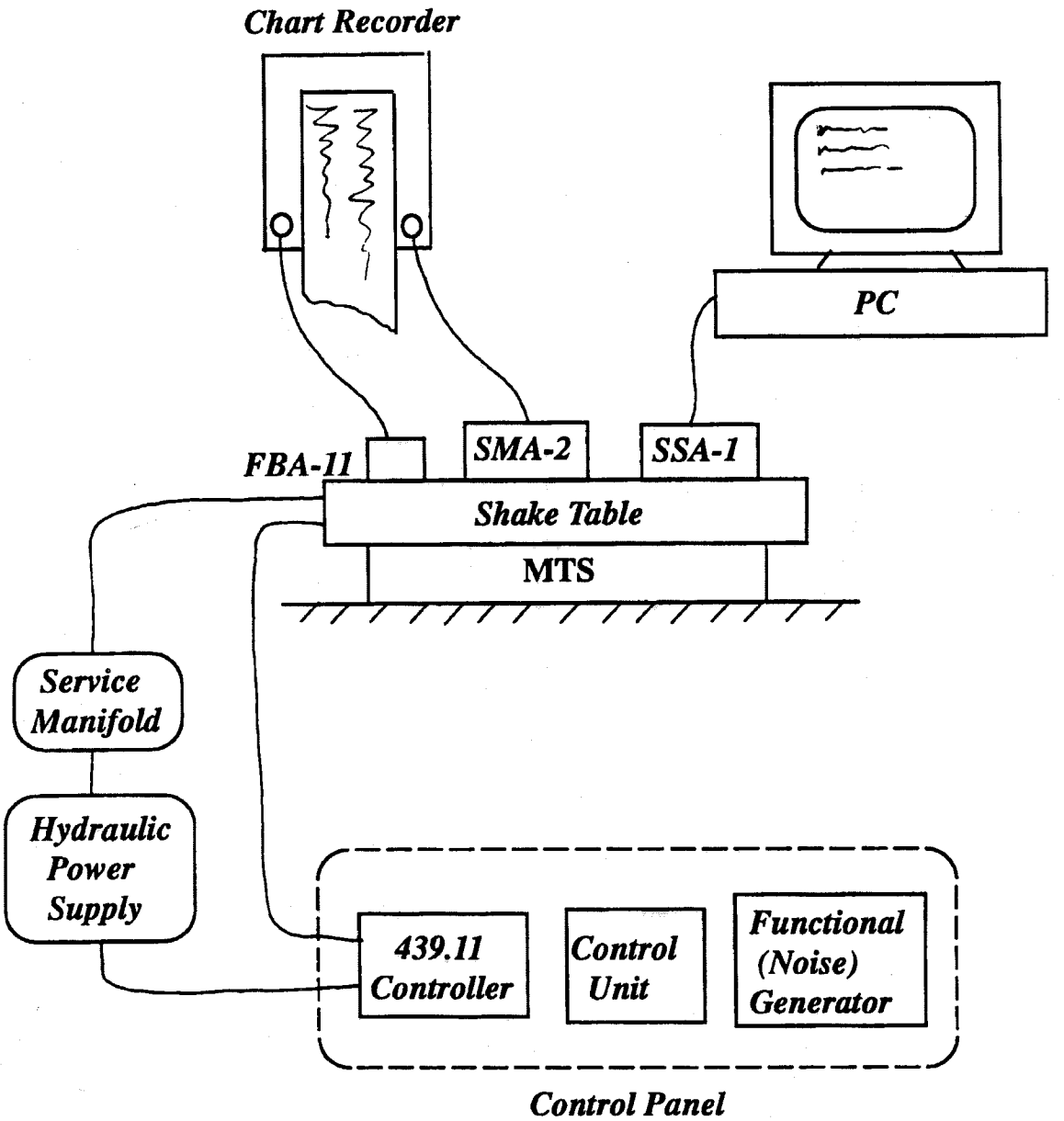

Figure 4.1 Instrument Setup.

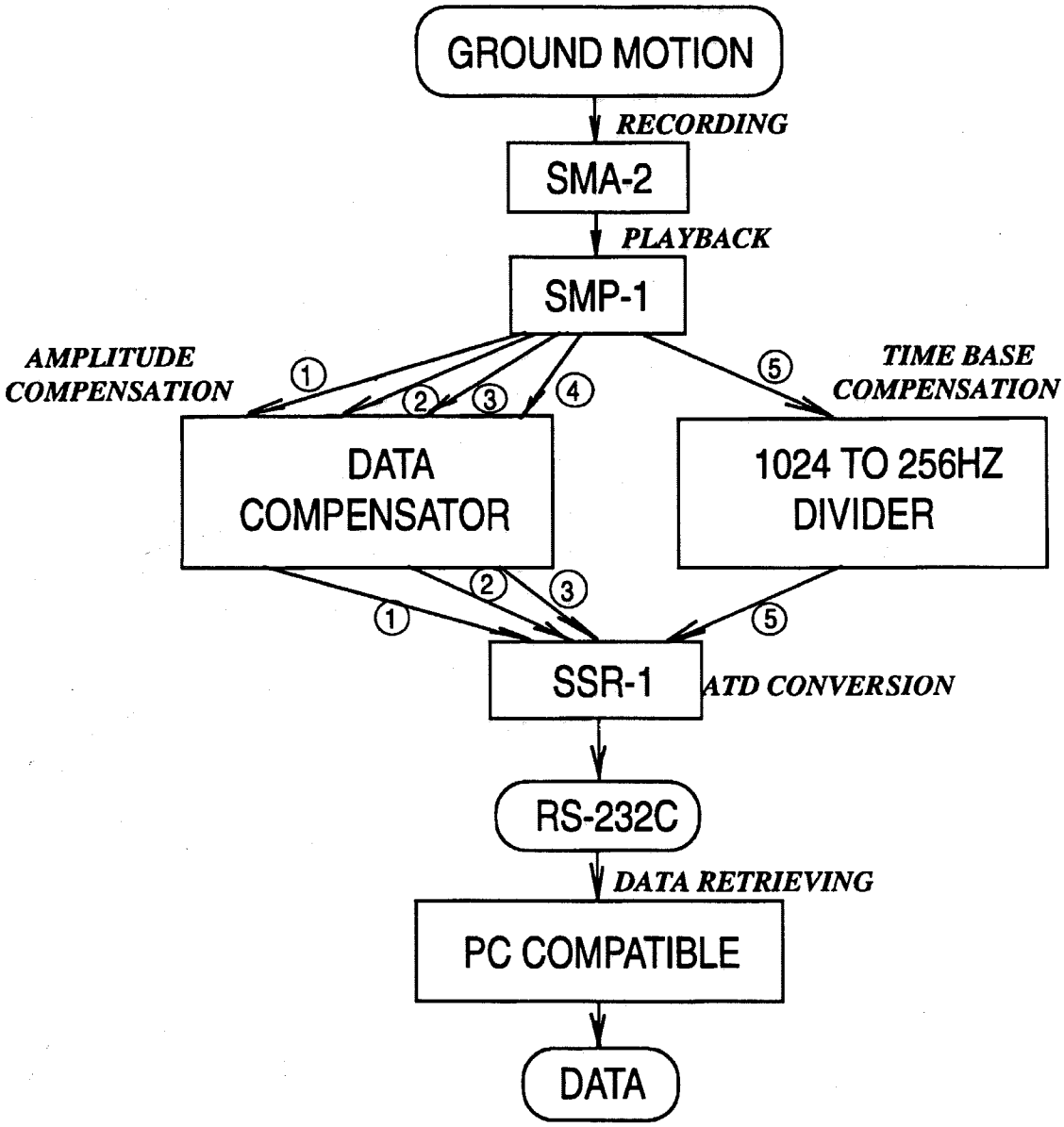

Figure 4.2 Global View of Earthquake Recording and Playback.

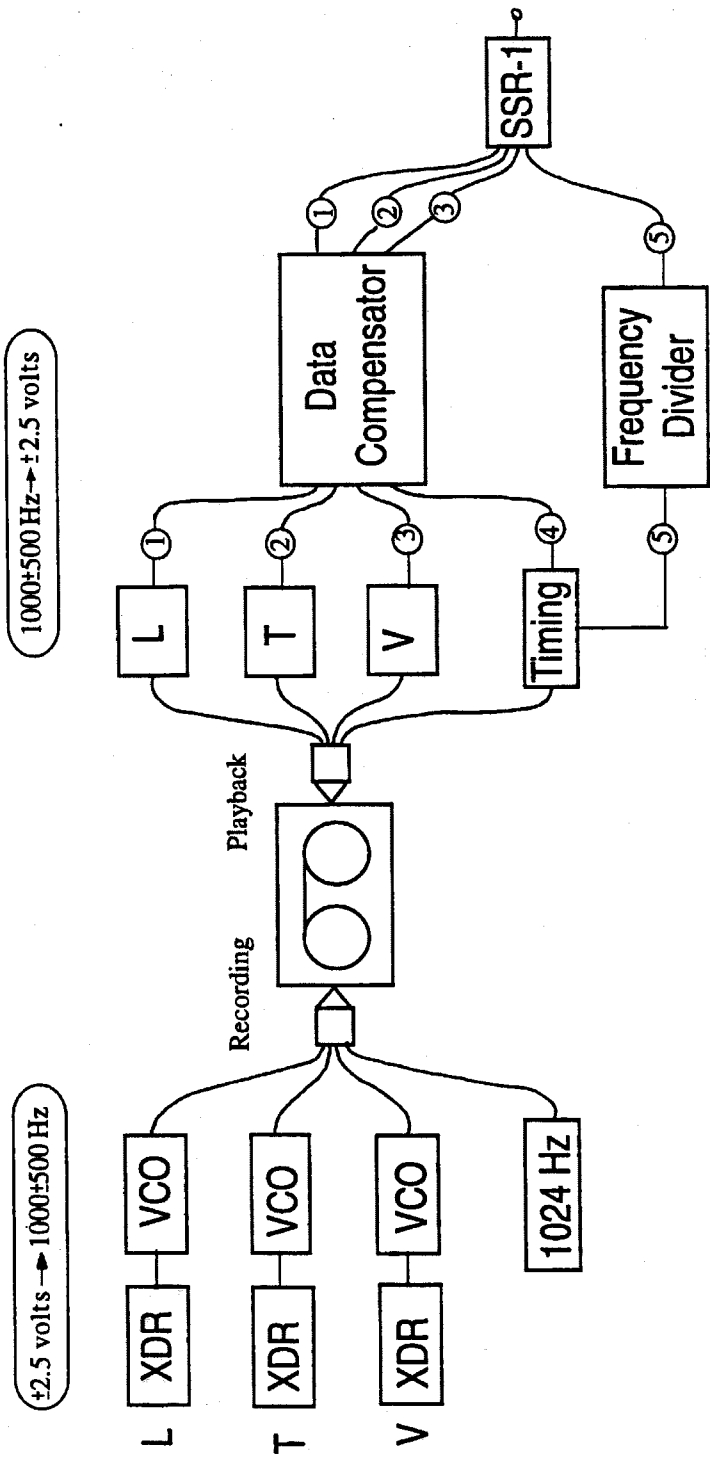

Figure 4.3 Details of Recording and Playback.

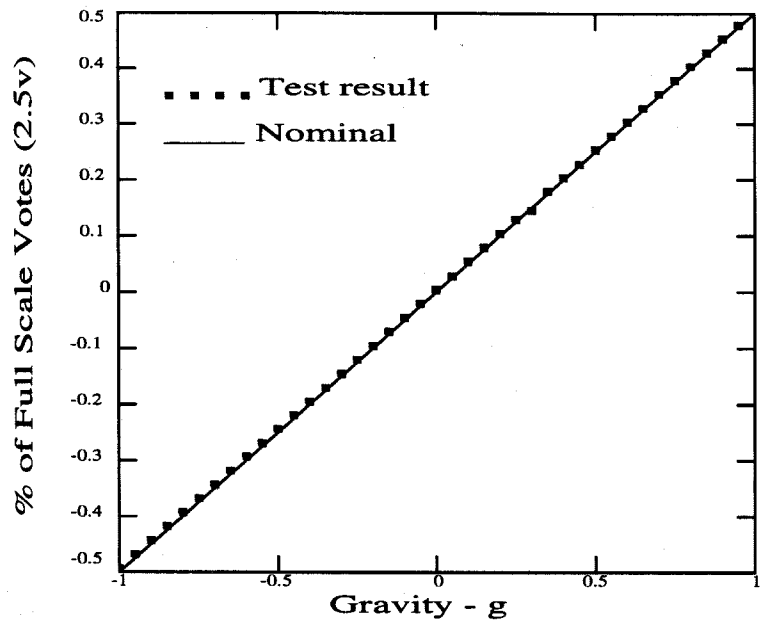

(a) Longitudinal

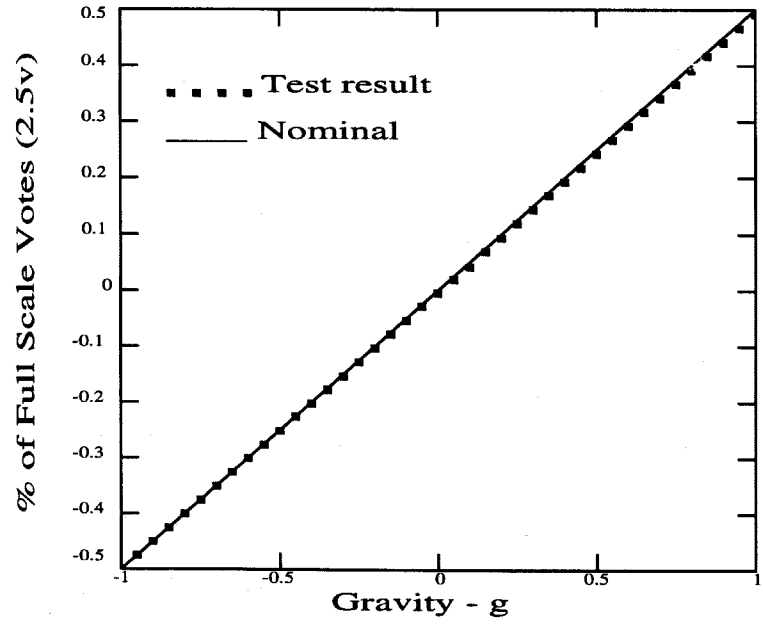

(b) Transverse

Figure 4.4 Tilt Test of the SSA-1 for Longitudinal and Transverse Components.

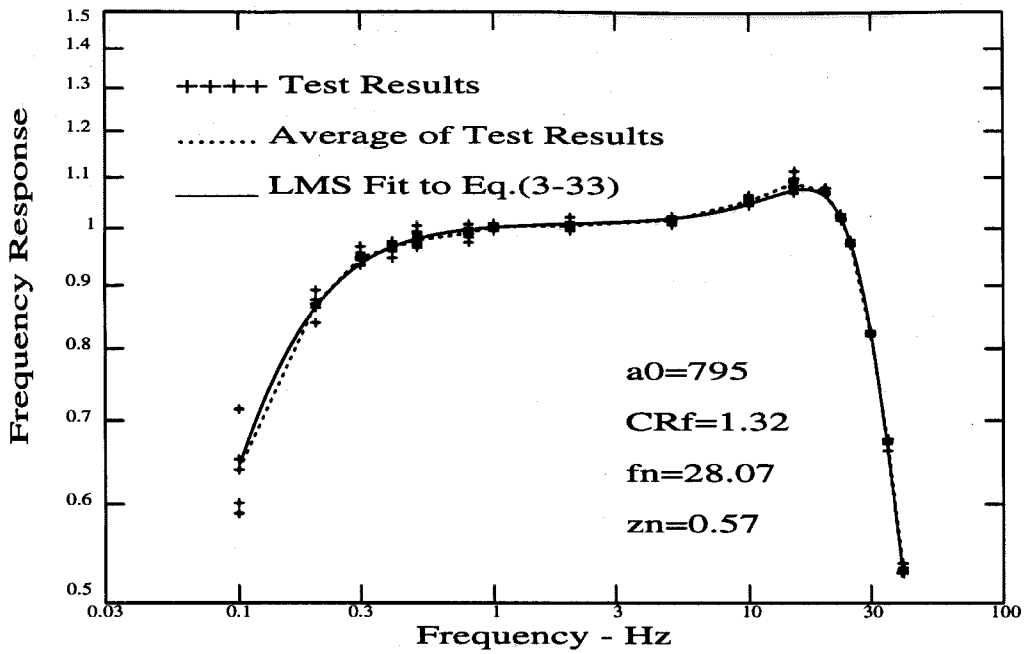

(a) Longitudinal

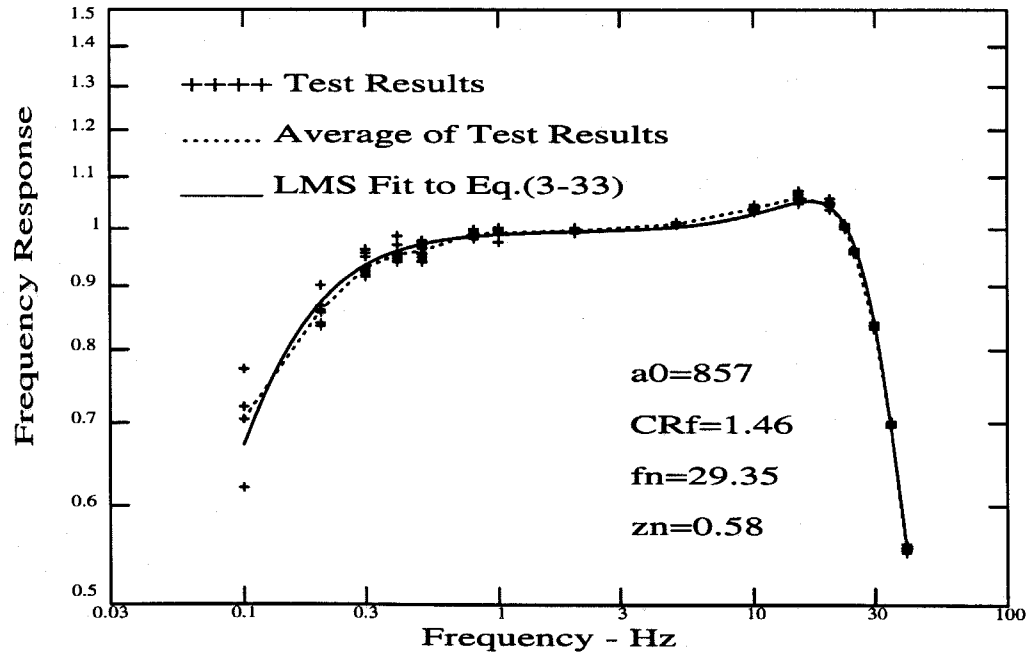

(b) Transverse

Figure 4.5 Test Results of Transfer Function for the EMA Transducers, (a) Longitudinal, (b) Transverse.

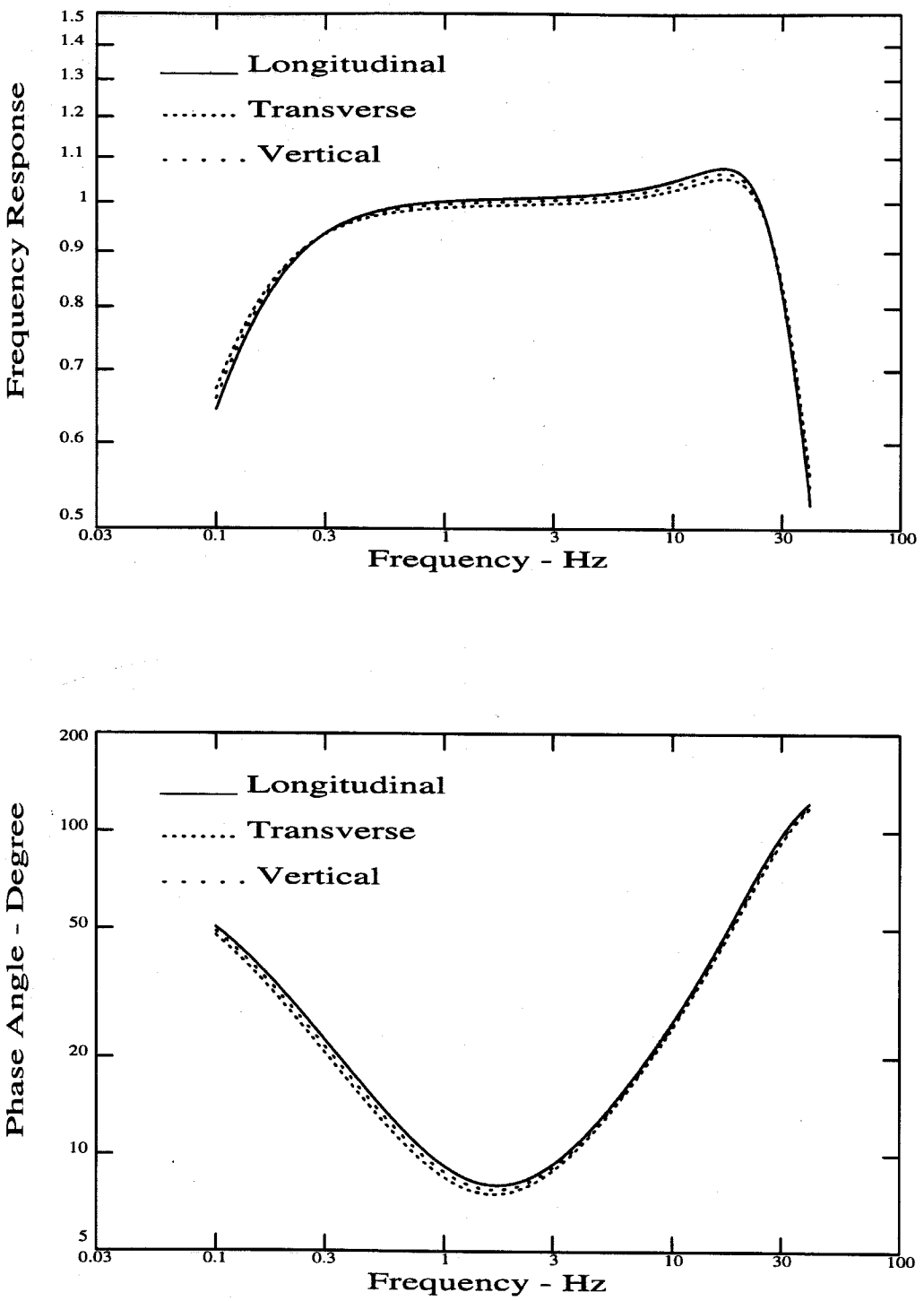

Figure 4.6(a) Transfer Function and Phase Angle Plots for Three Transducers (in Logarithmic Scale).

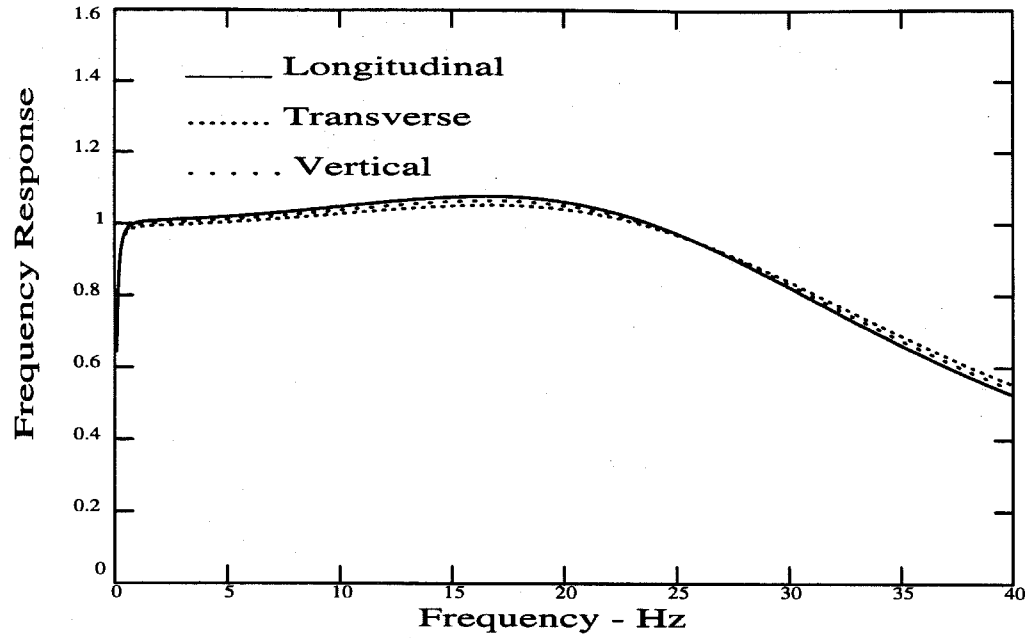

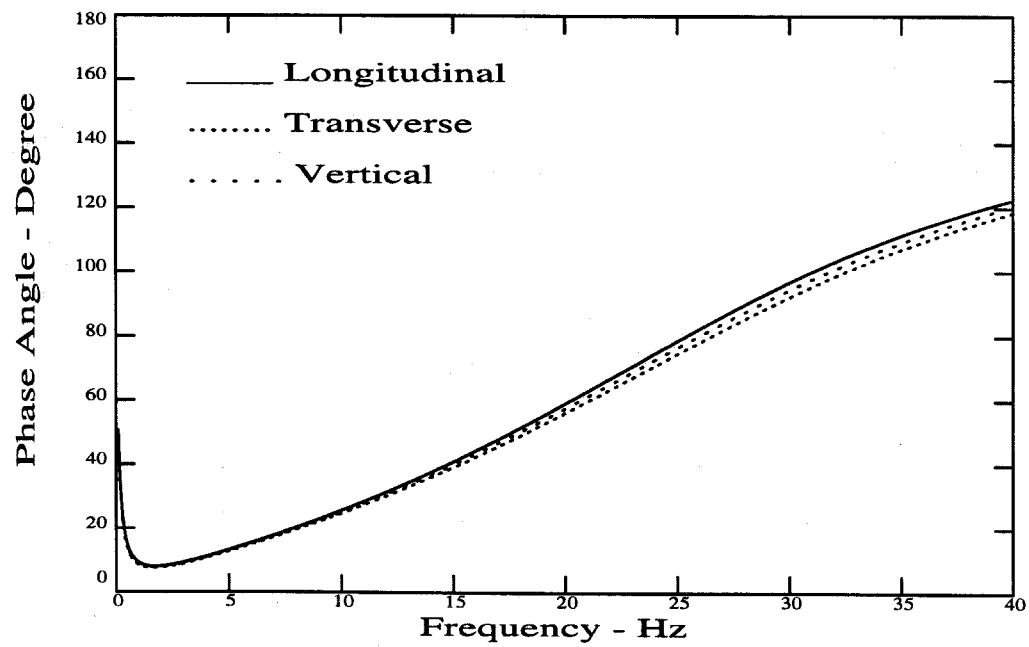

Figure 4.6(b) Transfer Function and Phase Angle Plots for Three Transducers (in Linear Scale).

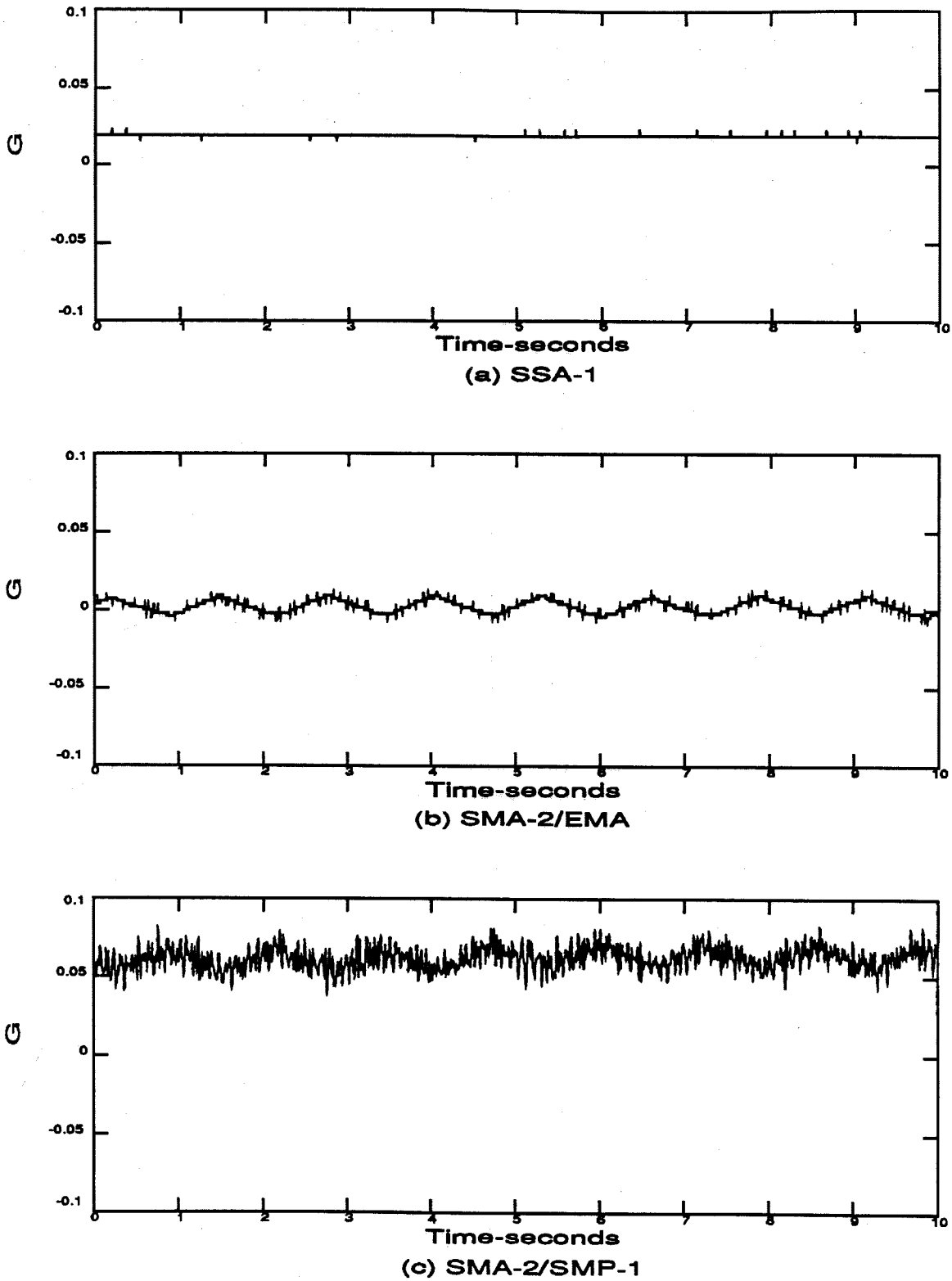

Figure 4.7 Noise Signals Recorded by the SSA-1, SMA-2/EMA and SMA-2/SMP-1.

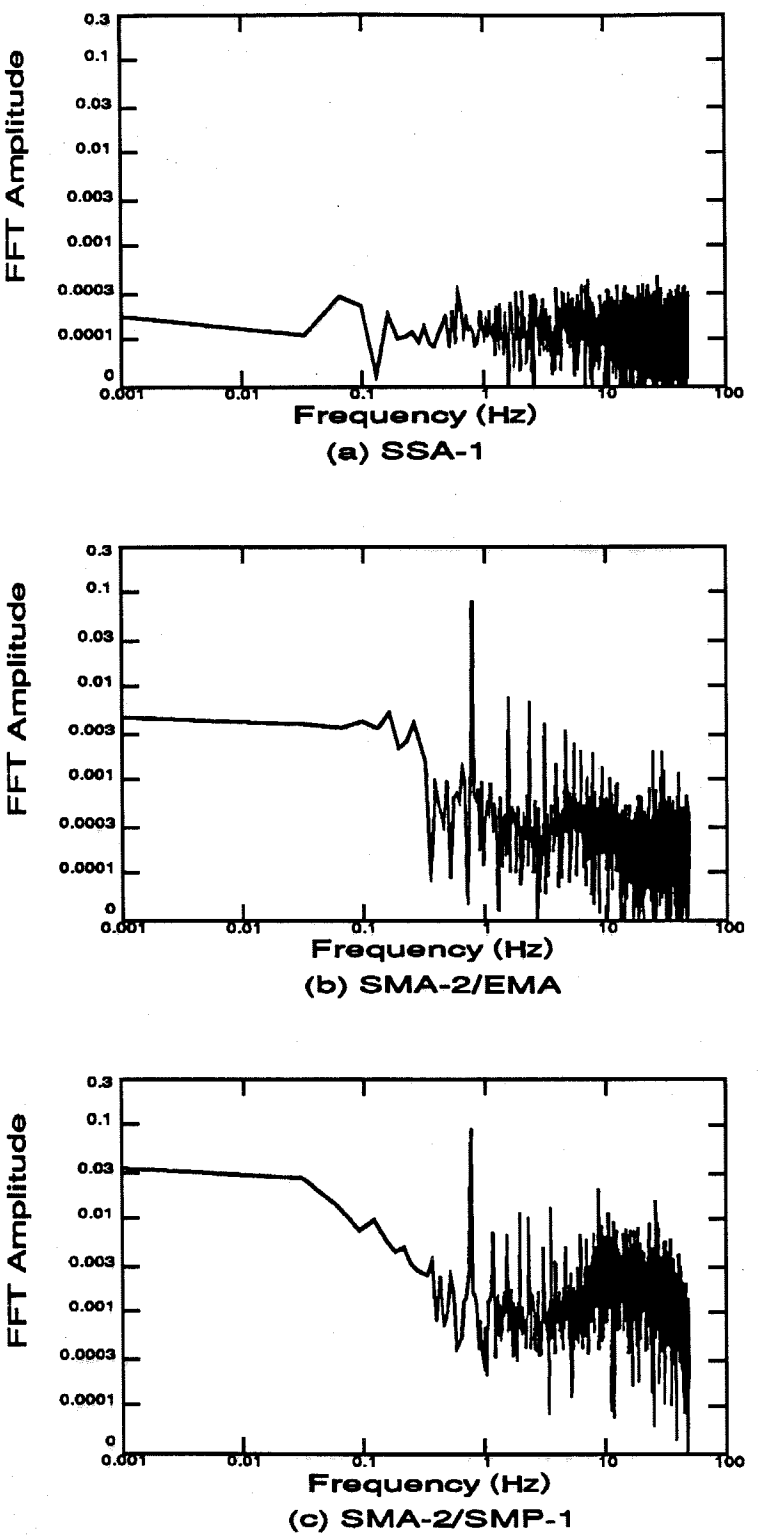

Figure 4.8 Fourier Spectra of the Noise Signals Recorded by the SSA-1, SMA-2/EMA and SMA-2/SMP-1.

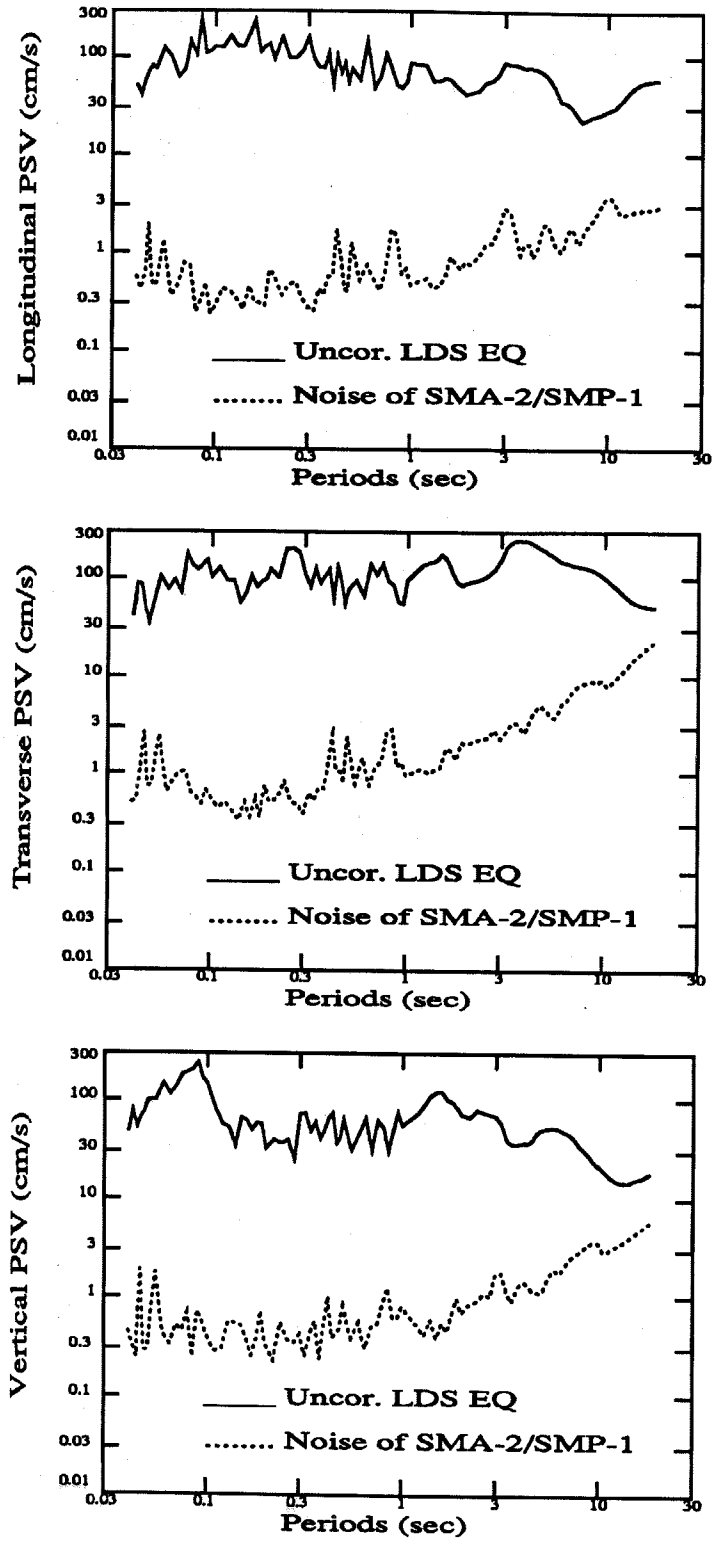

Figure 4.9 Pseudo-Velocity Spectra of the Uncorrected Landers Earthquake Data and the Instrument Noise.

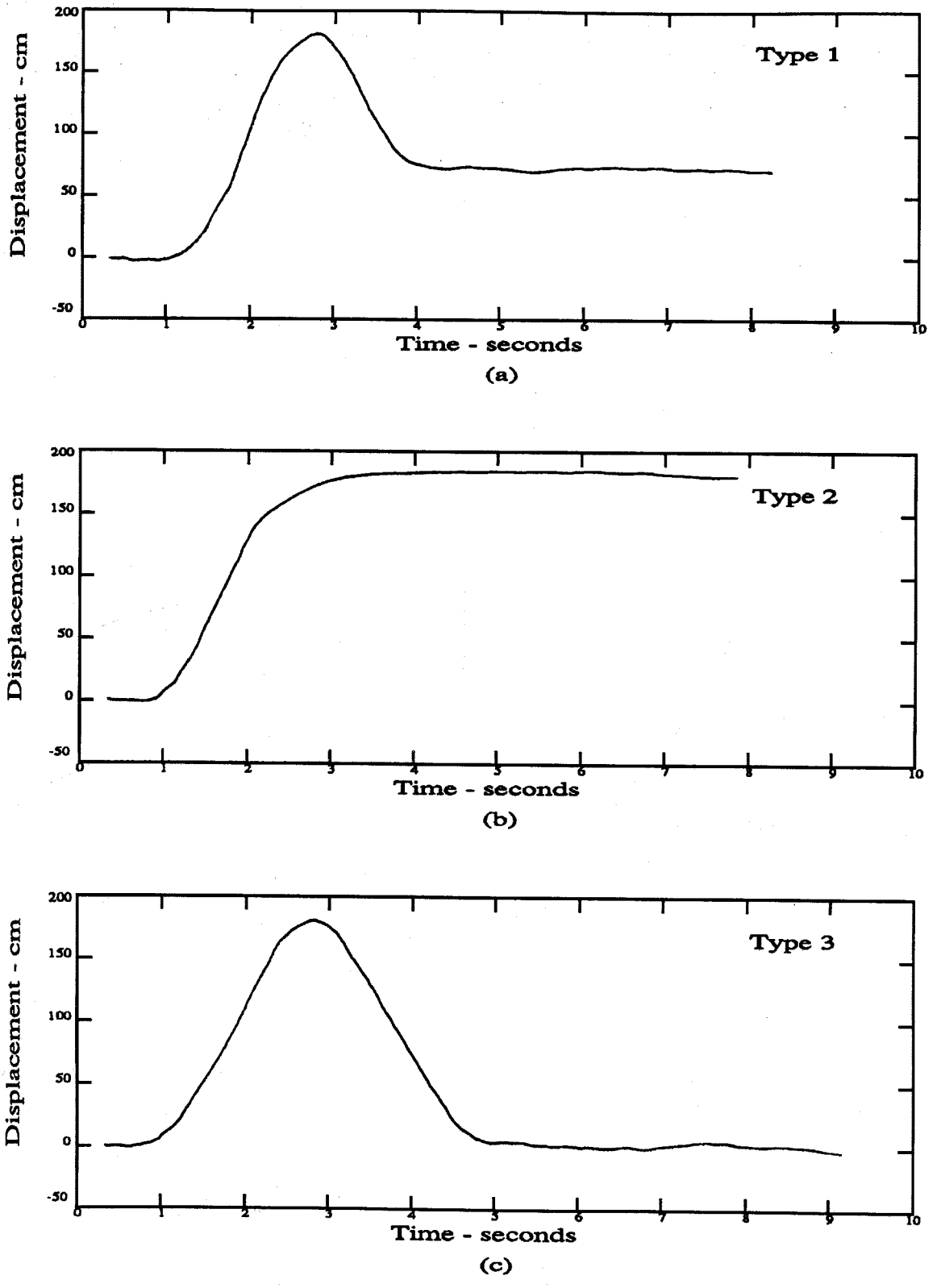

Figure 4.10 Three Types of Ground Motion for Simulated Long-Period Accelerograms.

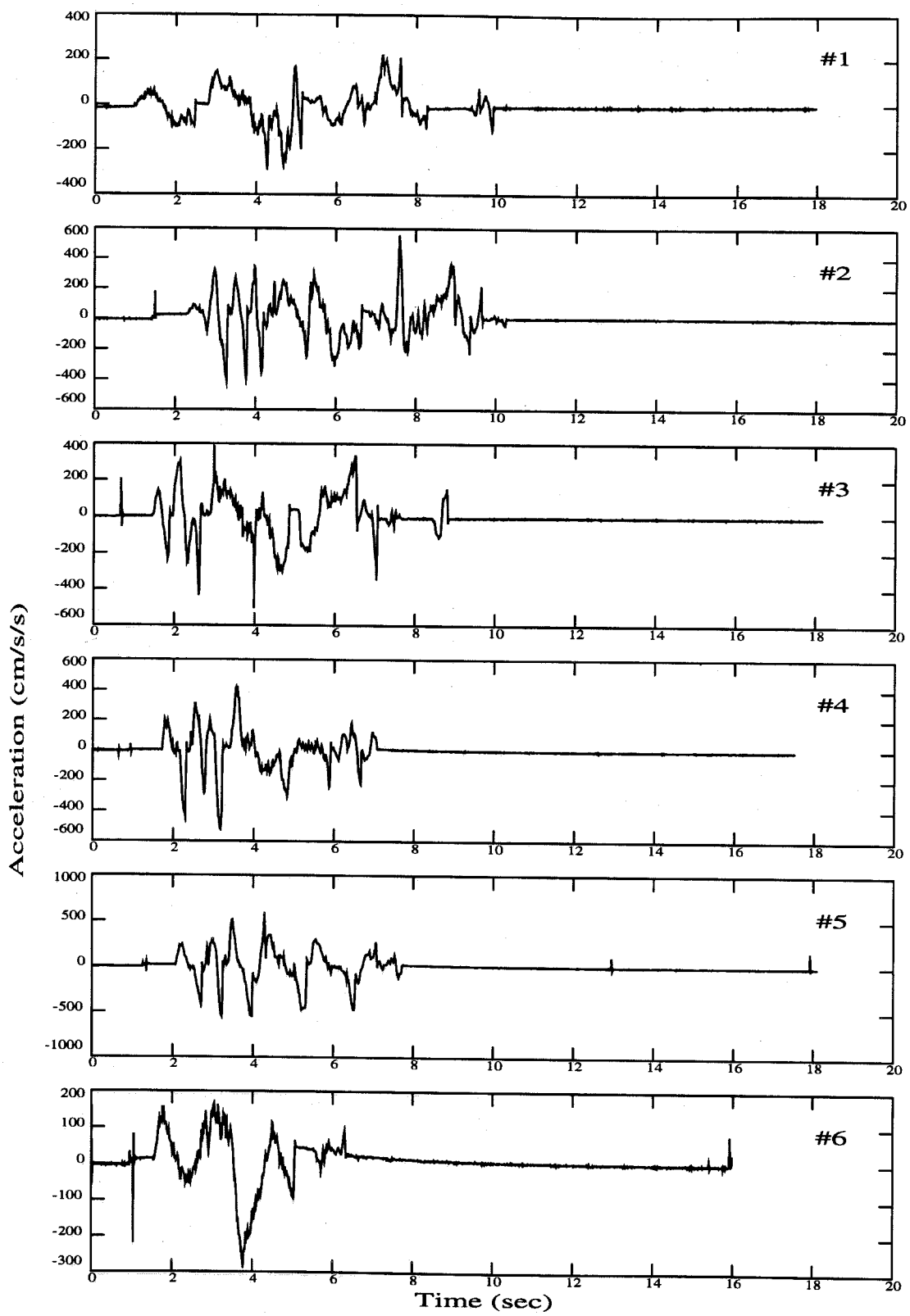

Figure 4.11(a) Twelve Different Simulated Long-Period Accelerograms (#1 to #6).

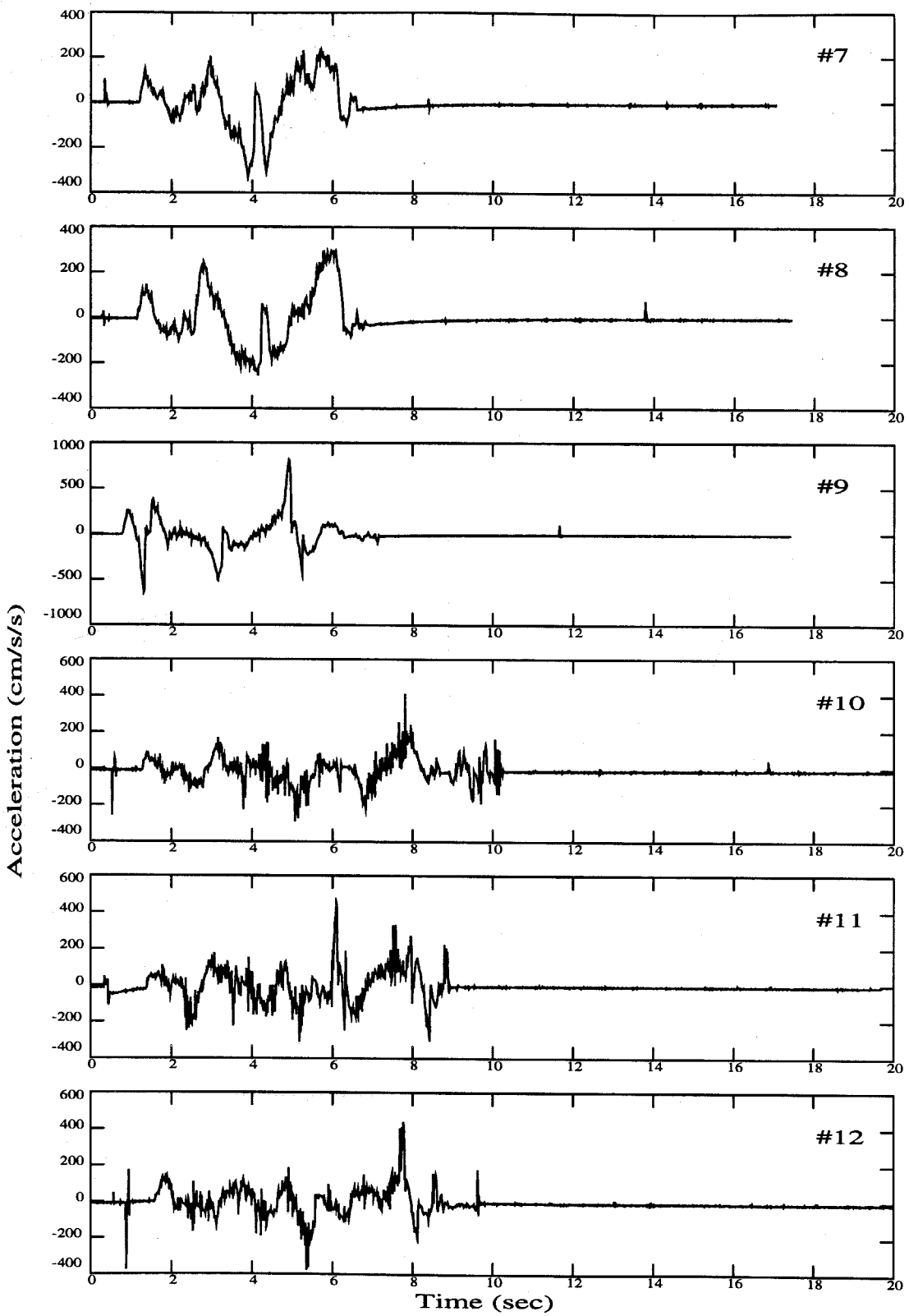

Figure 4.11(b) Twelve Different Simulated Long-Period Accelerograms (#7 to #12).

Chapter 5

A New Procedure for the Processing of Strong-Motion Data

5.1 Introduction

The strong motion data recorded on an accelerograph never exactly represent the real ground motion. Errors from the recording and retrieving system always exist in the earthquake records. The correction of these errors is very important because strong-motion accelerograms are frequently used in research studies as well as in engineering practice.

The errors involved in the recorded data can be roughly classified into two categories: system errors and noise errors. The main difference in the nature of these two types of errors is that one is generated by imperfections in the transducer and recorder system and can be determined, the other is random and cannot be determined.

Strong-motion accelerographs are mainly constructed out of mechanical and electronic components. Hence, system errors include mechanical system errors and electronic system errors. These errors can be identified by careful studies of the characteristics of the instrument structure. The instrument consists of three tri-axial transducers and a recording device. Each transducer is a single-degree-of-freedom oscillator. The relative displacement of the transducer mass in the SDOF system is designed to be proportional to the ground acceleration in the frequency range of interest. In practice, the frequency response or transfer function of the system is not exactly "flat" in any frequency range. For the SMA-2/EMA instrument, the electronic integrator of the EMA transducer acts like a high-pass filter for the relative displacement input signal due to leakage of the capacitor (see Chapter 3 for details).

Therefore, an instrument correction needs to be performed on the recorded earthquake data. The parameters used for the instrument correction are determined by the instrument calibration (Chapter 4). They are: the natural frequency, electronic damping, time constant of the integrator, and the sensitivity of each transducer.

System noise includes both instrument noise and background noise. These noises are introduced by random error sources during the recording and retrieving procedures. These kinds of errors are not easy to determine because of their random nature. Many efforts have been made to correct these noise errors. The existing standard method uses a high-pass filter and a low-pass filter to reduce the low frequency and high frequency noises. This procedure takes the risk of filtering out the real information from earthquake records, especially for near-field earthquake records. The standard data processing results of the Lucerne Valley record from the Landers earthquake is a good example of the effect of a filter on long-period information. Therefore, an improved error correction procedure needs to be found.

The main contribution of this work is the development of a new data processing scheme which can better recover long-period information from near-field earthquake records. The proposed new method is verified by processing of simulated near-field ground motion on the Lucerne Valley SMA-2/EMA instrument. Then, the new method is applied to the actual Lucerne Valley record of the Landers earthquake in Chapter 6.

5.2 Data Processing Procedure for Strong-Motion Accelerograms

Data processing of strong-motion accelerograms mainly includes three elements: (1) digitization, (2) baseline correction and instrument correction, and (3) calculation of the response spectrum and Fourier spectrum.

Digitization has been accomplished through a variety of means varying from hand digitization to automatic digitization. Hand digitization is a manual process and consumes tremendous time. Hand-digitized data are not only poor in accuracy but also of low resolution. Automatic digitization was developed using an image processing technique. It greatly speeds up the digitization process and reduces the noise by almost 2 to 3 times compared to the hand digitization [32]. With the development of digital instruments, it has become possible to record the ground

acceleration in a digital format. The sample rate of the digital instrument is as high as 1024 Hz. Study has shown [33] that the digital instrument reduces the noise by 1 order of magnitude in retrieving short-period information and reduces the noise by 2 orders of magnitude in retrieving long-period information compared to automatic digitization of analog instrument records. At present, most of the instruments in the field are still analog instruments because of their low cost. Normally a sample rate of 200 per second or 256 per second is selected to digitize analog records. The selected sample rates provide a Nyquist frequency of at least 100 Hz. With this sample rate, high frequency information is seldom lost.

The second step of the data processing procedure, baseline correction and instrument correction, is an important part of the data processing procedure. Instrument correction is mainly the correction of system errors, while baseline correction is essentially the correction of noise errors. How to correct the errors in the recorded data by data processing techniques has been an interesting topic for the past three decades. Various methods have been established to improve the baseline correction process. The most popular method is the CIT Vol. II standard data processing procedure, or variations of this approach. Since the resulting velocity and the displacement from these methods cannot represent the ground motion correctly in a physical sense, a new baseline correction scheme is studied here to give a more accurate version of the processed data.

Calculations of the response spectra and Fourier spectra are not discussed in detail here since existing methods at this step are well established and widely accepted in engineering practice.

5.3 Existing Data Processing Schemes

The attempt to correct earthquake data began in the 1960's. Berg and Housner [34] first applied a cubic-curve baseline correction to the velocity which is directly integrated from the acceleration. Brady [35] applied a parabolic baseline correction to the acceleration with minimization of the mean square value of the resulting velocity. In the 1970's, Trifunac *et al.* [36,37] applied low- and high-pass filters to strong-motion records to remove the low and high frequency errors in strong-motion accelerograms. In 1973, with the effort of Trifunac and Lee [11,37], the Caltech Vol. II

correction scheme was developed and the routine computer program for processing of strong motion accelerograms was established. A variation of the method called the Phase II method, was later developed by other organizations such as the California Division of Mines and Geology. The Vol. II correction method and its variations have been used as a standard data processing scheme for more than 20 years. Since the application of the filters in the standard data processing method introduces errors in the corrected data, different approaches and new filters were developed to reduce the errors in the corrections. The basics of the CIT Vol. II method and other methods are described briefly in the following sections.

5.3.1 CIT Vol. II Data Processing Scheme

By the 1970's, most of the accelerograms were recorded on photographic paper, or on 70 mm and 35 mm film. A digitization procedure was needed to obtain the earthquake acceleration data. Both high and low frequency errors were believed to be unavoidably introduced by the mechanical and manual processes. So, a data processing procedure was considered necessary to be performed on the strong-motion accelerograms. The first version of the data processing procedures are Caltech Vol. I, Vol. II, Vol. III and Vol. IV data processing procedures.

The Vol. II data were corrected based on the data processing of the Vol. I "uncorrected" accelerograms. The Vol. I data are generated by digitization of earthquake records to equally spaced 50 samples per second and smoothed with a $\frac{1}{4}$, $\frac{1}{2}$, $\frac{1}{4}$ running filter, having the zero axis translated to make the integral of the digitized acceleration zero. This is physically equivalent to making the velocity time history begin with zero and end with zero. In the strict sense, the Vol. I data are not uncorrected data.

The Vol. II data processing procedure includes instrument correction, baseline correction and double integration. This procedure can be briefly described by the following steps: 1) apply a low-pass Ormsby filter on the uncorrected data with a cut-off frequency f_c and a roll-off frequency f_t, 2) perform an instrument correction with the characteristic constants of the instrument, ω_n and ζ_n, which represent the natural frequency and critical damping fraction of the transducer, 3) apply a high-pass filter to the data with cut-off and roll-off frequencies which are determined by the signal-to-noise ratio of the each component, 4) perform an integration to obtain the velocity and displacement (in this step, a trapezoidal rule integration scheme is

used to carry through the double integration, and low-pass Omsby filter is used in obtaining the velocity and displacement), 5) apply a high-pass filter on the integrated velocity and displacement to avoid long-period errors in the record, and 6) remove the baseline shift to obtain the corrected acceleration.

In the Vol. II data processing procedure, the high-pass and low-pass filters were performed several times. Band-pass frequency limits of 0.05-0.07 to 25-27 Hz are typically assumed. The same band-pass limit is performed on the data each time. In the mean time, a least-mean-square fit to a straight line is also applied several times and decimation and interpolation was employed in the correction procedure to reduce the computational effort. Unfortunately, those numerical calculations introduce errors in the data processing at the same time that they attempt to reduce errors. The application of the filters may also remove useful information in the earthquake data. The detailed Vol. II data processing procedure can be found in Reference [27].

5.3.2 Other Development in Data Processing

Since errors and various problems still exist in the Caltech routine computer processing procedure, much effort has been made to improve the data processing technique [38,39,25,40,41,42,43]. In 1979, an automatic routine digitization system (ARDS) was developed at USC [32] to reduce the digitization error and save human time in digitization. In this system, the digitization of the records was completed with a resolution of more than 200 samples per second with the help of a modern computer system and a laser scanner device. This effectively extended the usable frequency range of the earthquake data.

Beginning in the 1980's, Sunder [38,39] introduced an infinite impulse response (IIR) nonlinear phase elliptic filter in the data processing scheme. In this improved data processing scheme, an IIR elliptic filter was used as a band-pass filter instead of the original low- and high-pass filters. Lee [25] then made several refinements in the routine data processing of strong-motion accelerograms following the development of the automatic routine digitization system, including a new differentiation filter in the instrument correction and an IIR filter in the double integration. The frequency limits for the band-pass filtering were also designed to be chosen automatically case-by-case.

Another branch of the development of routine processing of accelerograms based on early 1970's Caltech routines was undertaken in USGS. Converse, Brady and Joyner [41] at USGS developed the AGRAM computer program for processing digitized strong motion accelerograms with a new technique of filters to improve the data processing scheme. The program was designed to give better accuracy, versatility, speed and transportability based on the original CIT Vol. II processing program.

Although much effort has been made to develop data processing schemes, the resulting methods at some stage are still in question. For instance, the routine data processing procedures do not generally give the correct velocity and displacement time history compared to what is observed from field investigations. This is because the filtering procedures filter out the long-period information in the strong-motion accelerogram. The discrepancies may not appear significant when using the existing data processing scheme to process far-field strong-motion accelerograms, but they are significant in processing near-field accelerograms. The original data processing procedure cannot provide a static offset, and sometimes distort the large pulse-like signals observed in near-field accelerograms.

Iwan *et al.* [33,43] first developed a correction algorithm which can provide the permanent displacement according to the characteristics of a typical strong-motion recorder/transducer instrument, the Kinemetrics PDR-1/FBA-13. The algorithm was designed for correcting a digital instrument record which has pre-event memory. The acceleration data was first corrected for the DC offset observed in pre-event data and then the final offset of the acceleration. This was accomplished by removing the baseline shifts using segmented constant offsets in the acceleration time history. The value of the intermediate acceleration correction was selected so as to make the velocity correction continuous over the entire record. The final offset was determined by a least-squares fit to the final portion of the velocity data.

5.4 Proposed Data Processing Scheme

The study here is focused on providing a better method of baseline correction and instrument correction. Since the research is motivated by the correction of the Lucerne Valley record from the Landers earthquake, the instrument correction here is based on the SMA-2/EMA instrument. The test of the SMA-2/EMA instrument

as discussed in Chapter 4 provides the calibration data for the instrument correction. The instrument correction for the SMA-2/EMA should follow the formulation derived in Section 3.3.2. The corrections for other instruments with force-balance type of transducers should use the formulation presented in Section 3.3.1. In this chapter, the baseline corrections of a strong-motion accelerogram are discussed in detail.

5.4.1 Error Sources of the Earthquake Data

Since errors are inevitably introduced into earthquake records from various sources, baseline correction or noise reduction needs to be performed on these records. To perform the correction, one should be aware of where the errors come from.

To identify the error sources, the data recording and playback procedures should be investigated. The equipment or devices associated with the recording and playback are the most likely sources of errors. To classify the errors from different sources, a flow chart of the recording and playback procedure for the SMA-2/EMA instrument is given in Figure 5.1. The first oval in flow chart represents the real ground motion or earthquake accelerogram, box 1 represents the SDOF transducer, box 2 represents the integration amplifier, box 3 represents the recording device in the SMA-2/EMA instrument, box 4 represents the playback device such as the SMP-1, box 5 represents the SSR-1 digital instrument, box 6 represents a Personal Computer, and the last oval represents the recorded earthquake accelerogram.

The flow chart shows that the input ground motion is transformed into an electronic signal through a transducer and then recorded on a magnetic tape. The signal is then played back by the SMP-1 instrument. After playback, the analog electronic signal is digitized by an SSR-1 Solid State Recorder and is finally retrieved by a PC computer. The possible error sources from this procedure are 1) the transducer system, 2) the integration amplifier, 3) the recording deck, and 4) the playback device. The total errors from each of these error sources are denoted as E_1, E_2, E_3 and E_4 respectively. As mentioned, the errors include both system errors and noise errors. System errors arise from both the mechanical system and the electronic system. They are denoted by $\bar{E}$ and $\tilde{E}$ respectively. Noise error is denoted as N. Error sources 1), 3) and 4) will introduce mechanical system errors $\bar{E}_1$, $\bar{E}_3$, $\bar{E}_4$ and the error sources 2), 3) and 4) will introduce electronic system errors $\tilde{E}_2$, $\tilde{E}_3$ and $\tilde{E}_4$. Noise errors are most likely introduced by error sources 1), 3) and 4) and then are denoted as N_1, N_3

and N_4. The sensitivity errors from the recording system and playback system are denoted as S_1 and S_2.

Error $\bar{E}_1$ arises from the fact that the transfer function of the transducer is not flat over the entire frequency range. Error $\tilde{E}_2$ arises from the fact that the amplifier is not an ideal integrator. The amplifier high passes the recorded signal and therefore the low frequency information is lost. Error $\tilde{E}_3$ is due to the shift of the central frequency of VCOs in the recording system. Error $\tilde{E}_4$ arises from the shift of the central frequency of the demodulator in the playback device. Errors $\bar{E}_3$ and $\bar{E}_4$ are tape speed errors from both the recording and playback systems. They result from the fluctuations of the signal amplitudes and changes of the time duration in the recorded data. Sensitivity errors S_1, S_2 are the deviations of the gains of the SMA-2 and SMP-1 devices from their nominal values. Errors N_1, N_3 and N_4 are the noises generated by the various uncertainties.

In summary, the errors from the four error sources can be represented by the following relationships

$$E_1 = \bar{E}_1 + N_1 \tag{5.1}$$

$$E_2 = \tilde{E}_2 \tag{5.2}$$

$$E_3 = \bar{E}_3 + \tilde{E}_3 + N_3 \tag{5.3}$$

$$E_4 = \bar{E}_4 + \tilde{E}_4 + N_4 \tag{5.4}$$

Where

$\bar{E}_1$ – Error caused by the transducer response.

$\tilde{E}_2$ – Error from the integrator.

$\tilde{E}_3$ – Error resulting from the shift of the central frequency of the VCOs.

$\tilde{E}_4$ – Error resulting from the shift of the central frequency of the demodulators.

$\bar{E}_3$ – Tape speed error from the recording system.

$\bar{E}_4$ – Tape speed error from the playback system.

S_1 – Sensitivity error from the SMA-2/EMA.

S_1 – Sensitivity error from the SMP-1 Playback machine.

N_1, N_3, N_4 – Noise errors from the recording and playback procedures.

The purpose of the error analysis is to find appropriate means to correct the errors. The correction of these errors is the main function of baseline correction.

5.4.2 Correction of the Errors

The correction of the data should be performed in the inverse procedure of the recording and playback as shown in Figure 5.1. Errors represented by Equation (5.1) to (5.4) can be corrected by both instrument correction and baseline correction. Errors $\bar{E}_1$ and $\tilde{E}_2$ can be corrected by instrument correction through the use of a filter which consists of a SDOF oscillator and an integrator. The calculation can be done by employing Equation (3.33). Errors $\bar{E}_3$ and $\bar{E}_4$ are corrected by the Data Compensator and the Frequency Divider [22] which are part of the accessories of the playback system (refer to Chapter 4). The sensitivity errors S_1 and S_2 are corrected by the instrument calibration. The rest of the errors $\tilde{E}_3$, $\tilde{E}_4$, N_1, N_3 and N_4 are corrected by the baseline correction. Errors $\tilde{E}_3$ and $\tilde{E}_4$ result from the central frequency shifts. They can be simply removed by linear baseline correction. The noise errors are not easy to correct due to their nature of uncertainties. These noise errors should be carefully studied before being removed. Since low frequency noise causes the main distortion in the final displacement of the record, the correction should be focused on minimizing the low frequency noise.

Assume that the noise introduced by each source is a low-order polynomial function of time expressed by

$$N = a_0 + a_1\ t + a_2 t^2 + a_3 t^3 \tag{5.5}$$

The noise from step 1 in Figure 5.1 will pass through step 2, 3 and 4, the noise from step 3 will pass through step 4, and the noise from step 4 will be directly included in the retrieved data. The resulting noises from step 3 will still be a polynomial function since step 4 is a linear operator. The noise from step 1 will become a polynomial function plus an exponential function $e^{-\frac{1}{CR_f}t}$ after passing through step 2 which is an integration amplifier, and maintain the same characteristics after passing through step 4.

The exponential function results from solving Equation (3.19). Assume that the input noise is N_i and the output noise is N_o for the integrator, then the relationship between N_i and N_o is obtained from Equation (3.19) as

$$\dot{N}_o + \frac{1}{CR_f} N_o = -\frac{\alpha}{CR_i} \dot{N}_i \tag{5.6}$$

Solving this differential equation gives

$$N_o = -\frac{\alpha}{CR_i}\int_0^t \dot{N}_i e^{\frac{1}{CR_f}(\tau - t)} d\tau \tag{5.7}$$

When the noise from the transducer is a polynomial function

$$N_i = a_0 + a_1\ t + a_2\ t^2 + a_3\ t^3 + a_4\ t^4 \tag{5.8}$$

the solution of equation (5.7) will be

$$N_o = b_0\left(1 - e^{-\frac{1}{CR_f}t}\right) + b_1\ t + b_2\ t^2 + b_3\ t^3 \tag{5.9}$$

where

$$b_0 = -\tfrac{\alpha}{CR_i}\left(a_1 CR_f - 2a_2(CR_f)^2 + 6a_3(CR_f)^3 - 24a_4(CR_f)^4\right)$$
$$b_1 = -\tfrac{\alpha}{CR_i}\left(2a_2 CR_f - 6a_3(CR_f)^2 + 24a_4(CR_f)^3\right)$$
$$b_2 = -\tfrac{\alpha}{CR_i}\left(3a_3 CR_f - 12a_4(CR_f)^2\right)$$
$$b_3 = -\tfrac{\alpha}{CR_i}\left(4a_4 CR_f\right)$$

Equation (5.9) shows that the output of the integrator is a polynomial plus an exponential function. The output polynomial function is one order lower than the input polynomial function and the constant term is decayed by an exponential function of $1 - e^{-\frac{1}{CR_f}t}$.

The constant value of CR_f can be determined from the instrument calibration. The nominal CR_f value with the manufacturer-designed integrator corner frequency of 0.1 Hz can be calculated as

$$CR_f = \frac{10}{2\pi} = 1.57$$

The CR_f value of the integrator for the SMA-2/EMA in this test is based on the calibration results. After t_1 seconds, the constant term will be decayed by $1 - e^{-\frac{1}{CR_f}t_1}$. When $t_1 = 2$ seconds and $CR_f = 1.4$ seconds, the amount of decay will be

$$1 - e^{-\frac{2}{1.4}} = 1 - e^{-\frac{1}{0.7}} = 75\%$$

when $t_1 = 3$ seconds and $CR_f = 1.4$ seconds, the amount of decay becomes

$$1 - e^{-\frac{3}{1.4}} = 88\%$$

Since the exponential part of the noise error is generated by the transducer and an amplifier, it is corrected by the instrument correction. After instrument correction, the long-period noise errors, which have been assumed to be a low-order polynomial function, still exist in the record.

The long-period noise errors are associated with a non-physical trend of the record since the actual baseline should be aligned to zero. To better observe the long-period errors, an integration is performed on the instrument-corrected acceleration time history to obtain a velocity time history. The non-physical trend in the velocity time history is identified by applying a least-mean-square fit to a segmented polynomial function. As the polynomial baseline is found, it is subtracted from the velocity time history. The remaining part of the velocity time history represents the actual ground velocity.

The baseline could be a continuous or segmented polynomial function. In the case of three segments, the first and third segments are adjusted forcing the velocity time history to zero since the ground motion must start and end at zero. The second segment is then smoothly connected the first and third segments. The integral of the velocity time history represents the final displacement offset, which may be zero or some finite value.

The length of the segment is determined by careful examination of the earthquake record. Since P-wave travels faster than S-wave, the vertical transducer of the instrument first starts to record significant ground motion. The two horizontal transducers are generally actuated at the same time as the vertical transducer. After a short period of time, which is proportional to the fault-to-station distance, the horizontal transducers begin to record the strong ground motion. Hence, the horizontal recording before the arrival of the S-wave gives an estimate of the zero ground motion state. This is especially true if the instrument has a pre-event memory. The baseline correction should, on average, correct this part of record to zero.

When the ground motion ceases, the instrument continues to run for a certain amount of time before stopping. This part of the recording also represent a zero ground velocity state. The baseline correction should correct this part of the average velocity to zero. Figure 5.2 is a schematic diagram to show a segmented polynomial

baseline correction, where t_1 roughly represents the S-wave arrival time and t_2 represents the approximate time at the end of the strong motion phase of the record. The time t_1 and t_2 are determined by a visual examination of the record. Though the selection of t_1 and t_2 is not exact, the whole baseline procedure results in a physically correct picture close to the actual ground motion.

In summary, the baseline corrections are completed in two steps: 1) remove any linear baseline trend from the recorded acceleration before the instrument correction is performed. The baseline is obtained by applying a linear least-mean-square fit to the accelerogram. For records from EMA transducers, skip the first 2 seconds of the transient response, 2) remove the polynomial baseline from the instrument-corrected data. The polynomial baseline is obtained by applying a continuous or segmented polynomial least-mean-square fit to the velocity time history. The velocity time history is directly integrated from the instrument corrected accelerogram by a trapezoidal rule with an appropriate time interval.

5.4.3 Summary of the Proposed Data Processing Procedure

To describe the data processing procedure more clearly, a flow chart of Figure 5.3 is made to show the details of the proposed data processing scheme. The whole data processing scheme is summarized in the following steps:

1) Apply a linear least-mean-square fit to the uncorrected accelerograms (raw data) and remove the straight baseline from the uncorrected accelerograms.

A straight baseline is first removed from the uncorrected accelerograms. For the tape-recorded accelerograms from the instrument with EMA transducers, the first 2 seconds may contain an exponential transient response of the baseline shift introduced by the integration amplifier. The linear least-mean-square baseline fit is performed on the acceleration time history after the first 2 seconds. For the film-recorded accelerograms from instruments such as the SMA-1, the straight baseline fit is performed on the whole acceleration time history. After removal of the straight baseline, the ground acceleration is indicated as $(\ddot{x}_g)_1$ in Figure 5.3.

2) Apply instrument correction.

The instrument correction corrects two parts of the errors: the error from the transducer response and the error from the integrator output. For the instrument with EMA transducers, these errors can be removed by executing Equation (3.58) or

(3.59) with the input acceleration signal $(\ddot{x}_g)_1$ on the left side of the equation. The parameters of Equation (3.58) are determined from the laboratory test or calibration of the SMA-2/EMA (refer to Chapter 4). Similarly, for the SMA-1 instrument, Equation (3.9) is used to perform the instrument correction. If calibration data are not available, the nominal parameters provided by the manufacturer are used. A central difference scheme and a trapezoidal integration rule are used in performing the differentiation and integration involved in the instrument correction. After instrument correction, the ground acceleration is indicated as $(\ddot{x}_g)_2$ in Figure 5.3.

3) Integrate to obtain velocity.

Direct integration of $(\ddot{x}_g)_2$ gives the velocity $(\dot{x}_g)_2$. A trapezoidal integration rule is used in performing the integration and a zero initial velocity is assumed. At this stage, higher order errors (higher than first order) still exist in the data since only a linear baseline is removed in the first step.

4) Segmented polynomial baseline correction to the velocity.

The existing displacement offset in the near-field earthquake ground motion requires that the integration of the velocity time history should not be averaged to zero as is the case for conventional data processing. Based on the fact that the ground velocity starts at zero and ends at zero, a segmented polynomial function is fit to the initial and final portions of the velocity time history to remove any non-physical trend. The corrected velocity at this step is then indicated as $(\ddot{x}_g)_3$ in the flow chart.

5) Direct integration to obtain displacement.

Since the velocity is corrected based on the understanding of the ground motion in a physical sense, the integrated displacement is believed to be true. Direct integration of the velocity $(\dot{x}_g)_3$, assuming that the initial displacement is zero, gives the displacement $(x_g)_3$.

6) Subtract the derivative of the velocity correction from the acceleration time history.

The derivative of the segmented polynomial function from the velocity correction is equal to the non-physical trend of the acceleration time history. After the acceleration baseline correction, the corrected acceleration is denoted as $(\ddot{x}_g)_3$ in Figure 5.3.

The above data processing procedures use a trapezoidal integration rule and a central difference differentiation scheme. These numerical computations will also

introduce errors at each computational step. The accuracy of the numerical calculations is discussed in the next section.

The proposed data processing procedure is verified by the processing of the simulated long-period earthquake data. The detailed discussions are shown in the last section of this chapter.

5.5 Accuracy of the Numerical Calculations

One of the major concerns of the computational accuracy in the data processing procedure is aliasing. For example, high frequency information in earthquake data may be lost or distorted when the sample rate of the earthquake accelerogram is not high enough to represent the wave form. It is easy to show [44] that aliasing can be avoided by choosing a sample interval Δt, which is equal to one-half the reciprocal of the highest frequency of interest, f_N. That is

$$\Delta t = \frac{1}{2f_N} \tag{5.10}$$

The f_N in Equation (5.10) is known as Nyquist frequency. In strong-motion data processing, the time interval of the data should be small enough so that the Nyquist frequency of the digital signal is high enough to at least include the frequency range of interest in structural response. Since most strong ground motions contain energy within the frequency range of 25 Hz, a time step of 0.02 seconds is usually considered sufficient to represent the wave form of a strong-motion accelerogram.

Another concern in the data processing procedure are the errors introduced by numerical integrations and differentiations. It will be shown in the following that a time interval of 0.02 seconds is not small enough for the data to perform an accurate numerical calculation. In the proposed data processing procedure, a central difference scheme is adopted to perform the numerical differentiations and a trapezoidal rule is selected to calculate the numerical integrations. Since the numerical calculation results are not exact, the accuracy of the computational results of the data processing needs to be studied and controlled within an acceptable range by choosing an appropriate time interval for the digitization of an earthquake record.

This section discusses the accuracy of each numerical calculation applied in the earthquake data processing. The numerical calculations involved are the first- and

second-order differentiations and the integration. Since each computational step can be viewed as a filter, the judgement of the computational accuracy is made by comparison of the numerical and analytical results of the filters for the same computation. This procedure is completed through the transfer functions of those filters. The accuracy of those numerical filters and their performance is discussed in the following.

1. First-order differentiation.

The numerical scheme of the central difference representation for the first-order differentiation is:

$$y_i = \frac{1}{2\Delta t}(x_{i+1} - x_{i-1}) \tag{5.11}$$

The transfer function of this formula, denoted by $H_N(f_k)$, can be represented by:

$$H_N(f_k) = \frac{i}{\Delta t}\ sin(2\pi f_k \Delta t), \quad k = 0, 1, 2, ...N-1 \tag{5.12}$$

where f_k is the discrete frequency for $k = 0, 1, 2, ...N-1$, and Δt is the time interval between x_i and x_{i+1}. Substituting Δt in terms of the Nyquist frequency, Equation (5.12) can be written as

$$H_N(f_k) = i\ 2f_N\ sin(\frac{\pi f_k}{f_N}) \tag{5.13}$$

Since the exact representation for the first-order differentiation filter at discrete value f_k is

$$H(f_k) = i2\pi f_k, \tag{5.14}$$

The absolute error E_a in the numerical differentiation filter of Equation (5.13), which is the deviation of the $H_N(f_k)$ from $H(f_k)$, can be calculated and obtained by

$$E_a = -\frac{1}{6}(\frac{\pi f_k}{f_N})^2 + fourth\ order\ and\ higher \tag{5.15}$$

Assuming that f_k is small compared with f_N, the high order terms of $(\frac{\pi f_k}{f_N})$ can be neglected. To control the error within a small number ϵ, the following inequality should be satisfied

$$\frac{f_k}{f_N} \leq \frac{\sqrt{6\epsilon}}{\pi} \tag{5.16}$$

2. Second-order differentiation

A second-order central difference scheme is used to perform the second-order differentiation. This numerical scheme is formulated as

$$y_i = \frac{1}{\Delta t^2}(x_{i+1} - 2x_i + x_{i-1}) \tag{5.17}$$

The transfer function of Equation (5.17) is obtained as

$$H_N(f_k) = -16 f_N^2 \ sin^2(\frac{\pi}{2}\frac{f_k}{f_N}) \tag{5.18}$$

The exact transfer function for second-order differentiation at a discrete frequency f_k is represented by

$$H(f_k) = -(2\pi f_k)^2 \tag{5.19}$$

Then, the absolute error of the numerical calculation represented by Equation (5.18) is

$$E_a = -\frac{1}{3}(\frac{\pi}{2}\frac{f_k}{f_N})^2 + fourth\ order\ and\ higher \tag{5.20}$$

Neglecting the high order terms, the largest acceptable frequency f_k which controls the error within ϵ should satisfy the relationship

$$\frac{f_k}{f_N} \leq \frac{2\sqrt{3\epsilon}}{\pi} \tag{5.21}$$

3. Integration

The trapezoidal numerical integration scheme is represented by

$$y_{i+1} = y_i + \frac{\Delta t}{2}(x_i + x_{i+1}) \tag{5.22}$$

The transfer function of Equation (5.22) is then

$$H_N(f_k) = \frac{1}{i4f_N} \ ctan(\frac{\pi}{2}\frac{f_k}{f_N}) \tag{5.23}$$

The exact transfer function of Equation (5.22) at discrete frequency f_k is

$$H(f_k) = \frac{1}{i2\pi f_k} \tag{5.24}$$

Then, the absolute error in the numerical filter of Equation (5.23) is estimated as

$$E_a = -\frac{1}{3}(\frac{\pi}{2}\frac{f_k}{f_N})^2 + fourth\ order\ and\ higher \tag{5.25}$$

Neglecting the higher order term of $\left(\frac{\pi}{2}\frac{f_k}{f_N}\right)$, the maximum acceptable f_k for the integration filter with the computational errors controlled within ϵ is

$$\frac{f_k}{f_N} \leq \frac{2\sqrt{3\epsilon}}{\pi} \tag{5.26}$$

All of the numerical schemes presented above are non-recursive filters and no phase shift occurred in those filters. So the error controls are on their amplitudes. By comparison of the inequalities of Equation (5.16), (5.21) and (5.26), the common criterion of error control for the differentiations and integration is concluded to be

$$\frac{f_k}{f_N} \leq \frac{\sqrt{6\epsilon}}{\pi} \tag{5.27}$$

For example, to control the error within 10% in the frequency range of 0 to 25 Hz, the Nyquist frequency of the data should be four times larger than this frequency range, which means that the time interval should be not larger than 0.005 seconds.

Based on the above analysis, the instrument correction filter for the SMA-2/EMA instrument can also be derived. The numerical and analytical instrument correction filters for this instrument are:

$$H_N(f_k) = \left[2\zeta_n\frac{f_{cr}}{f_n} + 1 - \left(\frac{2f_N}{\pi f_n}\right)^2 sin^2\left(\frac{\pi f_k}{2f_N}\right)\right]$$

$$+i\left[\left(\frac{f_{cr}}{f_n} + 2\zeta_n\right)\frac{f_N}{\pi f_n}sin\left(\frac{\pi f_k}{f_N}\right) - \frac{\pi f_{cr}}{2f_N}ctan\left(\frac{\pi f_k}{2f_N}\right)\right] \tag{5.28}$$

and,

$$H(f_k) = \left[2\zeta_n\frac{f_{cr}}{f_n} + 1 - \left(\frac{f_k}{f_n}\right)^2\right] + i\left[\left(\frac{f_cr}{f_n} + 2\zeta_n\right)\frac{f_k}{f_n} - \frac{f_{cr}}{f_k}\right] \tag{5.29}$$

To compare the numerical and the analytical instrument correction filters, the amplitudes of their frequency response and the phase shifts are calculated and plotted in Figure 5.4. Three cases with sampling periods of Δt=0.02, 0.01 and 0.005 seconds are considered. The Nyquist frequencies for those sampling periods are then f_N=25, 50 and 100 Hz respectively. The other parameters in the instrument filters are taken from their nominal or optimal design values, which are $f_n = 25$ Hz, $\zeta_n = 0.6$, $f_{cr} = 0.1$ Hz. Figure 5.4 shows that the accuracy of the numerical instrument correction filter is very good in the low frequency range. In the high frequency range, the distortion of the numerical filter increases rapidly as frequency increases.

The frequency range in which the errors are controlled under 5% and 10% for different sampling periods are calculated and listed in Table 5.1. The results show that in order to control the error under 5% and 10% in a frequency range of 20 Hz to 25 Hz, a sampling period of 0.005 seconds is required. Any other time interval lower than that will reduce the high frequency information by 10% or more during the numerical calculations. For the SMA-2/EMA instrument, the analog signal is retrieved at a sample rate of 256 samples per second. The Nyquist frequency is then 128 Hz which gives the frequency range of about 25 Hz to an accuracy within 10%. Hence, a sample rate of 256 samples per seconds is sufficient for the numerical computations in data processing of the earthquake data recorded on the SMA-2/EMA accelerograph.

5.6 Application of the Proposed Method to Simulated Earthquake Data

Since the displacements of a simulated earthquake data are known *a priori*, the proposed new data processing scheme can be verified by its application to simulated earthquake data. Several cases are selected to discuss this new data processing method. As described in Section 4.3.4, the simulated earthquakes were generated manually by moving the SMA-2/EMA instrument. Three types of the simulated earthquake accelerograms were generated to have displacement time histories with the shapes of Figure 4.10(a)(b)(c).

A first look is taken at the simulated earthquake record #3. It was generated by horizontally moving the instrument in the longitudinal direction of the transducer. The instrument was moved 6 feet (183 cm) in a positive direction and 3 feet (91 cm) in the negative direction, and then stopping. The generated displacement time history belongs to Type One in Figure 4.10(a).

To test the proposed data processing scheme, several different cases of processing are investigated. They are: 1) direct integration without correction, 2) integration with baseline correction but without instrument correction, 3) integration with instrument correction but without baseline correction, and 4) integration with both instrument correction and baseline correction. The results are shown in Figure 5.5(a)(b)(c)(d) for the four different cases.

The results from the case 1) processing are shown in Figure 5.5(a). These results are obviously not true since the velocity baseline is not zero and the final displacement is not constant after the stopping of the instrument. The errors result from the imperfect transducer response as well as the baseline shift from the recording and playback.

Figure 5.5(b) is the results of the case 2) processing on the same simulated ground motion. In this case, two baseline corrections are applied to the recorded data. First, a linear baseline correction is performed on the acceleration. Second, a segmented polynomial baseline correction is applied to the velocity time history after the integration. With one more integration, the displacement time history is obtained. In this way, it is hard to make a correct judgement as to whether the processed results are correct or not, providing the instrument displacement is not known *a priori*. But in this test, the shape of the displacement time history of simulated earthquake record #3 is known. Comparing the displacement time history in Figure 5.5(b) to the displacement time history in Figure 4.10(a), it can be seen that the processed result is obviously different from the real instrument motion. The final displacement from the "corrected data" shows a negative offset, while the real offset should be positive according to the instrument performance during the test. So, only applying a baseline correction is not sufficient to give the correct results, especially for the long-period earthquake records recorded on the instruments with EMA transducers.

Figure 5.5(c) presents the results of the case 3) processing, still for the same simulated earthquake. The record is instrument corrected but not baseline corrected. After instrument correction and integration, a velocity time history is obtained and shown in the second plot of Figure 5.5(c). The velocity time history shows that the instrument distortion is recovered so that the polynomial baseline shift can be clearly observed from the velocity time history. So, without baseline correction, the tail portion of the velocity time history will be nonzero and the integrated displacement time history will be distorted.

Figure 5.5(d) shows the results of the case 4) processing which is an application of the proposed data processing method including all the steps shown in Figure 5.3. The results are very much like they should be. The magnitude of the pulse and the final displacement are very close to what were measured from the test. The errors

from the calculated displacement are about 10% which is considered acceptable. This case proves that the new data processing method is successful and taking off either step of baseline or instrument correction from the data processing procedure will lead to wrong results.

Some other simulated earthquake records are also processed with the new proposed method. Records #4 and #7 were recorded by the longitudinal transducer of the instrument. These records represent ground displacements with the characteristics of parallel and perpendicular motions relative to the fault. The same procedures of the four different cases are performed on these two records. The processed results are shown in Figure 5.6(a)(b)(c)(d) and Figure 5.7(a)(b)(c)(d). These figures also show that only the results from case 4) processing present good agreements to the real instrument motions. The errors in the calculated displacements are also around 10%. These examples further prove that both the baseline and instrument corrections are very important in data processing.

It can be seen from the above case studies that the baseline correction serves to remove the curved baseline shift from the records, while the instrument correction serves to recover the amplitude and phase distortion which cannot be observed as obviously as the baseline shift. The amplitude and the phase distortions are caused by imperfection in the transducer design. The correction of these distortions is very important for the SMA-2/EMA instrument correction, especially when it records long-period information.

The above examples show that the proposed data processing technique works fairly well on correcting the simulated accelerograms. The results of the case studies are sufficient to show that the proposed method can also work well on real earthquake accelerograms.

5.7 Summary and Conclusions

This chapter presents the study of the possible error sources associated with the data processing of strong-motion accelerograms and proposes a new data processing method to recover these errors. The new data processing method is verified using simulated long-period accelerograms. In addition, the accuracy of the numerical calculations is also discussed and the maximum sampling period is selected to control

the computational errors to an acceptable level. The study leads to the following conclusions:

(1). It is possible to recover long-period information from near-field strong-motion accelerograms by the proposed data processing scheme. The new method uses special baseline and instrument correction procedures which are based on an understanding of the physics of the earthquake and the nature of the instrument as well as the data recording and retrieving procedure.

(2). The use of filters is not recommended in the data processing of the near-field strong-motion accelerograms since the filtering procedure will distort the signal information. This has also been concluded from the conventional processing of the Lucerne Valley record in Chapter 2.

(3). The sampling period of digitized earthquake data should not be larger than 0.005 seconds so that the numerical calculation errors can be controlled to be less than 10% in the frequency range of interest. Otherwise, a better numerical differentiation and integration scheme than the central difference differentiation and trapezoidal integration rule should be employed.

Sampling Period	Errors under 5%	Errors under 10%
0.005 sec	20.2 Hz	25.1 Hz
0.01 sec	14.6 Hz	17.3 Hz
0.02 sec	11.1 Hz	13.4 Hz

Table 5.1 The Frequency Range of the Numerical Filter with Errors Less Than 5% and 10% for Different Sampling Periods

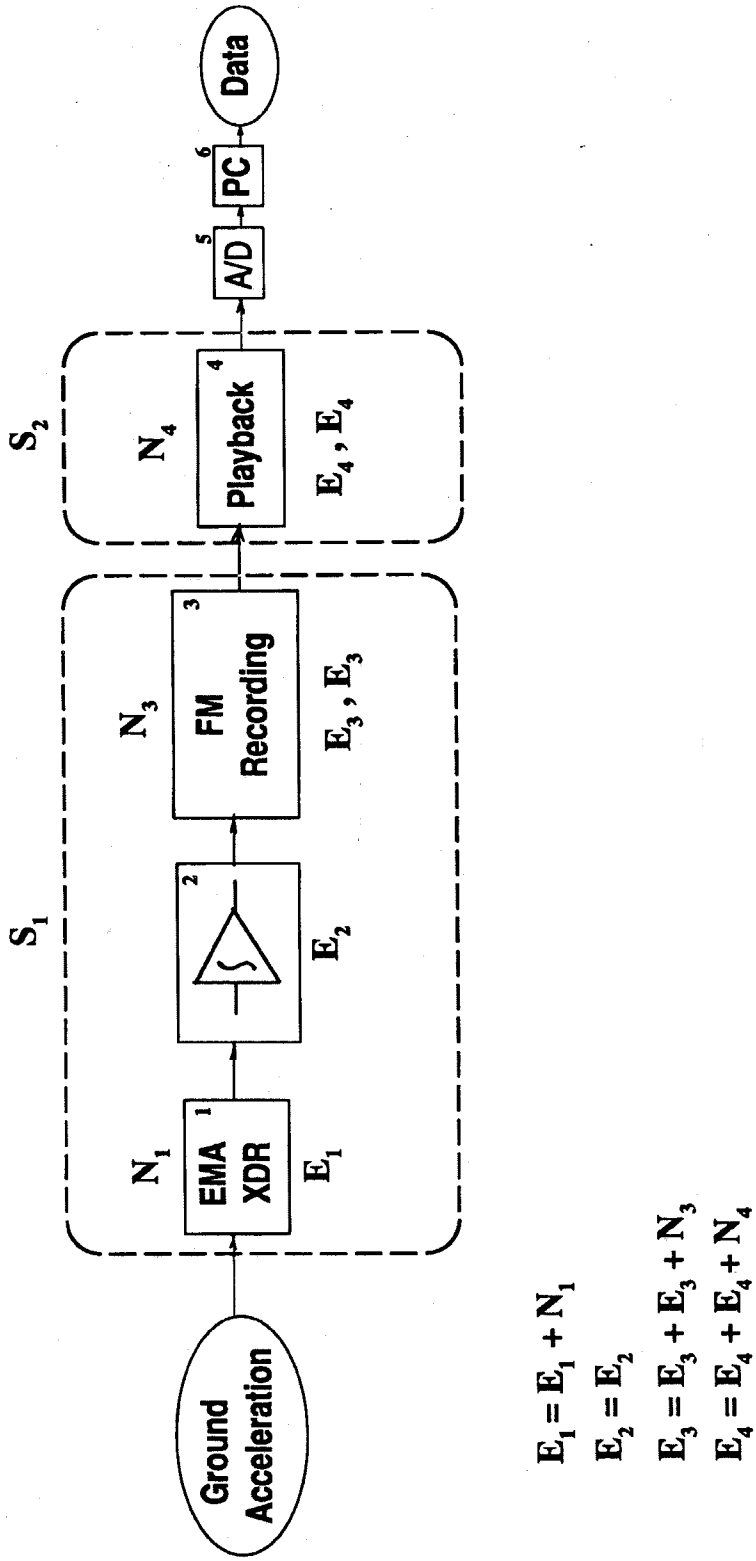

Figure 5.1 Errors From the Recording and Retrieving Procedure.

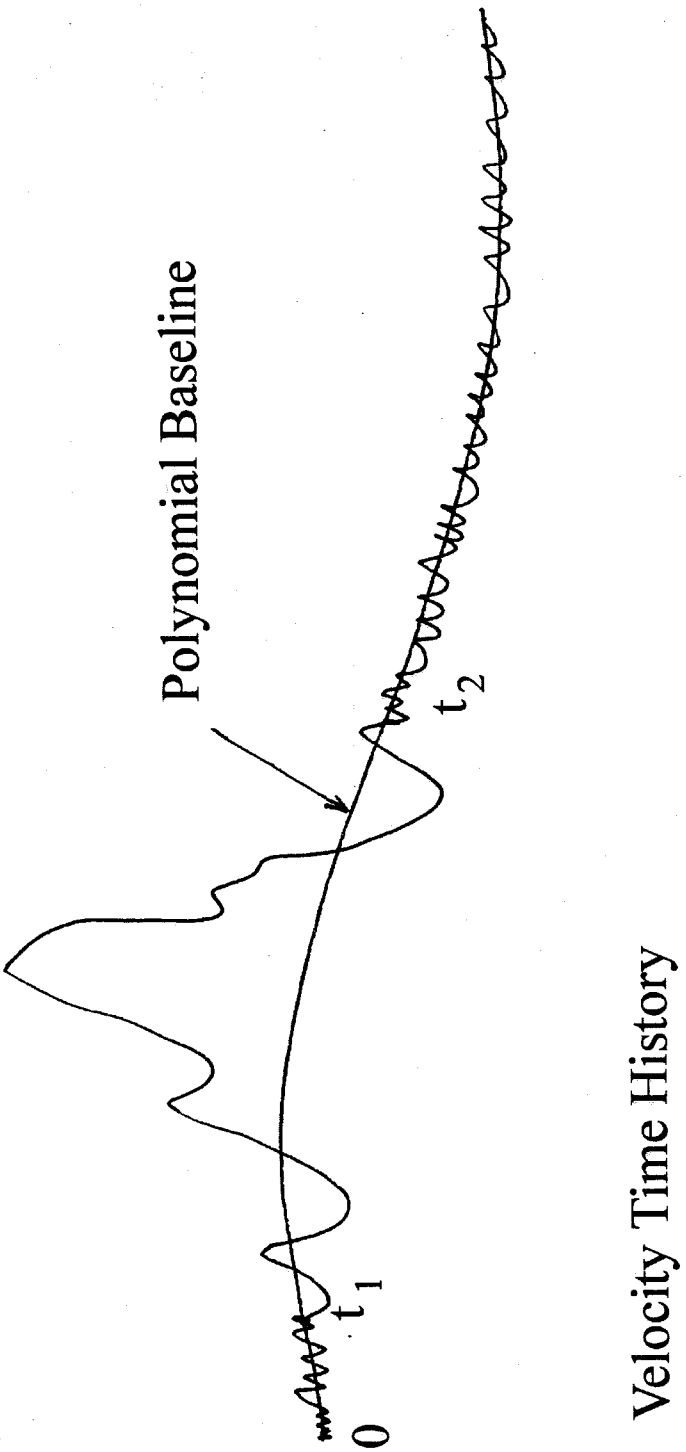

Figure 5.2 Schematic Diagram of Segmented Polynomial Baseline Correction.

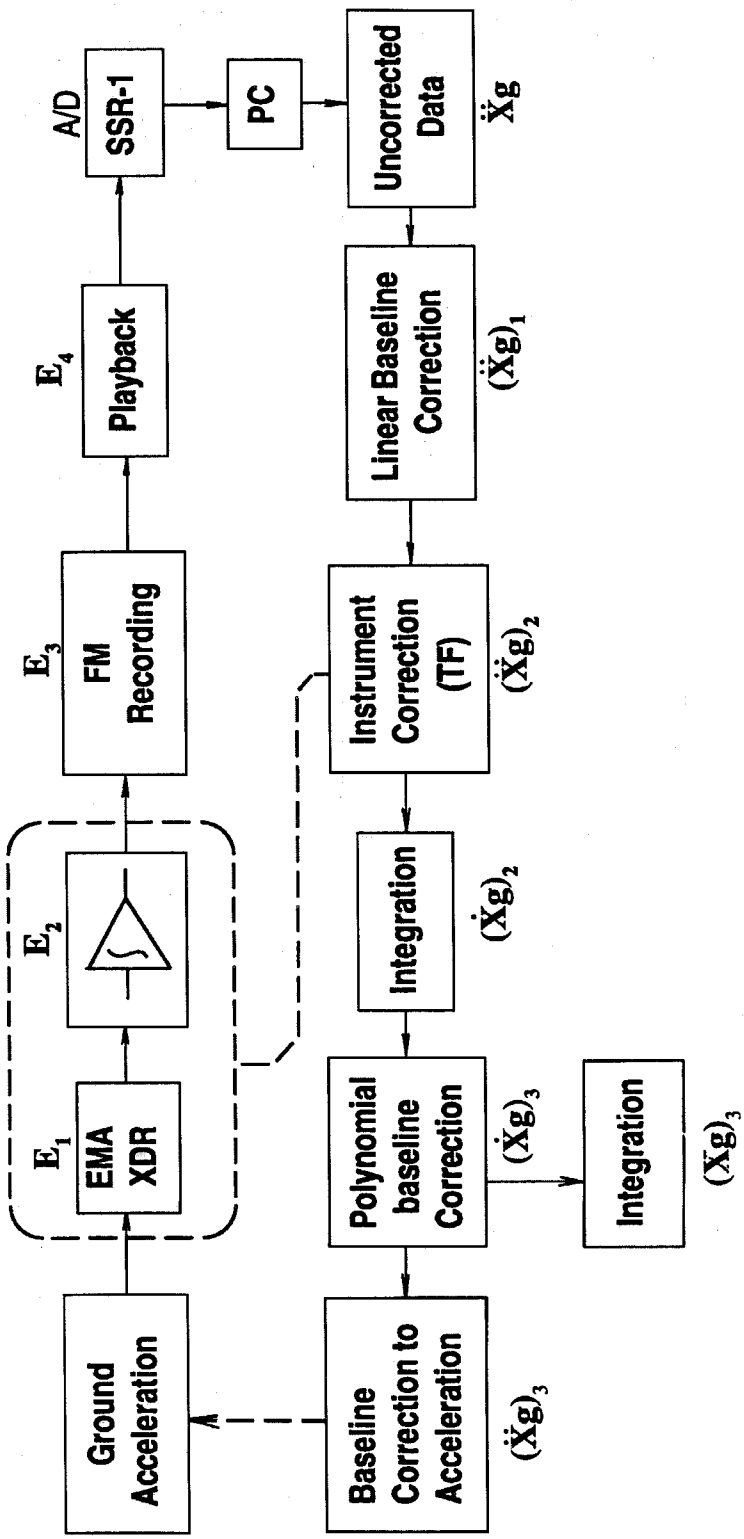

Figure 5.3 Data Processing Procedure.

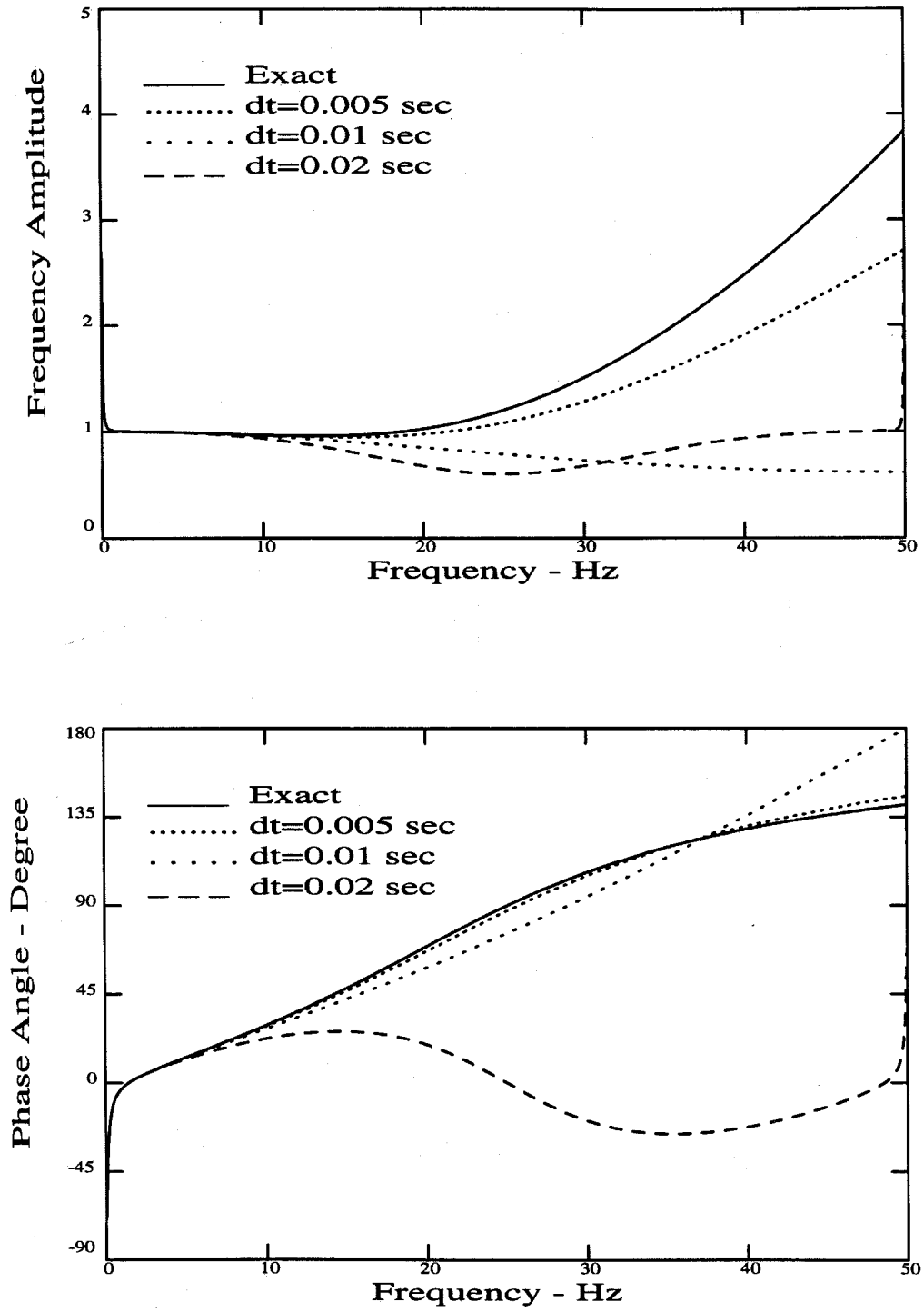

Figure 5.4 Amplitude and Phase Response of Exact and Numerical Instrument Correction Filters.

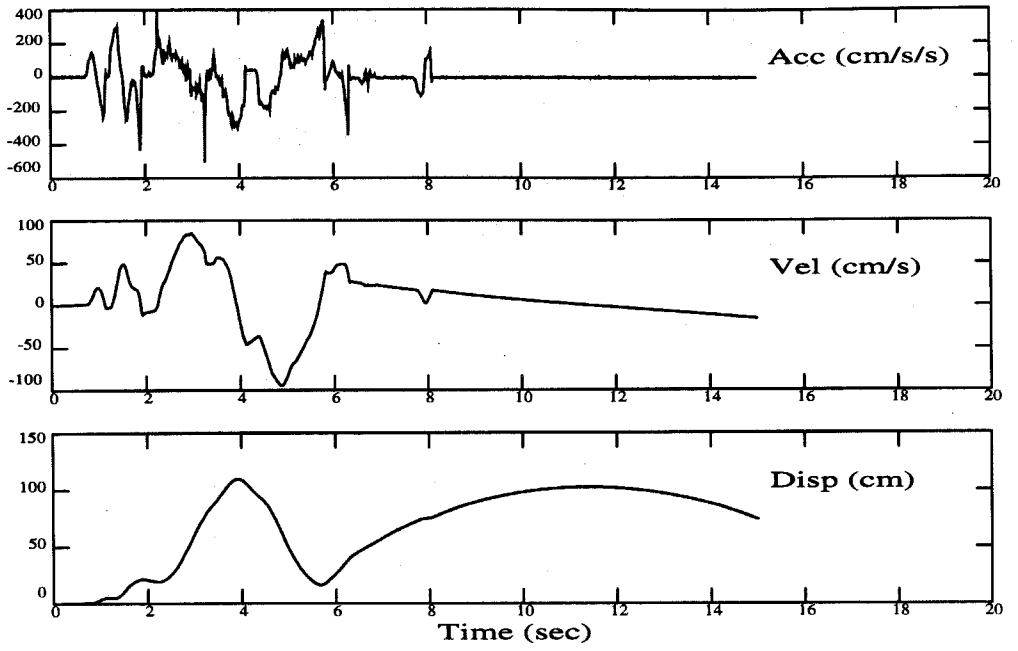

Figure 5.5(a) Case 1) Processing of Simulated Earthquake Record #3 Without Any Correction.

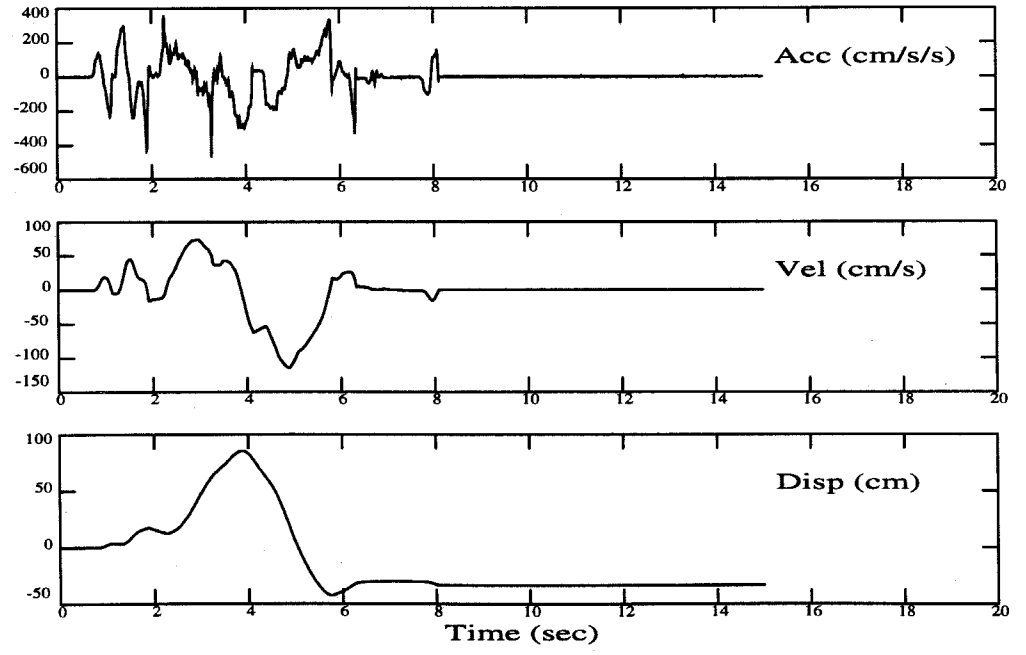

Figure 5.5(b) Case 2) Processing of Simulated Earthquake Record #3 With Baseline Correction but Without Instrument Correction.

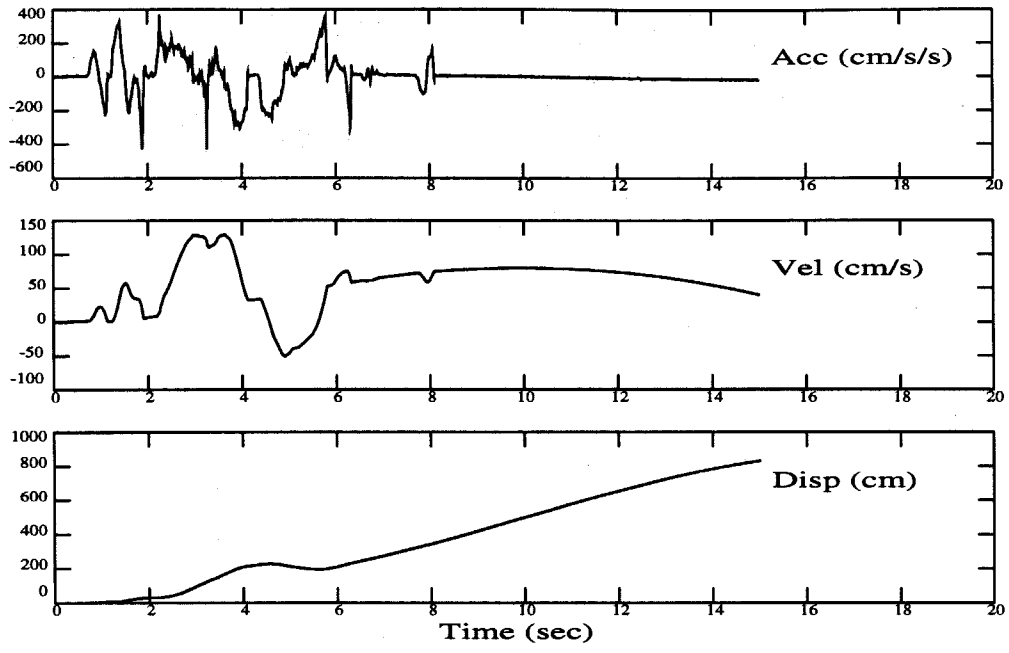

Figure 5.5(c) Case 3) Processing of Simulated Earthquake Record #3 With Instrument Correction but Without Baseline Correction.

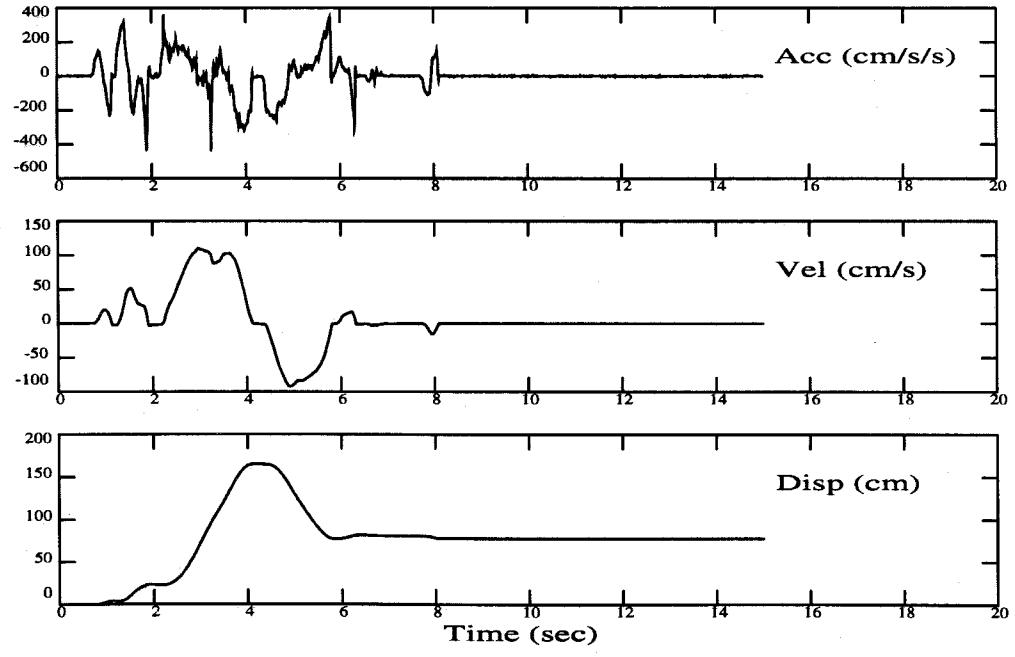

Figure 5.5(d) Case 4) Processing of Simulated Earthquake Record #3 With Both Instrument Correction and Baseline Correction.

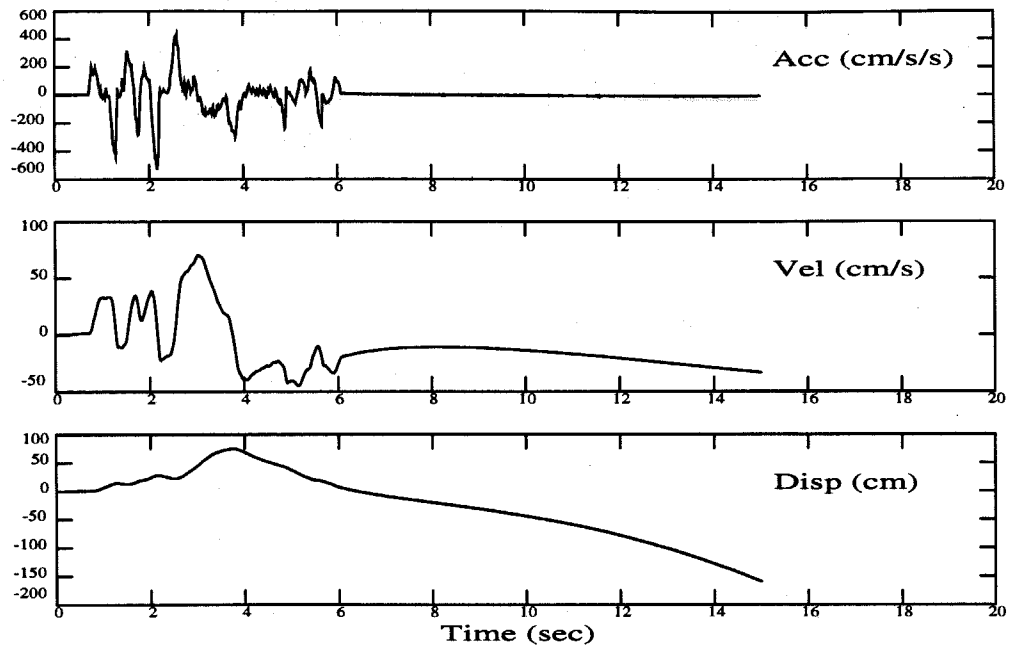

Figure 5.6(a) Case 1) Processing of Simulated Earthquake Record #4 Without Any Correction.

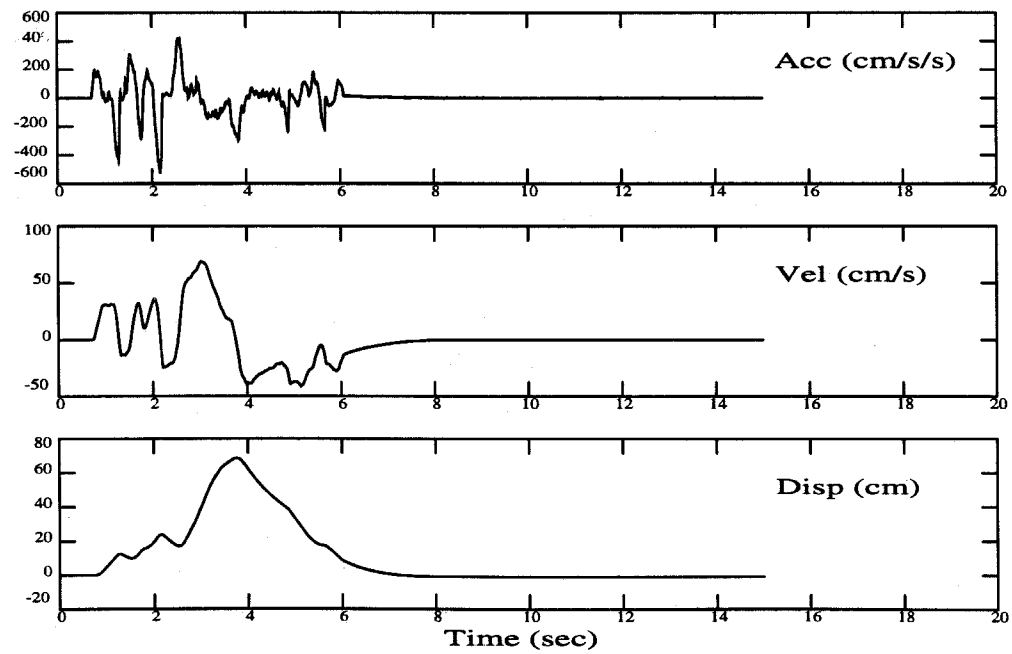

Figure 5.6(b) Case 2) Processing of Simulated Earthquake Record #4 With Baseline Correction but Without Instrument Correction.

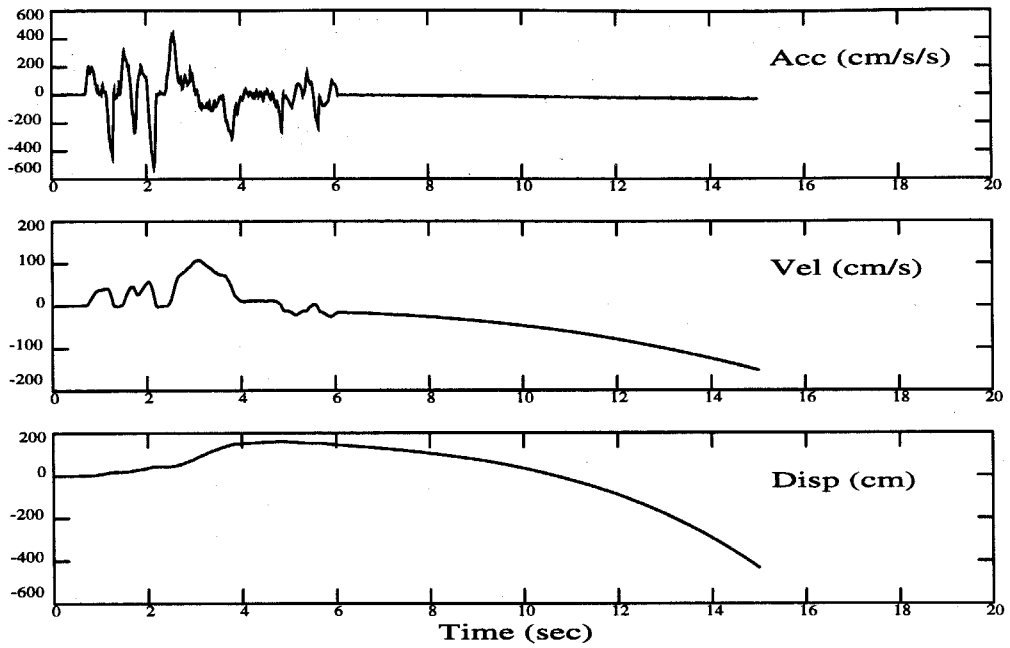

Figure 5.6(c) Case 3) Processing of Simulated Earthquake Record #4 With Instrument Correction but Without Baseline Correction.

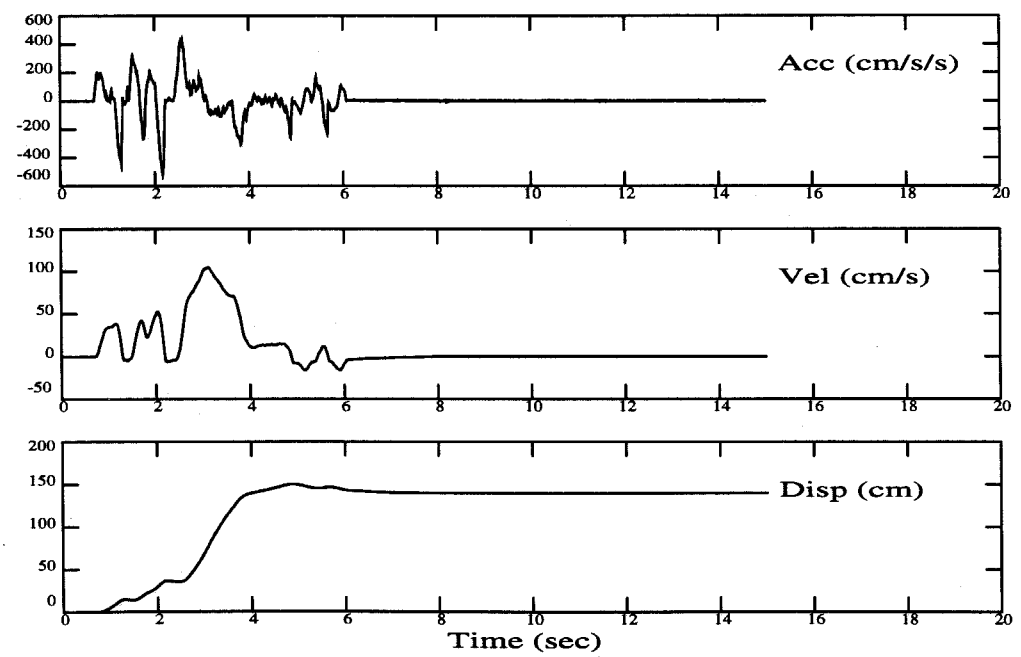

Figure 5.6(d) Case 4) Processing of Simulated Earthquake Record #4 With Both Instrument Correction and Baseline Correction.

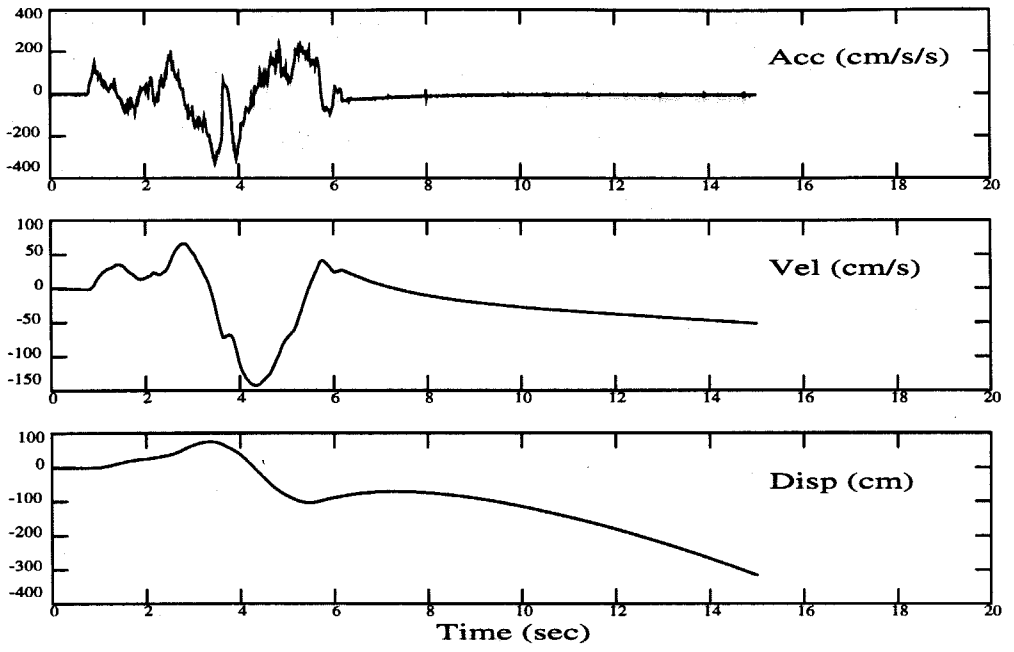

Figure 5.7(a) Case 1) Processing of Simulated Earthquake Record #7 Without Any Correction.

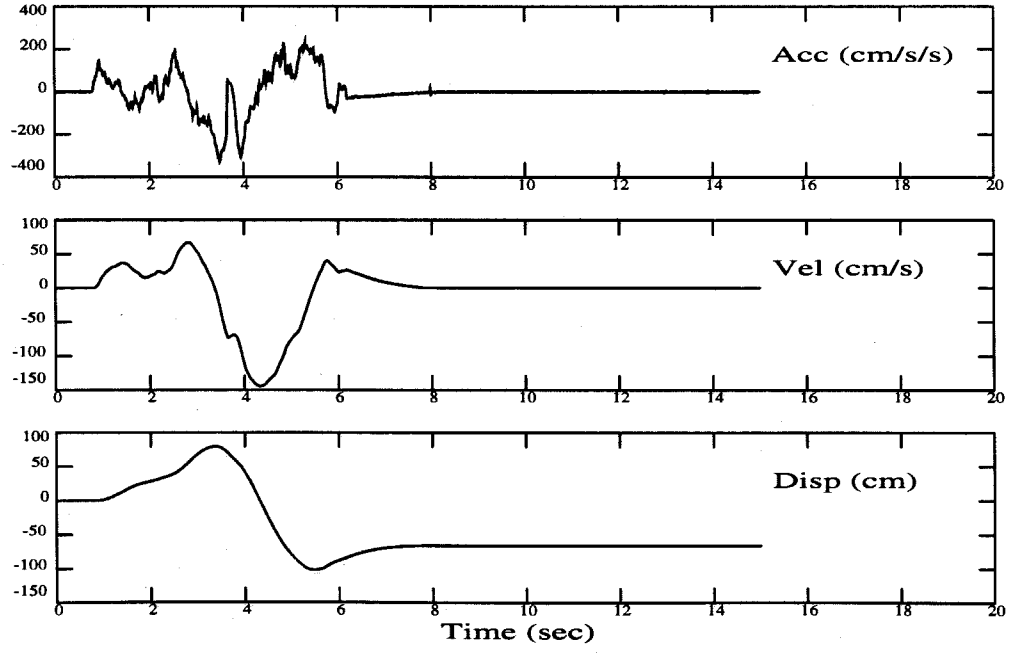

Figure 5.7(b) Case 2) Processing of Simulated Earthquake Record #7 With Baseline Correction but Without Instrument Correction.

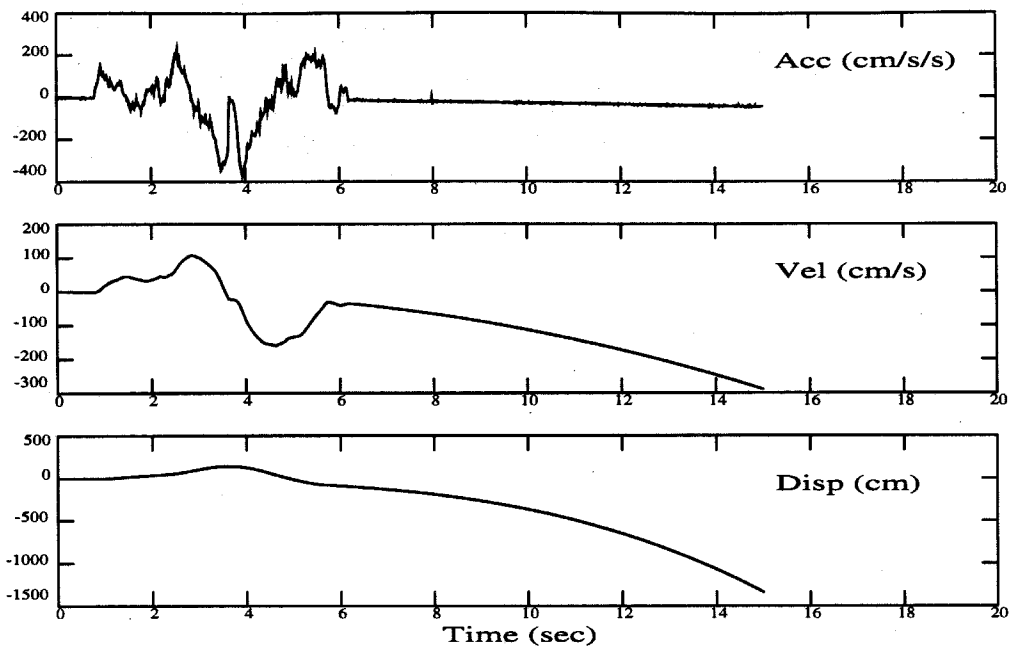

Figure 5.7(c) Case 3) Processing of Simulated Earthquake Record #7 With Instrument Correction but Without Baseline Correction.

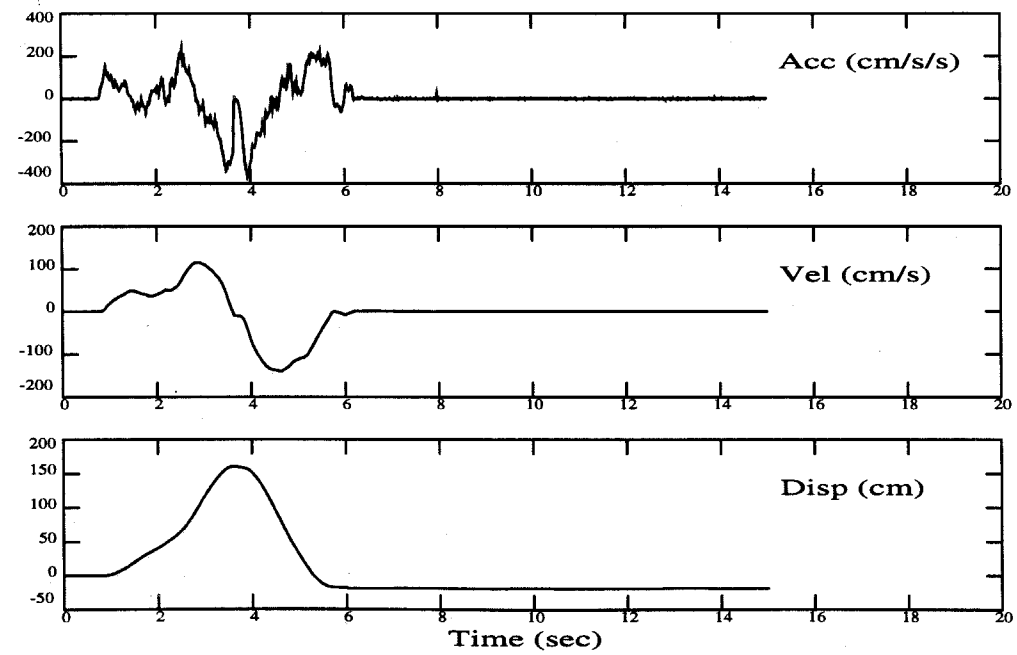

Figure 5.7(d) Case 4) Processing of Simulated Earthquake Record #7 With Both Instrument Correction and Baseline Correction.

Chapter 6

Data Processing of the Landers Earthquake Data

6.1 Introduction

As described in Chapter 2, the Landers earthquake ($M_L = 7.4$) was the largest event in the past 50 years and the Lucerne Valley record was one of the first recorded near-field ground motions. Large offsets on the fault near the station were observed from the field investigation. Another important fact is that the fault-to-station distance of the Lucerne Valley record, 2 km, is one of the closest in strong-motion recording history. In this chapter, the new data processing scheme developed in Chapter 5 is employed to process the Lucerne Valley record, and the instrument parameters obtained in Chapter 4 are used for the instrument correction. The response spectra and the Fourier spectra of the new and conventional processed record are also presented and discussed.

6.2 Data Processing of the Lucerne Valley Record

By applying the new data processing procedure described in Section 5.2.2, the acceleration, velocity and displacement of the Lucerne Valley record are obtained and shown in Figure 6.1. The baseline corrections for the three velocity components are also displayed in Figure 6.2. A segmented polynomial baseline is obtained by the least-mean-square fit to each of the velocity time histories which are integrated from the instrument corrected accelerograms. Figure 6.2 shows that the polynomial baseline represents the nonphysical trend of the velocity time history in a good manner. After subtracting the polynomial baseline, the calculated velocity time history and

the integrated displacement time history present a reasonable ground behavior of the earthquake (see Figure 6.1).

6.2.1 Comparison of the New and Conventional Data Processing

The results of new data processing (Figure 6.1) are obviously different from the results of conventional data processing (Figure 2.10). The new data processing gives maximum displacements of about 75 cm (longitudinal component) and 260 cm (transverse component) while conventional data processing only gives maximum displacements of 3.5 cm and 9 cm respectively. The final offsets of 72 cm (longitudinal component) and 180 cm (transverse component) that are shown in the results of new data processing do not appear in the results of conventional processing. The maximum peak-to-peak velocities for the two horizontal components are around 50 cm/sec (longitudinal) and 200 cm/sec (transverse) from the new data processing but are around 40 cm/sec and 80 cm/sec from the conventional data processing respectively. Also, the maximum peak velocity from the new data processing, which is 146 cm/sec, is much larger than that from the conventional processing, which is 49 cm/sec. In Table 6.1 are listed the peak values of acceleration, velocity and displacement from the results of the new data processing and those from the results of conventional data processing (shown in the parentheses).

In summary, the major differences between the results of the new data processing and conventional data processing are: 1) the results of the new data processing show large displacement offsets and the results of conventional data processing show a zero displacement offset for each component which is inconsistent with the geological data obtained from the field, and 2) the maximum peak velocity of the horizontal components from the new data processing also differs from that from the conventional data processing. This quantity is believed to be the major concern in causing large strains in structures subject to earthquakes.

6.2.2 Rotations of Horizontal Components

Since it is more instructive to view ground motion in the direction parallel and perpendicular to the fault, rotations of the two horizontal components are performed and the results are shown in Figure 6.3. A permanent offset of 150 cm is shown in the fault-parallel displacement and a permanent offset of 118 cm is shown in the

fault-perpendicular displacement. The maximum velocities for the fault-parallel and -perpendicular components are 83 cm/sec and 129 cm/sec respectively. It should be mentioned here that the transverse transducer was not aligned perpendicular to the longitudinal transducer in the Lucerne Valley instrument. The angle between the two transducers was about 85°. This fact has been taken into account when performing the rotations of the horizontal components of the processed record.

The fault orientation near the Lucerne Valley station is slightly different from the global fault orientation (see Figure 2.1). The local fault direction near the station was measured to be about N55°W, while the global direction of the fault is about N45°W. Assuming that the ground motion mainly follows the global fault direction, then, the two horizontal components of the processed record are rotated to the directions N45°W and S45°W respectively. The N45°W displacement component presents a positive permanent offset and the S45°W one shows a positive large pulse perpendicular to the fault. These are exactly the expected properties of the near-field ground motion of an earthquake on a strike-slip fault. Compared to synthetic earthquake records generated for a strike-slip fault by Hartzell and Heaton [4], the resulting perpendicular component does not come back to the origin but shows an offset, probably because the local fault near the Lucerne Valley station is kinked (Figure 2.1).

The maximum velocity direction is found to be approximately S80°W. The velocity time history in that direction is plotted in Figure 6.4, which is almost the same as the original transverse velocity time history since the maximum velocity direction is nearly the same. The value of the maximum velocity is 146 cm/sec. This kind of velocity pulse can generate very large strain forces in structures and should be considered in structural design.

6.2.3 Particle Trajectory of the Lucerne Valley Station

To investigate the ground motion more directly, the particle ground displacement and velocity trajectory of the Lucerne Valley station are plotted in Figure 6.5 and 6.6. The time interval between the solid diamond squares is 0.16 seconds for both displacement and velocity plots.

The plots show that the ground motion in the vicinity of the fault shows a large single pulse. The particle motion starts from the original position, moving away

from the fault and then coming back to the fault, towards northwest direction. The pulse is almost perpendicular to the fault direction. It can also be seen that the maximum velocity occurs approximately in the same direction as the displacement pulse direction. Since the station is on the left side of the fault, the particle motions of the ground show a right-lateral strike-slip fault behavior. The results also show that the velocity components are very similar to the synthetic earthquake records generated by the strike-slip seismic model studied by Heaton [7].

6.3 Response Spectra

Response spectrum is one of the methods to measure the strength of earthquake ground motion. It is widely used for structural design purposes. Response spectra are defined as the maximum responses of a SDOF damped oscillator subjected to an earthquake. The maximum response is usually either the maximum absolute value of the relative displacement, relative velocity or absolute acceleration of the SDOF oscillator. In engineering practice, a pseudo-velocity spectrum is commonly used for design criteria. It is often graphed on a tripartite logarithmic paper so that the maximum relative displacement (SD), maximum pseudo-velocity (PSV) and maximum pseudo-acceleration (PSA) values can be read from one plot. This is because these quantities can be approximately calculated from each other by the relationship

$$SD = \frac{T}{2\pi}(PSV) = (\frac{T}{2\pi})^2(PSA) \tag{6.1}$$

In the following sections, the PSV spectra for the Lucerne Valley record are calculated and plotted in a tripartite logarithmic form. The PSV spectra calculated from the data corrected by the new data processing are compared with the PSV spectra calculated from the uncorrected data as well as the data corrected by the conventional data processing.

6.3.1 Response Spectra of Corrected and Uncorrected Record

The response spectra for the three components of the Lucerne Valley record are calculated for the damp ratios of 0%, 2%, 5% and 10% respectively, and the results are shown in Figure 6.7. The solid lines represent the response spectra calculated from the records corrected by the new data processing method and the dotted lines represent the results calculated from the uncorrected record. The two sets of results

are very close in the short-period range of the response spectra. However, in the long-period range, the two set of the results are very different. In the long-period range near 10 seconds, the response spectra of the new processed data are higher than that of the uncorrected data, which indicated that the long-period distortions in that range have been corrected; while in the long-period range beyond 20 seconds, the response spectra of new processed record are lower than that of the uncorrected record, which means that the new data processing effectively filters out the low frequency noises. The high frequency noise does not seem to be filtered out by any noticeable amount from the new data processing. This has been proved to be acceptable for the reasons that: 1) the signal-to-noise ratio for the Lucerne Valley record is as high as 100 (see Figure 4.9) in the short-period range, which implies that the high frequency signal mostly represents the real ground motion, and 2) the instrument correction filter suppresses the response amplitude of high frequency beyond 25 Hz by more than 10%. So, it is unnecessary to apply a filter on the Lucerne Valley record during data processing.

6.3.2 Response Spectra of New and Conventional Processed Record

The PSV spectra calculated from the record corrected by the proposed data processing method are also compared with the PSV spectra calculated from the record corrected by the conventional data processing method. The results are plotted in Figure 6.8 to 6.10. The solid lines represent the PSV spectra calculated from accelerations corrected by the proposed data processing procedure, and the dotted lines represent the PSV spectra calculated from accelerations corrected by the conventional data processing procedure. The plots show that the solid lines are considerably higher than dotted lines in both the high and low frequency range. This is because the application of high- and low-pass filters in the conventional data processing eliminates high and low frequency information from the original records. Based on the analysis presented in this study, the author believes that the conventional method filters out real information. More importantly, the response spectra of the conventional processed record result in lower design loads which will lead to a less conservative design.

Not only is real information lost from the record of conventional data processing, but also the response spectra do not in general have an asymptotic displacement that

is equal to the maximum displacement of the time history (compare the maximum displacement in Figure 2.10 and the dotted lines in Figure 6.8 to 6.10 at long-period ends). This is because the application of the filters in the conventional data processing distorts the velocity and displacement signals. In the conventional data processing procedure, the band-pass filters are not only applied to the acceleration time history but also to the velocity and displacement time histories. In this way, the integral of the acceleration will not be equal to the velocity and the integral of the velocity will not be equal to the displacement. The same discrepancies can also be observed from the pseudo-velocity spectra in CIT Vol III and the others calculated from the records processed by the conventional data processing method.

The PSV spectra calculated from the record corrected by the proposed data processing method show that the maximum acceleration in each of the three components asymptotically approaches the peak acceleration when the natural period of the structure tends to zero, and the maximum displacement asymptotically approaches the peak displacement when the natural period of the structure tends to a large value. These can be observed from comparing the maximum values in Figure 6.1 to the solid lines in Figure 6.8 to 6.10 at both short- and long-period ends.

6.4 Fourier Spectra

Like the response spectrum, the Fourier spectrum is another method of measuring the strength of the earthquake ground motion. It is implemented by use of the fast-Fourier-transform algorithm. The Fourier spectra of ground accelerations represent the frequency content of the acceleration time histories. The area under the Fourier spectrum actually measures the energy of the ground motion. It is closely related to the relative velocity response spectrum of an undamped oscillator. In general, the velocity spectrum is always greater than the Fourier spectrum. Here, the Fourier spectra are calculated for both the corrected and uncorrected Lucerne Valley records.

The Fourier spectra of ground accelerations corrected by the new data processing (solid lines) and the Fourier spectra of uncorrected data (dotted lines) are calculated and shown in Figure 6.11. The two sets of results do not show obvious differences in the high frequency range. In low frequency range, especially near the zero frequency,

the Fourier amplitudes are reduced significantly by the new procedure. This implies that a large amount of baseline shift has been corrected, though a small amount of errors still exist due to the numerical calculations. In the frequency range near 0.1 Hz, the Fourier amplitudes of the new processed record are in general higher than that of the uncorrected record, which implies that the low frequency distortions in that frequency range have been recovered.

Figure 6.12 presents plots of Fourier spectra for the new processed record (solid lines) and those of the conventional processed record (dotted lines). Similar to the comparisons made for response spectra, the Fourier amplitudes of the new processed record are considerably higher in both the high and low frequency ranges than those of the conventional processed record.

6.5 Conclusions

The corrected Lucerne Valley record from the Landers earthquake is believed to be the first successfully processed near-field earthquake record that shows the dynamic behavior of the typical characteristics of near-field ground motion. It provides valuable information for seismological studies of the earthquake mechanism as well as engineering studies of earthquake resistant design.

The present investigation shows that the new data processing method maintains more useful information in the earthquake record than the conventional data processing method in the following aspects:

(1). The maximum peak values of the new processed record are significantly larger than those of the conventional processed record. In conventional data processing, the large velocity pulses are under-represented and the displacement offsets are not presented in the corrected data.

(2). The response spectra and the Fourier spectra calculated from data corrected by the two methods show that the response spectra of the conventional processed record are considerably lower than those of the new processed record in both the high and the low frequency range for the Lucerne Valley record. The use of response spectra derived from conventional processed records may lead to less conservative structural design.

(3). Using the proposed algorithm, the maximum accelerations or displacements obtained from the pseudo-velocity spectra asymptotically approach the peak acceleration or displacement when the period of the oscillator tends to zero or infinite. The same spectra calculated using conventional methods are not consistent on this point.

The long-period information in a strong-motion record can be very important for structural engineers in the analysis of long-period structures. The large pulse presented in the velocity component of near-field ground motion is believed capable of generating significant strain forces or shears in structures and may cause serious structural damages.

Components	Peak Acc	Peak Vel	Peak Disp
Longitudinal (N15W)	-0.83 (-0.88) g	33 (22) cm/s	75 (-4) cm
Transverse (S80W)	-0.75 (0.63) g	146 (49) cm/s	260 (9) cm
Vertical (Up)	0.92 (-0.68) g	-41 (-33) cm/s	41 (7) cm

Table 6.1 Peak Values of Acceleration, Velocity and Displacement of the Three Components of the Lucerne Valley Record from the Landers Earthquake

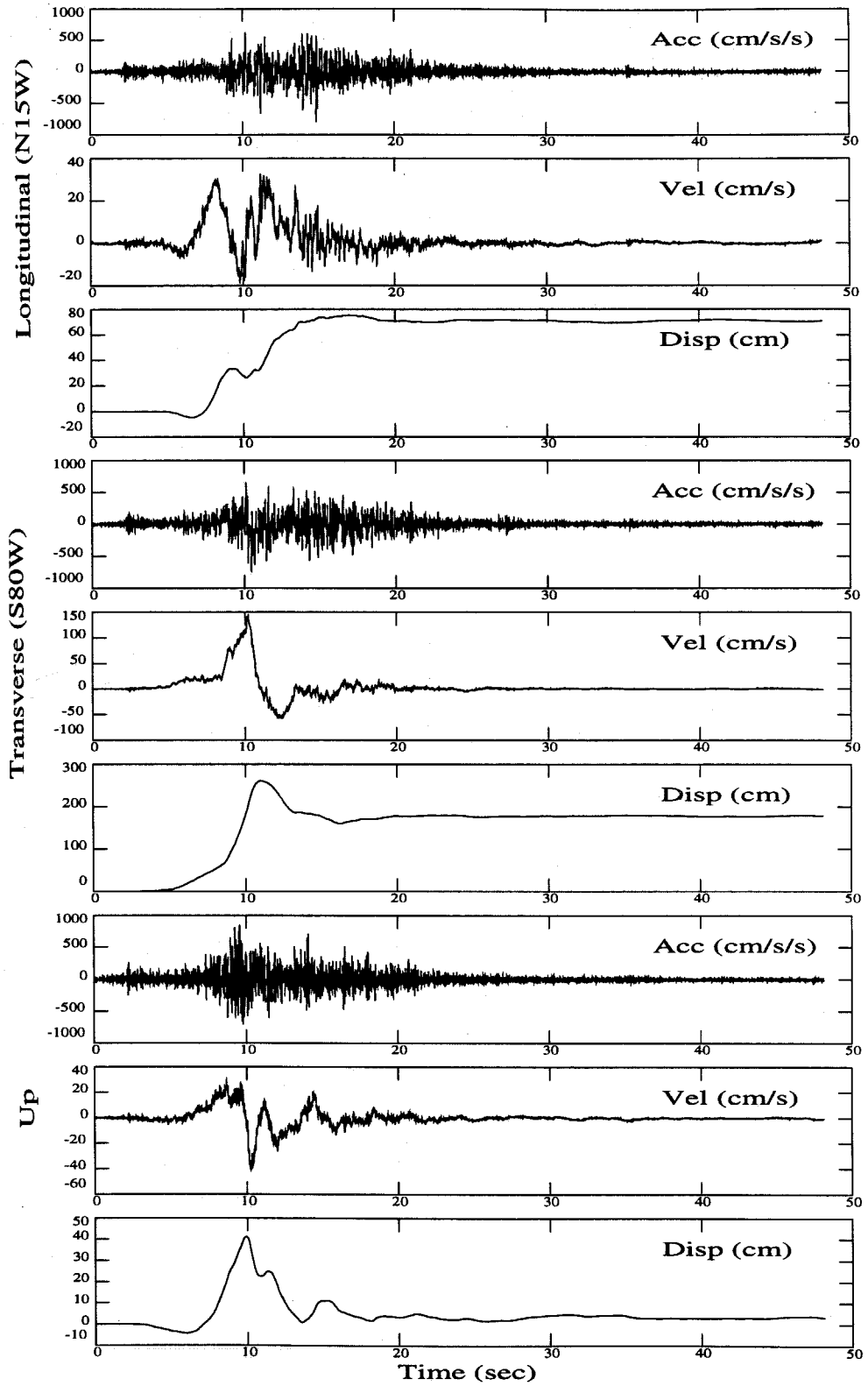

Figure 6.1 Corrected Acceleration, Velocity and Displacement of the Lucerne Valley Record from the Landers Earthquake.

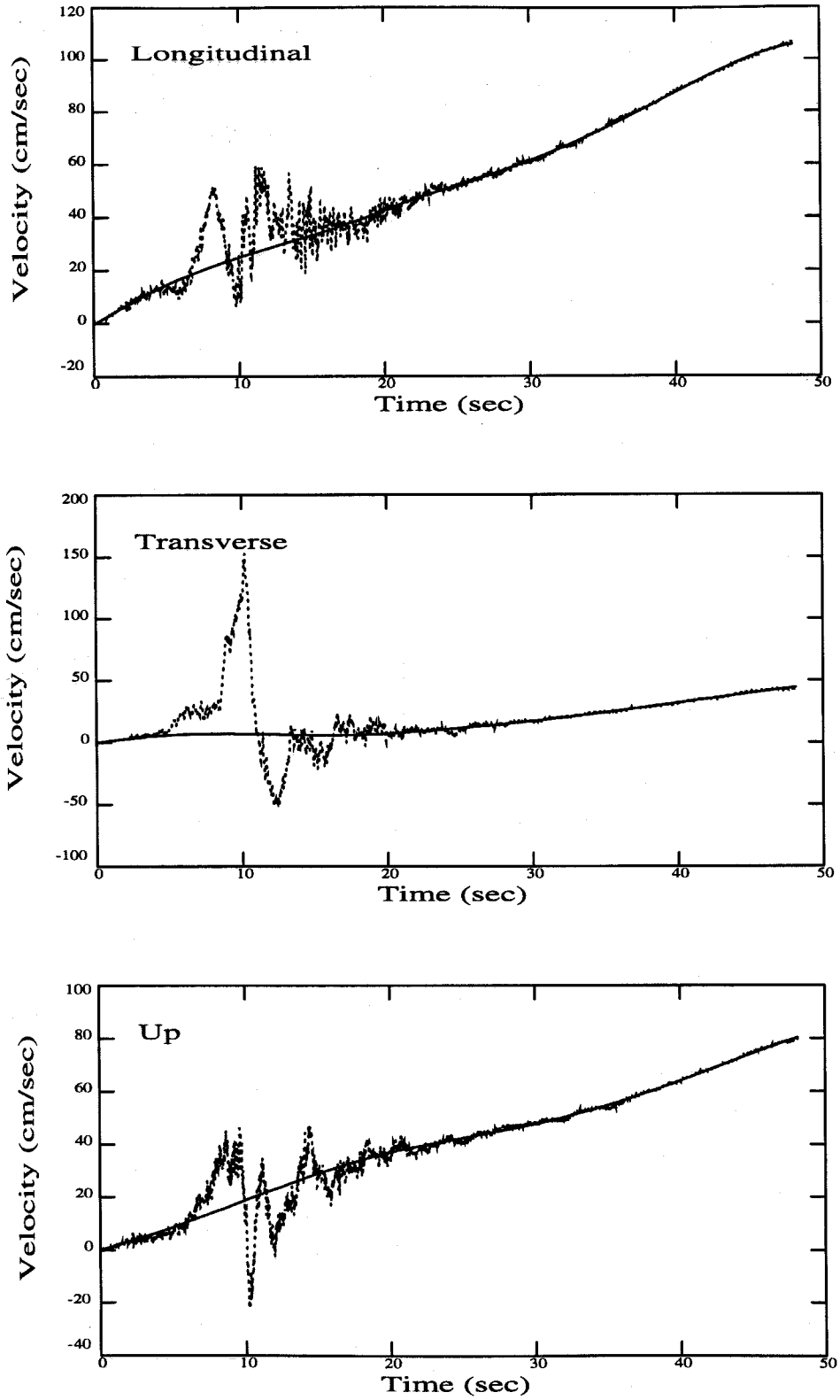

Figure 6.2 Baseline Correction on three Velocity Components of the Lucerne Valley Record. —— Baseline, ····· Velocity Time History.

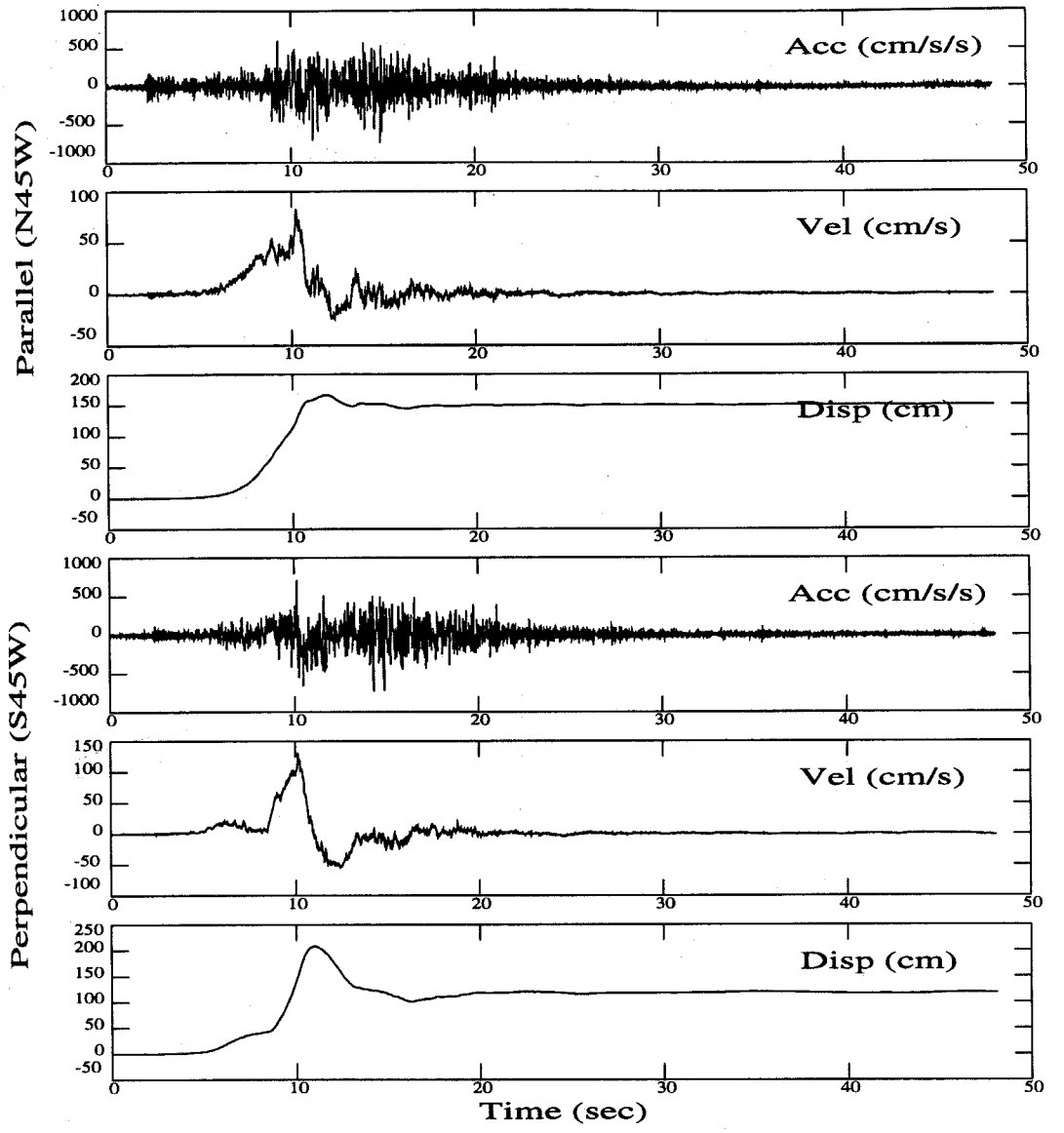

Figure 6.3 Horizontal Components of the Lucerne Valley Record Rotated to the Directions Parallel and Perpendicular to the Fault.

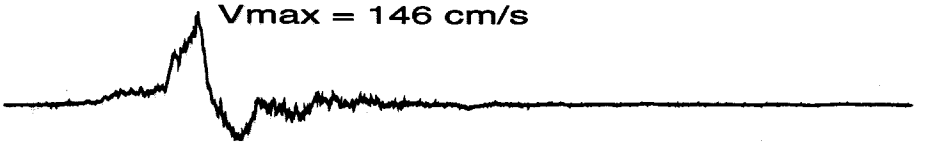

Figure 6.4 Horizontal Maximum Velocity Component (S80°W) of the Lucerne Valley Record.

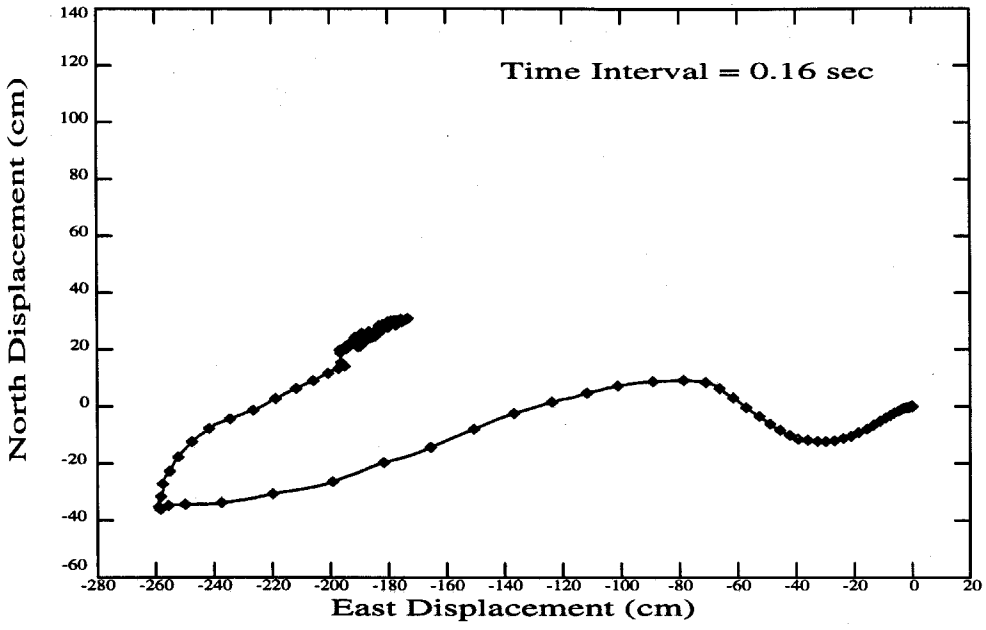

Figure 6.5 Ground Displacement Trajectory of the Lucerne Valley Station.

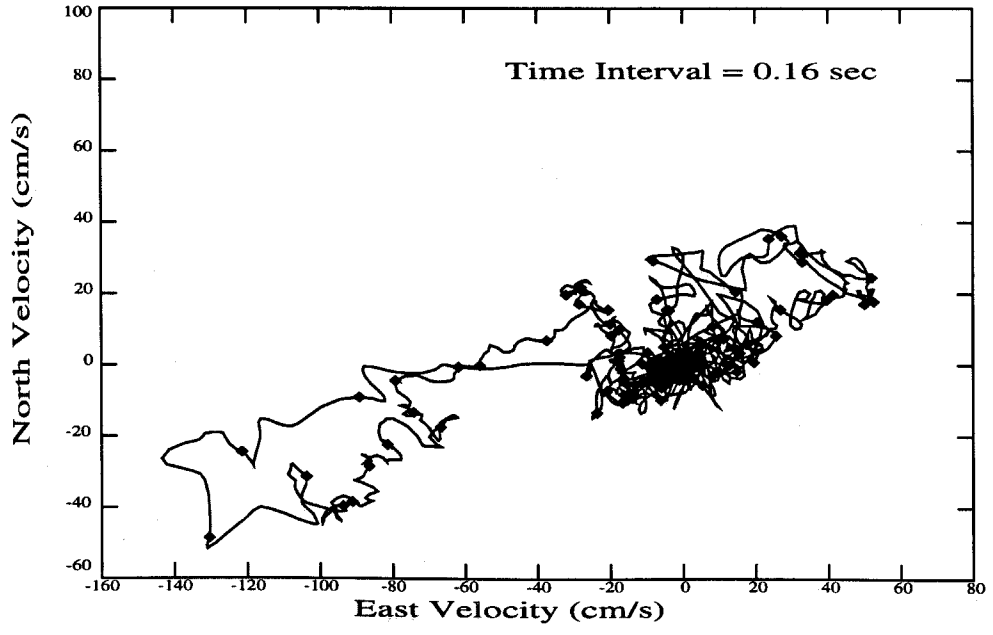

Figure 6.6 Ground Velocity Trajectory of the Lucerne Valley Station.

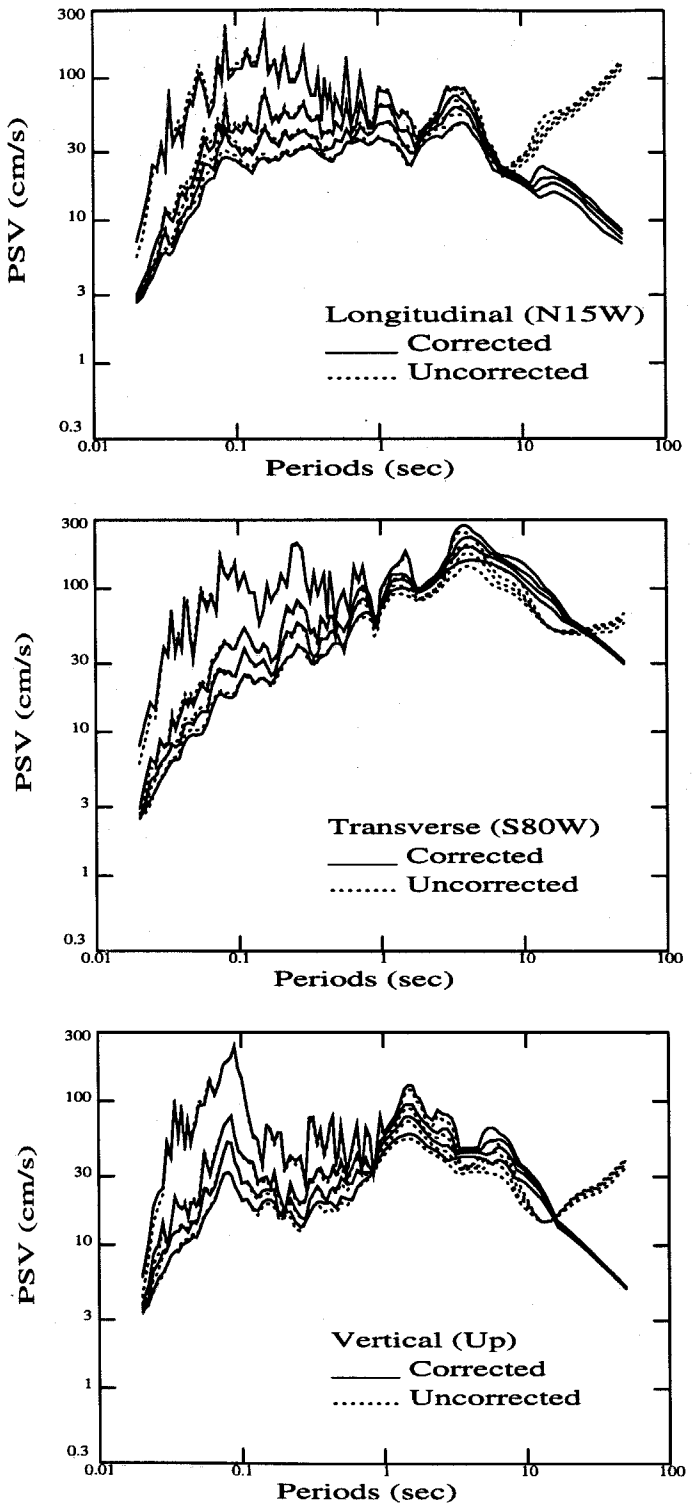

Figure 6.7 Pseudo-Velocity Spectra of the Lucerne Valley Record with Damping Ratio of 0%, 2%, 5%, 10%.
—— Result of the Newly Processed Record,
····· Result of the Uncorrected Record.

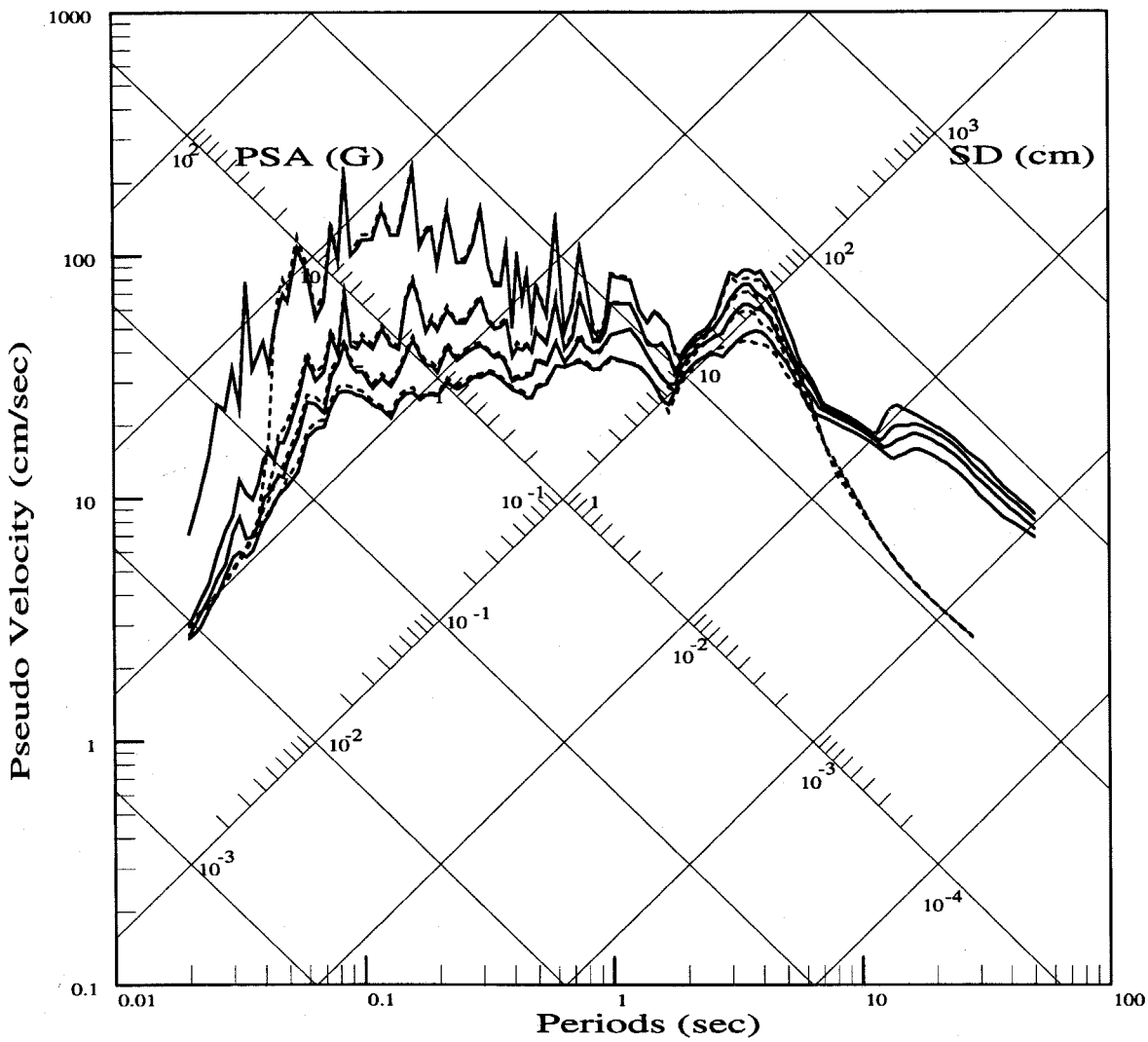

Figure 6.8 Response Spectrum of Longitudinal Component of the Lucerne Valley Record with Damping Ratio of 0%, 2%, 5%, 10%.
—— Result of the Newly Processed Record,
····· Result of the Conventionally Processed Record.

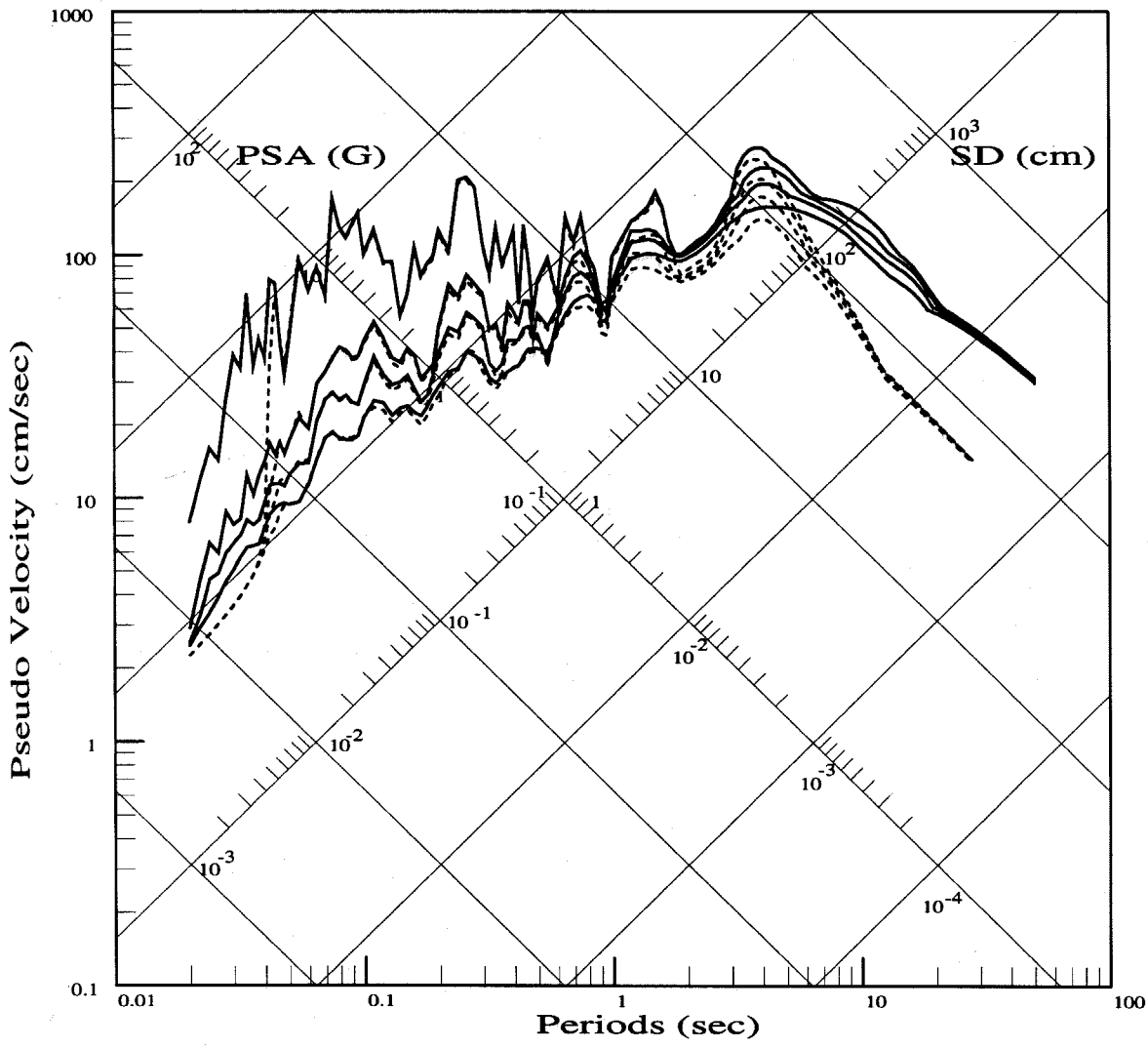

Figure 6.9 Response Spectrum of Transverse Component of the Lucerne Valley Record with Damping Ratio of 0%, 2%, 5%, 10%.
—— Result of the Newly Processed Record,
····· Result of the Conventionally Processed Record.

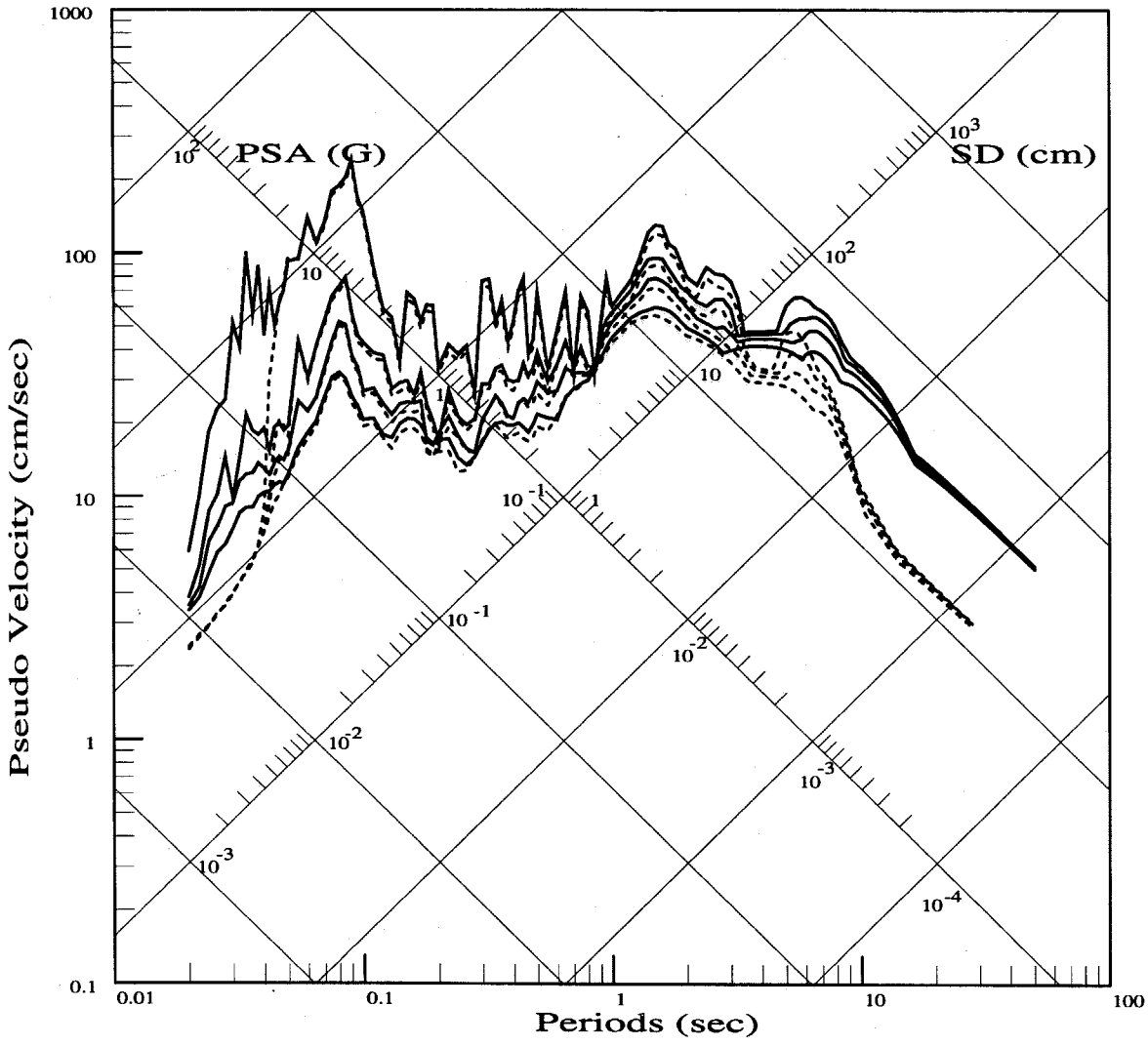

Figure 6.10 Response Spectrum of Vertical Component of the Lucerne Valley Record with Damping Ratio of 0%, 2%, 5%, 10%.
—— Result of the Newly Processed Record,
····· Result of the Conventionally Processed Record.

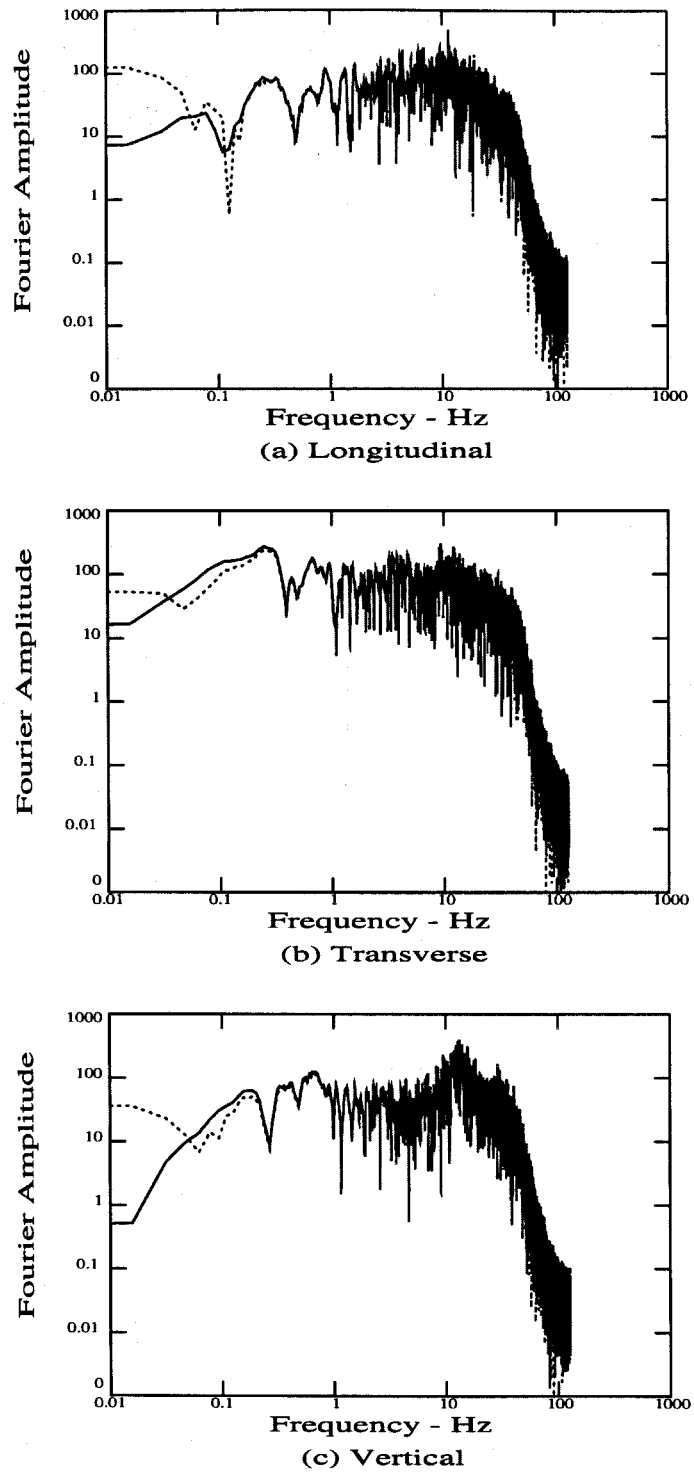

Figure 6.11 Fourier Spectra of the Lucerne Valley Record.
—— Fourier Spectra of the Newly Processed Record,
····· Fourier Spectra of the Uncorrected Record.

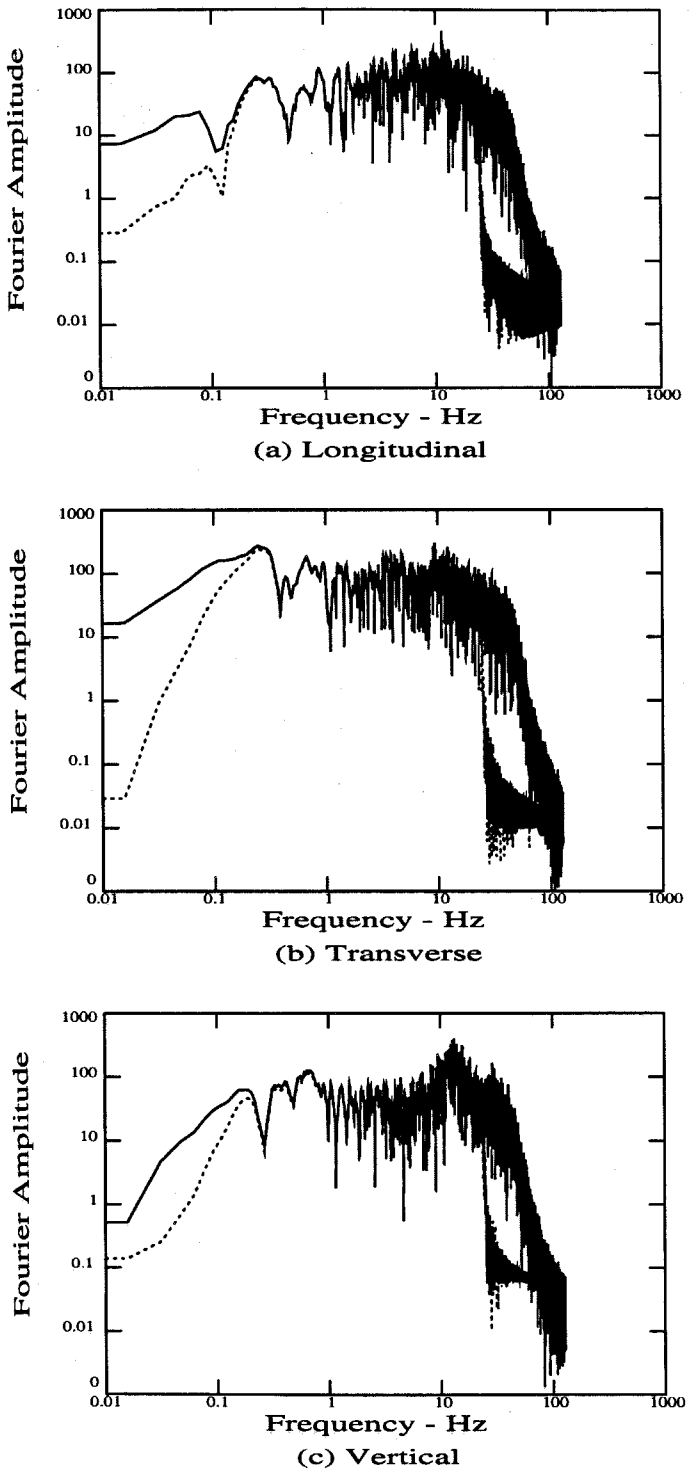

Figure 6.12 Fourier Spectra of the Lucerne Valley Record.
—— Fourier Spectra of the Newly Processed Record,
····· Fourier Spectra of the Conventionally Processed Record.

Chapter 7

Summary and Recommendations

The new data processing method is believed to be better than existing conventional methods in that the new method is developed based on a physical understanding of the earthquake ground motion plus a detailed evaluation of the instrument performance. Earthquake ground motion is rather complex due to many deterministic and indeterministic factors such as faulting type, epicentral or hypocentral distance, station-fault distance, soil condition, and wave path. Recorded strong ground motions, or accelerograms, are also affected by the instrument type and instrument conditions. Therefore, to design a good data processing scheme, one needs to understand the nature of the ground motion as well as the characteristics of the instrument which is used to record the motion. The new data processing scheme is aimed at retaining real information and removing nonphysical trends in the recorded earthquake data, and therefore provides a reliable data for seismologists to pursue ground motion studies as well as for engineers to perform dynamic analysis of the structures response. Since the primary purpose of the study is to provide a basis for engineering analysis, the discussions and the suggestions in the following are focused on engineering applications.

The development of the new data processing scheme was motivated by the need to process accelerograms from near-field ground motions. The applications of the new data processing scheme to simulated earthquake data and the Lucerne Valley record show that it can recover long-period information such as displacement offsets and large pulse-like waves from near-field earthquake records. For an earthquake associated with strike-slip fault, the ground motion near the vicinity of the fault presents a permanent offset along the fault and large pulse-like motion perpendicular

to the fault. For other types of earthquake mechanism, the near-field ground motions are most likely to be combinations of these two types of motions. Therefore, the new data processing scheme should also work for the near-field records from other types of earthquake mechanism. This needs further applications of the method to the various near-field earthquake data. Some refinements for the new data processing method may be needed for different applications, but the basic idea should not be far from the proposed data processing scheme.

It should be pointed out that the instrument correction should be treated differently for different types of transducer, especially for those which do not respond perfectly in the low-frequency range. It is suggested that if the instrument characteristics are unknown, an experimental test on the instrument should be conducted to see whether the instrument response is represented by a standard instrument correction formula. In processing the Lucerne Valley record, the instrument correction formula is different than what has been used in the conventional data processing due to an electro-magnetic tape recording instrument. The integration amplifier in the EMA transducer reduces the amplitudes of long-period waves. It is especially important to consider the effects of integration amplifiers in correcting near-field earthquake records since near-field ground motion may be dominated by long-period components. In conclusion, the new data processing scheme requires that the instrument correction be varied subjected to the instrument type.

As mentioned, the purpose of the study is to develop a new data processing scheme so as to provide reliable ground motion data for structural response studies. Many accomplishments have been made in the past in establishing design criteria that can prevent the collapse of a building during an earthquake. But little has been done for structures to resist an earthquake at a close fault location. Preliminary study has shown that the near-field ground motion has much greater damage potential to structures. To resist near-field ground motion, higher demand design criteria should be implemented. The recent Northridge earthquake ($M_L = 6.4$) on Jan 17, 1994 caused significant damage to the highway system as well as to highly densed residential areas. The earthquake had a blind fault with a fault plane of 10 $\times$ 10 miles, a dipping angle of 35° to 45°, and a fault depth of 3 to 12 miles. Since the earthquake had shallow focus and the fault plane was right underneath the city, numerous structures suffered near-field ground motion. This example tells us that

the study of structural effects of near-field ground motion is an important task for structural engineers and research workers.

The important conclusions obtained from this thesis are included at the end of each chapter. The most important conclusion of this study is: the data processing of the Lucerne Valley record with the proposed data processing method shows that it is now possible to recover long-period information from near-field ground motions. Furthermore, the processed Lucerne Valley record can be used for many structural and earthquake engineering studies. The record is particularly important in the sense that:

1) It is a typical record of near-field ground motion and presents high damage potential to the structures, especially the long-period structures. All the other important records obtained in the past, including the El Centro earthquake record, lack information in the low frequency range.

2) The typical geological behaviors of large displacement and pulse-like motion may generate unexpected large strain in structures, and also cause base-isolated structures to move beyond the displacement control level for the base-isolators. These important investigations would be difficult to perform using earthquake records corrected by the conventional data processing method.

3) Current design criteria may need to be revised to consider the effects of near-field ground motions. The Lucerne Valley record may be used as a basis earthquake to test the safety of a structure in its lifetime.

Finally, future studies based on this investigation are recommended as follows:

1. Application of the new data processing scheme to records from other important earthquakes such as the Northridge earthquake.

Study various fault mechanisms and investigate their geological behaviors during the data processing. If the instrument transducer cannot be simply represented by a SDOF oscillator or as an EMA type transducer, an appropriate instrument correction filter should be derived for instrument correction and the possible error sources introduced by the particular instrument should be considered.

2. Use of processed Lucerne Valley record to study the structural effects of near-field ground motion.

A preliminary study [8] has shown that the pulse-like near-field ground motion is a major contributor to large strain in structures. The large strain energy may cause tremendous shear force in the base of a structure or cause drift between the stories of a high-rise building. To better understand how structures respond to the near-field ground motion, further study and analysis are needed.

3. Use of the processed Lucerne Valley record to study the dynamic behavior of base-isolated structures.

The basic idea of base-isolation is to build a structure on soft isolators so that part of the energy transferred from the earthquake ground motion is absorbed by the isolators and the vibration of the structure is reduced. Since the building is relatively rigid compared to the base-isolators, a base-isolated structure can often be modeled as a SDOF oscillator with very soft springs. When the ground shakes, the motion of the building will lag behind the ground motion due to the inertia of the building mass. The gap between the building and the displacement control barrier should be larger than the maximum displacement of the building during an earthquake. Since near-field ground motion is characterized by large displacement motion, impact of the barrier and the building may be unavoidable for base-isolated structures which are located in the near-field area. Solving this problem needs further investigations.

4. The Lucerne Valley record may also be used to study various dynamic problems such as dynamic response of nonlinear structures, structural control system, and other structural dynamic systems.

References

[1] Richter, Charles Francis, "Elementary Seismology," W.H. Freeman and Company, Inc., San Francisco and London, 1958.

[2] Halverson, Harry T., "The Strong-Motion Seismograph," United ElectronicDynamics, Inc., Pasadena, California, 1963.

[3] Bolt, Bruce A., "Earthquakes, Newly Revised and Expanded," W.H. Freeman and Company, Inc., New York, 1993.

[4] Hartzell, Stephen and Thomas Heaton, "Earthquake Ground Motion at Close Distance," EERI/STANFORD/USGS Workshop, Stanford University, Sep.5 and 6, California, 1990.

[5] Heaton, Thomas H., "Overview of Seismological Methods for the Synthesis of Strong Ground Motion," Unpublished Notes, U.S. Geological Survey, Pasadena, California, 1992.

[6] Heaton, Thomas H., and Stephen H. Hartzell, "Earthquake Ground Motions," Ann. Rev. Earth Planet. Sci. 16:121-145, 1988.

[7] Heaton, Thomas H., "Generalized Ray Models of Strong Ground Motion," Ph.D. Thesis, California Institute of Technology, Pasadena, California, 1978.

[8] Iwan, Wilfred D. and Xiaodong Chen, Summer Research (Unpublished Notes), California Institute of Technology, Pasadena, California, 1991.

[9] Sieh, Kerry et al., "Near-Field Investigations of the Landers Earthquake Sequence, April to July 1992," Science, Vol. 260, pp. 171-176 April 9, 1993.

[10] Hart, Earl W., William A. Bryant, and Jerome A. Treiman, "Surface Faulting Associated with the June 1992 Landers Earthquake, California," California Geology January/February, pp. 10-16, 1993.

[11] Trifunac, M. D. and V. Lee, "Routine Computer Processing of Strong-Motion Accelerograms," Report No. EERL 73-03, Earthquake Engineering Research Laboratory, California Institute of Technology, Pasadena, California, 1973.

[12] Dullien, Robert C., "Laboratory Evaluation of the SMA-2 Magnetic Tape-type Strong Motion Accelerograph," Earthquake Engineering Research Laboratory, California Institute of Technology, Pasadena, California, 1972.

[13] Hudson, D. E., "History of Accelerograph Development," *Proceedings of the Golden Anniversary Workshop on Strong Motion Seismometry*, pp. 29-56, 1983.

[14] Cloud, William K., "Early Days of Strong Motion Seismometry in the United States," *Proceedings of the Golden Anniversary Workshop on Strong-Motion Seismometry*, pp. 25-28, 1983.

[15] Hudson, D. E., "Strong Motion Instrumentation Systems," *Proceedings of the Golden Anniversary Workshop on Strong-Motion Seismometry*, pp. 73-85, 1983.

[16] Hudson, D. E., "Strong-Motion Accelerograph Systems – Problems and Prospects," *Proceedings of the 8th World Conference on Earthquake Engineering*, Vol. II, pp. 39-45, 1984.

[17] Hudson, D. E., "Design of Strong-Motion Instruments, Networks and Arrays," *Proceedings of the Seventh European Conference on Earthquake Engineering, Athens, Greece*, pp. 153-160, 1982.

[18] Amini, Ali and Trifunac, M. "Analysis of a Feedback Transducer,"Report No. 83-03, Civil Engineering Department, University of Southern California, Los Angeles, California, 1983.

[19] Kinemetrics, Inc., "Model SMA-2 Strong Motion Accelerograph, Operation and Field Service," Kinemetrics, Pasadena, California, 1989.

[20] Rihn, W. J., "Magnetic Tape Recording And Processing of Strong-Motion Data," *Proceedings: Fifth World Conference on Earthquake Engineering*, Vol. I, pp. 1069-1072, 1974.

[21] Hudson, D.E. Unpublished Lecture Notes, Earthquake Engineering Research Laboratory, California Institute of Technology, Pasadena, California, 1979.

[22] Kinemetrics Document, "Conditioning and Correction of Strong Motion Data on Analogy Magnetic Tapes," No. 7, Pasadena, California, February 1986.

[23] Hudson, D. E., A. G. Brady, M. D. Trifunac and A. Vijayaraghavan, "Strong-Motion Earthquake Accelerograms, Volume II-Corrected Accelerograms and Integrated Ground Velocity and Displacement Curves," Report No. EERL 71-50, Earthquake Engineering Research Laboratory, California Institute of Technology, Pasadena, California, 1971.

[24] Lee, V. W. and M. D. Trifunac, "Current Development in Data Processing of Strong-Motion Accelerograms," Report No. 84-01, Civil Engineering Department, University of Southern California, Los Angeles, California, 1984.

[25] Lee, V. W., "Recent Development in Data Processing of Strong-Motion Accelerograms," *Proceedings of the 8th World Conference on Earthquake Engineering,* Vol. II, pp. 119-126, 1984.

[26] Amini, A., M.D. Trifunac and R.L. Nigbor, "A Note on the Noise Amplitudes in Some Strong Motion Accelerographs," *Soil Dynamics and Earthquake Engineering,* Vol. 6, No. 3, pp. 180-185, 1987.

[27] Hudson, D. E., "Reading and Interpreting Strong Motion Accelerograms," Monograph, Earthquake Engineering Research Institute, Berkeley, California, 1979.

[28] Trifunac, M. D., "Preliminary Empirical Model for Scaling Fourier Amplitude Spectra of Strong Ground Motion in Terms of Earthquake Magnitude, Source to Station Distance, and Recording Site Conditions," BSSA, Vol. 6, No. 4, August 1976.

[29] Kinemetrics, Inc., "SMP-1 Acceptance Test," Serial Number 259, Pasadena, California, 1992.

[30] Kinemetrics, Inc., "Channel Calibration of Magnetic Tape Playback Model SMP-1," Serial Number 136, Pasadena, California, 1992.

[31] Kinemetrics, Inc., "Surveillance Procedure Data Sheet, Channel Calibration of Triaxial Time-history Accelerograph," Kinemetrics Inc., Model SMA-2 (with electromagnetic accelerometers), Pasadena, California, July 14, 1992.

[32] Trifunac, M. D. and V. W. Lee, "Automatic Digitization and Processing of Strong Motion Accelerograms," Report No. 79-15, Civil Engineering Department, University of Southern California, Los Angeles, California, 1979.

[33] Iwan, W. D., "Characteristics of Digital Strong Motion Accelerographs," *Proceedings of International Workshop on Earthquake Engineering*, Shanghai, China, March 27-31, Vol. I, pp. A-19, 1984.

[34] Berg, G. V. and Housner, G. W., "Integrated Velocity and Displacement of Strong Earthquake Ground Motion," *Bulletin of Seismological Society of America*, Vol. 51, pp. 175-189, 1961.

[35] Brady, A. G. "Studies of Response to Earthquake Ground Motion," Ph. D. Thesis, Civil Engineering Department, California Institute of Technology, Pasadena, California, 1966.

[36] Trifunac, M. D., "Low Frequency Digitization Errors and New Method for Zero Baseline Correction of Strong-Motion Accelerograms," Report No. EERL 70-07, Earthquake Engineering Research Laboratory, California Institute of Technology, Pasadena, California, 1970.

[37] Trifunac, M. D., F. E. Udwdia and A. G. Brady, "High Frequency Errors and Instrument Corrections of Strong-Motion Accelerograms," Report No. EERL 71-05, Earthquake Engineering Research Laboratory, California Institute of Technology, Pasadena, California, 1971.

[38] Sunder S. S. and Jerome J. Connor, "A New Procedure for Processing Strong-Motion Earthquake Signals," *Bulletin of the Seismological Society of America.* Vol. 72, No. 2, pp. 643-661, April 1982.

[39] Sunder, S. S., "On the Standard Processing of Strong-Motion Earthquake Signals," Ph. D. Thesis, Research Report R80-38, School of Engineering, Massachusetts Institute of Technology, Cambridge, Massachusetts, 1980.

[40] Converse, A. M., A. G. Brady and W. B. Joyner, "Improvement In Strong-Motion Data Processing Procedures," *Proceedings of the 8th World Conference on Earthquake Engineering*, Vol. II, pp. 143-148, 1984.

[41] Levine, M-B. P., "Accelerogram Processing Using Reliability Bounds and Optimal Correction Methods," Report No. EERL 90-02, Earthquake Engineering Research Laboratory, California Institute of Technology, Pasadena, California, 1990.

[42] Stephens, J. E. and J. T. P. Yao, "Data Processing of Earthquake Acceleration Records," *Structural Engineering*, CE-STR, 85-5, 1985.

[43] Iwan, W. D., A. Moser and Chia-yen Peng, "Some Observations on Strong Motion Earthquake Measurement Using a Digital Accelerograph," *Bulletin of the Seismological Society of America*, Vol. 75, No. 5, pp. 1225-1246, 1985.

[44] Brigham, E. Oran, "The Fast Fourier Transform and Its Applications," Prentice-Hall, Inc., New Jersey, 1988.

CALIFORNIA INSTITUTE OF TECHNOLOGY

Reports Published by

Earthquake Engineering Research Laboratory
Disaster Research Center
Dynamics Laboratory
Soil Mechanics Laboratory

Reports with prices are available for purchase from:

Earthquake Engineering Research Library
Mail Stop 104-44
California Institute of Technology
Pasadena, California 91125 USA

Prepayment is required. Overseas orders please include shipping and handling charges of $3.00 per title.

Notes: N/A indicates that the report is no longer available for purchase from EERL.

(PB–) are Accession Numbers assigned by the National Technical Information Service (NTIS) and may be ordered through NTIS at 5285 Port Royal Road, Springfield, Virginia, 22161. For information about NTIS pricing, contact that address. The Caltech price is unrelated to that charged by NTIS.

Items marked N/A without PB- numbers are available only via interlibrary loan to the address above.

Earthquake Engineering Research Laboratory (EERL)

EERL 70–01	Trifunac, M.D., "Wind and Microtremor Induced Vibrations of a Twenty-Two Story Steel Frame Building," 1970.	5.00
EERL 70–02	Trifunac, M.D., "Ambient Vibration Tests of a Thirty-Nine Story Steel Frame Building," 1970.	4.50
EERL 70–03	Trifunac, M.D., "On the Statistics and Possible Triggering Mechanism of Earthquakes in Southern California," 1970.	6.00
EERL 70–04	Trifunac, M.D. and D.E. Hudson, "Laboratory Evaluations and Instrument Corrections of Strong-Motion Accelerographs," 1970.	11.50
EERL 70–05	Keightley, W.O., "A Strong-Motion Accelerograph Array with Telephone Line Interconnections," 1970.	4.00
EERL 70–06	Trifunac, M.D., "Response Envelope Spectrum and Interpretation of Strong Earthquake Ground Motion," 1970.	2.50
EERL 70–07	Trifunac, M.D., "Low Frequency Digitization Errors and a New Method for Zero Baseline Correction of Strong-Motion Accelerograms," 1970.	6.00
EERL 70-20	Strong-Motion Earthquake Accelerograms, Digitized and Plotted Data. Volume I: Uncorrected Accelerograms, part A. (PB 287 847)	N/A
EERL 70-21	Strong-Motion Earthquake Accelerograms, Digitized and Plotted Data. Volume I: Uncorrected Accelerograms, part B. (PB 196 823)	N/A
EERL 71–01	Jennings, P.C., R.B. Mathiesen and J.B. Hoerner, "Forced Vibrations of a 22-Story Steel Frame Building," 1971. (PB 205 161)	N/A
EERL 71–02	Jennings, P.C., "Engineering Features of the San Fernando Earthquake of February 9, 1971," 1971. (PB 202 550)	52.00
EERL 71–03	Adu, R.A., "Response and Failure of Structures Under Stationary Random Excitation," 1971. (PB 205 304)	N/A
EERL 71–04	Bielak, J., "Earthquake Response of Building-Foundation Systems," 1971. (PB 205 305)	N/A
EERL 71–05	Trifunac, M.D., F.E. Udwadia and A.G. Brady, "High Frequency Errors and Instrument Corrections of Strong-Motion Accelerograms," 1971. (PB 205 369)	5.00
EERL 71–06	Skattum, K.S., "Dynamic Analysis of Coupled Shear Walls and Sandwich Beams," 1971. (PB 205 267)	N/A
EERL 71–07	Hoerner, J.B., "Model Coupling and Earthquake Response of Tall Buildings," 1971. (PB 207 635)	16.50
EERL 71-20	Strong-Motion Earthquake Accelerograms, Digitized and Plotted Data. Volume I: Uncorrected Accelerograms, part C. (PB 204 364)	N/A
EERL 71-21	Strong-Motion Earthquake Accelerograms, Digitized and Plotted Data. Volume I: Uncorrected Accelerograms, part D. (PB 208 529)	N/A
EERL 71-22	Strong-Motion Earthquake Accelerograms, Digitized and Plotted Data. Volume I: Uncorrected Accelerograms, part E. (PB 209 749)	N/A
EERL 71-23	Strong-Motion Earthquake Accelerograms, Digitized and Plotted Data. Volume I: Uncorrected Accelerograms, part F. (PB 210 619)	N/A

EERL 71-50	Strong-Motion Earthquake Accelerograms, Digitized and Plotted Data. Volume II: Corrected Accelerograms and Integrated Ground Velocity and Displacement Curves, part A. (PB 208 283)	N/A
EERL 72–001	Jennings, P.C. and J. Bielak, "Dynamics of Building-Soil Interaction," 1972. (PB 209 666)	N/A
EERL 72–002	Udwadia, F.E., "Investigation of Earthquake and Microtremor Ground Motions," 1972. (PB 212 853)	15.50
EERL 72–004	Wood, J.H., "Analysis of the Earthquake Response of a Nine-Story Steel Frame Building During the San Fernando Earthquake," 1972. (PB 215 823)	15.50
EERL 72–005	Jennings, P.C., "Rapid Calculation of Selected Fourier Spectrum Ordinates," 1972.	3.50
EERL 72-020	Strong-Motion Earthquake Accelerograms, Digitized and Plotted Data. Volume I: Uncorrected Accelerograms, part G. (PB 211 357)	N/A
EERL 72-021	Strong-Motion Earthquake Accelerograms, Digitized and Plotted Data. Volume I: Uncorrected Accelerograms, part H. (PB 211 781)	N/A
EERL 72-022	Strong-Motion Earthquake Accelerograms, Digitized and Plotted Data. Volume I: Uncorrected Accelerograms, part I. (PB 213 422)	N/A
EERL 72-023	Strong-Motion Earthquake Accelerograms, Digitized and Plotted Data. Volume I: Uncorrected Accelerograms, part J. (PB 213 423)	N/A
EERL 72-024	Strong-Motion Earthquake Accelerograms, Digitized and Plotted Data. Volume I: Uncorrected Accelerograms, part K. (PB 213 424)	N/A
EERL 72-025	Strong-Motion Earthquake Accelerograms, Digitized and Plotted Data. Volume I: Uncorrected Accelerograms, part L. (PB 215 639)	N/A
EERL 72-026	Strong-Motion Earthquake Accelerograms, Digitized and Plotted Data. Volume I: Uncorrected Accelerograms, part M. (PB 220 554)	N/A
EERL 72-027	Strong-Motion Earthquake Accelerograms, Digitized and Plotted Data. Volume I: Uncorrected Accelerograms, part N. (PB 223 023)	N/A
EERL 72-033	Strong-Motion Earthquake Accelerograms, Digitized and Plotted Data. Volume I: Uncorrected Accelerograms, part Q. (PB 232 315/AS)	N/A
EERL 72-050	Strong-Motion Earthquake Accelerograms, Digitized and Plotted Data. Volume II: Corrected Accelerograms and Integrated Ground Velocity and Displacement Curves, part B. (PB 220 161)	N/A
EERL 72-051	Strong-Motion Earthquake Accelerograms, Digitized and Plotted Data. Volume II: Corrected Accelerograms and Integrated Ground Velocity and Displacement Curves, part C. (PB 220 162)	N/A
EERL 72-052	Strong-Motion Earthquake Accelerograms, Digitized and Plotted Data. Volume II: Corrected Accelerograms and Integrated Ground Velocity and Displacement Curves, part D. (PB 220 836)	N/A
EERL 72-080	Analyses of Strong-Motion Earthquake Accelerograms, Volume III: Response Spectra. Part A. (PB 212 602)	N/A
EERL 72-100	Analyses of Strong-Motion Earthquake Accelerograms, Volume IV: Fourier Amplitude Spectra. Part A. (PB 212 603)	N/A
EERL 73–001	Udwadia, F.E. and M.D. Trifunac, "The Fourier Transform, Response Spectra and Their Relationship Through the Statistics of Oscillator Response," 1973. (PB 220 458)	8.00
EERL 73–002	"Research Papers Submitted to Fifth World Conference on Earthquake Engineering, Rome, Italy, 25–29 June 1973," 1973. (PB 220 431)	11.00
EERL 73–003	Trifunac, M.D. and V. Lee, "Routine Computer Processing of Strong-Motion Accelerograms," 1973. (PB 226 047/AS)	N/A
EERL 73–004	Crouse, C.B., "Engineering Studies of the San Fernando Earthquake," 1973.	16.00
EERL 73–005	Wood, J.H., "Earthquake-Induced Soil Pressures on Structures," 1973.	33.00
EERL 73–006	Irvine, H.M., "The Veracruz Earthquake of 28 1973," 1973.	4.50
EERL 73–007	Iemura, H. and P.C. Jennings, "Hysteretic Response of a Nine-Story Reinforced Concrete Building During the San Fernando Earthquake," 1973.	6.00
EERL 73-020	Strong-Motion Earthquake Accelerograms, Digitized and Plotted Data. Volume I: Uncorrected Accelerograms, part O. (PB 222 417)	N/A
EERL 73-021	Strong-Motion Earthquake Accelerograms, Digitized and Plotted Data. Volume I: Uncorrected Accelerograms, part P. (PB 227 481/AS)	N/A
EERL 73-023	Strong-Motion Earthquake Accelerograms, Digitized and Plotted Data. Volume I: Uncorrected Accelerograms, part R. (PB 239 585/AS)	N/A
EERL 73-024	Strong-Motion Earthquake Accelerograms, Digitized and Plotted Data. Volume I: Uncorrected Accelerograms, part S. (PB 241 551/AS)	N/A
EERL 73-025	Strong-Motion Earthquake Accelerograms, Digitized and Plotted Data. Volume I: Uncorrected Accelerograms, part T. (PB 241 943/AS)	N/A
EERL 73-026	Strong-Motion Earthquake Accelerograms, Digitized and Plotted Data. Volume I: Uncorrected Accelerograms, part U. (PB 242 252/AS)	N/A
EERL 73-027	Strong-Motion Earthquake Accelerograms, Digitized and Plotted Data. Volume I: Uncorrected Accelerograms, part V. (PB 243 483/AS)	N/A
EERL 73-028	Strong-Motion Earthquake Accelerograms, Digitized and Plotted Data. Volume I: Uncorrected Accelerograms, part W. (PB 243 497/AS)	N/A
EERL 73-029	Strong-Motion Earthquake Accelerograms, Digitized and Plotted Data. Volume I: Uncorrected Accelerograms, part X. (PB 243 594/AS)	N/A

EERL 73-030	Strong-Motion Earthquake Accelerograms, Digitized and Plotted Data. Volume I: Uncorrected Accelerograms. part Y. (PB 242 947/AS)	N/A
EERL 73-050	Strong-Motion Earthquake Accelerograms, Digitized and Plotted Data. Volume II: Corrected Accelerograms and Integrated Ground Velocity and Displacement Curves, part E. (PB 223 024)	N/A
EERL 73-051	Strong-Motion Earthquake Accelerograms, Digitized and Plotted Data. Volume II: Corrected Accelerograms and Integrated Ground Velocity and Displacement Curves, part F. (PB 224 977/9AS)	N/A
EERL 73-052	Strong-Motion Earthquake Accelerograms, Digitized and Plotted Data. Volume II: Corrected Accelerograms and Integrated Ground Velocity and Displacement Curves, part G. (PB 229 239/AS)	N/A
EERL 73-080	Analyses of Strong-Motion Earthquake Accelerograms, Volume III: Response Spectra. part B. (PB 221 256)	N/A
EERL 73-081	Analyses of Strong-Motion Earthquake Accelerograms, Volume III: Response Spectra. part C. (PB 223 025)	N/A
EERL 73-082	Analyses of Strong-Motion Earthquake Accelerograms, Volume III: Response Spectra. part D. (PB 227 469/AS)	N/A
EERL 73-083	Analyses of Strong-Motion Earthquake Accelerograms, Volume III: Response Spectra. part E. (PB 227 470/AS)	N/A
EERL 73-084	Analyses of Strong-Motion Earthquake Accelerograms, Volume III: Response Spectra. part F. (PB 227 471/AS)	N/A
EERL 73-085	Analyses of Strong-Motion Earthquake Accelerograms, Volume III: Response Spectra. part G. (PB 231 223/AS)	N/A
EERL 73-100	Analyses of Strong-Motion Earthquake Accelerograms, Volume IV: Fourier Amplitude Spectra. Part B. (PB 220 837)	N/A
EERL 73-101	Analyses of Strong-Motion Earthquake Accelerograms, Volume IV: Fourier Amplitude Spectra. Part C. (PB 222 514)	N/A
EERL 73-102	Analyses of Strong-Motion Earthquake Accelerograms, Volume IV: Fourier Amplitude Spectra. Part D. (PB 222 969/AS)	N/A
EERL 73-103	Analyses of Strong-Motion Earthquake Accelerograms, Volume IV: Fourier Amplitude Spectra. Part E. (PB 229 240/AS)	N/A
EERL 73-104	Analyses of Strong-Motion Earthquake Accelerograms, Volume IV: Fourier Amplitude Spectra. Part F. (PB 229 241/AS)	N/A
EERL 73-105	Analyses of Strong-Motion Earthquake Accelerograms, Volume IV: Fourier Amplitude Spectra. Part G. (PB 231 224/AS)	N/A
EERL 74-001	Jephcott, D.K. and D.E. Hudson, "The Performance of Public School Plants During the San Fernando Earthquake," 1974. (PB 240 000/AS)	27.50
EERL 74-050	Strong-Motion Earthquake Accelerograms, Digitized and Plotted Data. Volume II: Corrected Accelerograms and Integrated Ground Velocity and Displacement Curves, part H. (PB 231 225/AS)	N/A
EERL 74-051	Strong-Motion Earthquake Accelerograms, Digitized and Plotted Data. Volume II: Corrected Accelerograms and Integrated Ground Velocity and Displacement Curves, part I. (PB 232 316/AS)	N/A
EERL 74-052	Strong-Motion Earthquake Accelerograms, Digitized and Plotted Data. Volume II: Corrected Accelerograms and Integrated Ground Velocity and Displacement Curves, part J, K. (PB 233 257/AS)	N/A
EERL 74-053	Strong-Motion Earthquake Accelerograms, Digitized and Plotted Data. Volume II: Corrected Accelerograms and Integrated Ground Velocity and Displacement Curves, part L, M. (PB 237 174/AS)	N/A
EERL 74-054	Strong-Motion Earthquake Accelerograms, Digitized and Plotted Data. Volume II: Corrected Accelerograms and Integrated Ground Velocity and Displacement Curves, part N. (PB 236 399/AS)	N/A
EERL 74-055	Strong-Motion Earthquake Accelerograms, Digitized and Plotted Data. Volume II: Corrected Accelerograms and Integrated Ground Velocity and Displacement Curves, part O, P. (PB 239 586/AS)	N/A
EERL 74-056	Strong-Motion Earthquake Accelerograms, Digitized and Plotted Data. Volume II: Corrected Accelerograms and Integrated Ground Velocity and Displacement Curves, part Q, R. (PB 239 587/AS)	N/A
EERL 74-057	Strong-Motion Earthquake Accelerograms, Digitized and Plotted Data. Volume II: Corrected Accelerograms and Integrated Ground Velocity and Displacement Curves, part S. (PB 241 552/AS)	N/A
EERL 74-080	Analyses of Strong-Motion Earthquake Accelerograms, Volume III: Response Spectra. part H. (PB 231 319/AS)	N/A
EERL 74-082	Analyses of Strong-Motion Earthquake Accelerograms, Volume III: Response Spectra. part J, K, L. (PB 236 110/AS)	N/A
EERL 74-083	Analyses of Strong-Motion Earthquake Accelerograms, Volume III: Response Spectra. part M, N. (PB 236 400/AS)	N/A
EERL 74-085	Analyses of Strong-Motion Earthquake Accelerograms, Volume III: Response Spectra. part Q, R. (PB 240 688/AS)	N/A
EERL 74-086	Analyses of Strong-Motion Earthquake Accelerograms, Volume III: Response Spectra. part S. (PB 241 553/AS)	N/A
EERL 74-100	Analyses of Strong-Motion Earthquake Accelerograms, Volume IV: Fourier Amplitude Spectra. Part H. (PB 232 327/AS)	N/A
EERL 74-101	Analyses of Strong-Motion Earthquake Accelerograms, Volume IV: Fourier Amplitude Spectra. Part I. (PB 232 328/AS)	N/A
EERL 74-102	Analyses of Strong-Motion Earthquake Accelerograms, Volume IV: Fourier Amplitude Spectra. Part J, K, L, M. (PB 236 111/AS)	N/A
EERL 74-103	Analyses of Strong-Motion Earthquake Accelerograms, Volume IV: Fourier Amplitude Spectra. Part N, O, P. (PB 238 447/AS)	N/A
EERL 74-104	Analyses of Strong-Motion Earthquake Accelerograms, Volume IV: Fourier Amplitude Spectra. Part Q, R, S. (PB 241 554/AS)	N/A
EERL 74-081	Analyses of Strong-Motion Earthquake Accelerograms, Volume III: Response Spectra. part I. (PB 232 326/AS)	N/A
EERL 74-084	Analyses of Strong-Motion Earthquake Accelerograms, Volume III: Response Spectra. part O, P. (PB 238 102/AS)	N/A

EERL 75–001	Wong, H.L., "Dynamic Soil-Structure Interaction," 1975. (PB 247 233/AS)	N/A
EERL 75–002	Foutch, D.A., G.W. Housner and P.C. Jennings, "Dynamic Responses of Six Multistory Buildings During the San Fernando Earthquake," 1975. (PB 248 144/AS)	11.00
EERL 75–003	Miller, R.K., "The Steady-State Response of Multidegree-of-Freedom Systems with a Spatially Localized Nonlinearity," 1975. (PB 252 459/AS)	20.50
EERL 75-050	Strong-Motion Earthquake Accelerograms, Digitized and Plotted Data. Volume II: Corrected Accelerograms and Integrated Ground Velocity and Displacement Curves, part T. (PB 242 433/AS)	N/A
EERL 75-051	Strong-Motion Earthquake Accelerograms, Digitized and Plotted Data. Volume II: Corrected Accelerograms and Integrated Ground Velocity and Displacement Curves, part U. (PB 242 949/AS)	N/A
EERL 75-052	Strong-Motion Earthquake Accelerograms, Digitized and Plotted Data. Volume II: Corrected Accelerograms and Integrated Ground Velocity and Displacement Curves, part V. (PB 242 948/AS)	N/A
EERL 75-053	Strong-Motion Earthquake Accelerograms, Digitized and Plotted Data. Volume II: Corrected Accelerograms and Integrated Ground Velocity and Displacement Curves, part W,Y. (PB 243 719)	N/A
EERL 75-080	Analyses of Strong-Motion Earthquake Accelerograms, Volume III: Response Spectra. part T. (PB 243 698/AS)	N/A
EERL 75-081	Analyses of Strong-Motion Earthquake Accelerograms, Volume III: Response Spectra. part U. (PB 242 940/AS)	N/A
EERL 75-082	Analyses of Strong-Motion Earthquake Accelerograms, Volume III: Response Spectra. part V. (PB 242 951/AS)	N/A
EERL 75-083	Analyses of Strong-Motion Earthquake Accelerograms, Volume III: Response Spectra. part W, Y. (PB 243 492/AS)	N/A
EERL 75-100	Analyses of Strong-Motion Earthquake Accelerograms, Volume IV: Fourier Amplitude Spectra. Part T,U. (PB 243 493/AS)	N/A
EERL 75-101	Analyses of Strong-Motion Earthquake Accelerograms, Volume IV: Fourier Amplitude Spectra. Part V,W,Y. (PB 243 494/AS)	N/A
EERL 76–01	Abdel-Ghaffar, A.M., "Dynamic Analyses of Suspension Bridge Structures," 1976. (PB 258 744/AS)	37.00
EERL 76–02	"Strong Motion Earthquake Accelerograms Index Volume," Earthquake Engineering Research Laboratory, 1976. (PB 260 929/AS)	7.50
EERL 76–03	Foutch, D.A., "A Study of the Vibrational Characteristics of Two Multistory Buildings," 1976. (PB 260 874/AS)	21.00
EERL 76–04	Spanos, P-T.D., "Linearization Techniques for Non-Linear Dynamical Systems," 1976. (PB 266 083/AS)	16.50
EERL 77–01	Abdel-Ghaffar, A.M. and G.W. Housner, "An Analysis of the Dynamic Characteristics of a Suspension Bridge by Ambient Vibration Measurements," 1977. (PB 275 063/AS)	8.50
EERL 77–02	Abdel-Ghaffar, A.M., "Studies of the Effect of Differential Motions of Two Foundations upon the Response of the Superstructure of a Bridge," 1977. (PB 271 095/AS)	9.50
EERL 77–03	Gates, N.C., "The Earthquake Response of Deteriorating Systems," 1977. (PB 271 090/AS)	14.00
EERL 77–05	Abdel-Ghaffar, A.M., "Engineering Data and Analyses of the Whittier, California Earthquake of January 1, 1976," 1977. (PB 283 750/AS)	26.00
EERL 77–06	Housner, G.W. and P.C. Jennings, "Earthquake Design Criteria for Structures," 1977 (PB 276 502/AS)	6.00
EERL 78–01	Beck, J.L., "Determining Models of Structures from Earthquake Records," 1978 (PB 288 806/AS)	31.00
EERL 78–02	Abdel-Ghaffar, A.M. and R.F. Scott, "An Investigation of the Dynamic Characteristics of an Earth Dam," 1978. (PB 288 878/AS)	20.00
EERL 78–03	Psycharis, I., "The Salonica (Thessaloniki) Earthquake of June 20, 1978," 1978. (PB 290 120/AS)	3.50
EERL 79–01	Mason, A.B., Jr., "Some Observations on the Random Response of Linear and Nonlinear Dynamical Systems," 1979. (PB 290 808/AS)	13.00
EERL 79–02	McVerry, G.H., "Frequency Domain Identification of Structural Models from Earthquake Records," 1979. (PB–80–194301)	22.00
EERL 80–01	Lee, D.M., P.C. Jennings and G.W. Housner, "A Selection of Important Strong Motion Earthquake Records," 1980. (PB 80 169196)	31.00
EERL 80–02	Abdel-Ghaffar A.M., R.F. Scott and M.J. Craig, "Full-Scale Experimental Investigation of a Modern Earth Dam," 1980. (PB–81–123788)	10.00
EERL 80–03	Rutenberg, A., P.C. Jennings and G.W. Housner, "The Response of Veterans Hospital Building 41 in the San Fernando Earthquake," 1980. (PB–82–201377)	14.50
EERL 80–04	Haroun, M.A., "Dynamic Analyses of Liquid Storage Tanks," 1980. (PB–81–123275)	29.00
EERL 80–06	Liu, W.K., "Development of Finite Element Procedures for Fluid-Structure Interaction," 1980. (PB 184078)	23.50
EERL 80–07	Yoder, P.J., "A Strain-Space Plasticity Theory and Numerical Implementation," 1980. (PB–82–201682)	13.50
EERL 80–08	Krousgrill, C.M., Jr., "A Linearization Technique for the Dynamic Response of Nonlinear Continua," 1980. (PB–82–201823)	13.50
EERL 80–09	Cohen, M., "Silent Boundary Methods for Transient Wave Analysis," 1980. (PB–82–201831)	20.00
EERL 81–01	Hall, S.A., "Vortex-Induced Vibrations of Structures," 1981. (PB–82–201849)	22.50
EERL 81–02	Psycharis, I.N., "Dynamic Behavior of Rocking Structures Allowed to Uplift," 1981. (PB–82–212945)	23.50
EERL 81–04	Shih, C.-F., "Failure of Liquid Storage Tanks Due to Earthquake Excitation," 1981. (PB–82–215013)	20.00
EERL 82–01	Lin, A.N., "Experimental Observations of the Effect of Foundation Embedment on Structural Response," 1982. (PB–84–163252)	33.00
EERL 82–02	Botelho, D.L.R., "An Empirical Model for Vortex-Induced Vibrations," 1982. (PB–84–161157)	12.00
EERL 82–03	Rashed, A., "Dynamic Analysis of Fluid-Structure Systems, " 1982. (PB–84–162916)	21.00

EERL 83–01	McVerry, G.H. and J.L. Beck, "Structural Identification of JPL Building 180 Using Optimally Synchronized Earthquake Records." 1983. (PB–84–162833)	7.50
EERL 83–02	Jain, S.K., "Analytical Models for the Dynamics of Buildings," 1983. (PB–84–161009)	20.00
EERL 83–03	Huang, M.-J., "Investigation of Local Geology Effects on Strong Earthquake Ground Motions," 1983. (PB–84–161488)	24.00
EERL 84–01	Wilson, J.C., "Analysis of the Observed Earthquake Response of a Multiple Span Bridge," 1984. (PB–85–240505/AS)	17.00
EERL 84–02	Iwan, W.D., M.A. Moser and C.-Y. Peng, "Strong-Motion Earthquake Measurement Using a Digital Accelerograph," 1984. (PB–91–170191/AS)	5.50
EERL 84–04	Cifuentes, A.O., "System Identification of Hysteretic Structures," 1984. (PB–240489/AS14)	17.00
EERL 85–01	Smith, K.S., "Stochastic Analysis of the Seismic Response of Secondary Systems," 1984. (PB–85–240497/AS)	14.00
EERL 85–02	Maragakis, E., "A Model for the Rigid Body Motions of Skew Bridges," 1984. (PB–85–248433/AS)	23.00
EERL 85–03	Jeong, G.D., "Cumulative Damage of Structures Subjected to Response Spectrum Consistent Random Process," 1985. (PB–86–100807)	10.50
EERL 85–04	Pak, R.Y.S., "Dynamic Response of a Partially Embedded Bar Under Transverse Excitations," 1985. (PB–87–232856/A06)	12.00
EERL 85–05	Chelvakumar, K., "A Simple Strain-Space Plasticity Model for Clays," 1985. (PB–87–234308/CC)	19.50
EERL 85–06	Beck, R.T. and J.L. Beck, "Comparison Between Transfer Function and Modal Minimization Methods for System Identification," 1985. (PB–87–234688/A04)	5.50
EERL 86–01	Peek, R., "Analysis of Unanchored Liquid Storage Tanks Under Seismic Loads," 1986. (PB–87–232872/A12)	23.50
EERL 86–02	Paparizos, L.G., "Some Observations on the Random Response of Hysteretic Systems," . 1986. (PB–88235668/CC)	18.00
EERL 86–03	Moser, M.A., "The Response of Stick-Slip Systems to Random Seismic Excitation," 1986. (PB–89–194427/AS)	15.00
EERL 87–01	Jayakumar, P., "Modeling and Identification in Structural Dynamics," 1987. (PB–89–194146/AS)	20.50
EERL 87–02	Duron, Z.H., "Experimental and Finite Element Studies of a Large Arch Dam," 1987. (PB–89–194435/AS)	17.00
EERL 87–03	Dowling, M.J., "Nonlinear Seismic Analysis of Arch Dams," 1987. (PB–89–194443/AS)	17.00
EERL 87–04	Whirley, R.G., "Random Response of Nonlinear Continuous Systems," 1987. (PB–89–194153/AS)	14.50
EERL 87–05	Peng, C.-Y., "Generalized Model Identification of Linear and Nonlinear Dynamic Systems," 1987. (PB–89–194419/AS)	15.00
EERL 88–01	Levine, M.B., J.L. Beck, W.D. Iwan, P.C. Jennings and R. Relles, "Accelerograms Recorded at Caltech During the Whittier Narrows Earthquakes of October 1 and 4, 1987: A Preliminary Report," 1988. (PB–91–170100)	5.50
EERL 88–02	El-Aidi, B., "Nonlinear Earthquake Response of Concrete Gravity Dam Systems," 1988. (PB–89–193124/AS)	18.00
EERL 88–03	Nowak, P.S., "Effect of Nonuniform Seismic Input on Arch Dams," 1988. (PB–89–194450/AS)	14.50
EERL 89–01	Donlon, W.P., Jr., "Experimental Investigation of the Nonlinear Seismic Response of Concrete Gravity Dams," 1989. (PB–91–170118)	23.00
EERL 89–02	Jensen, H.A., "Dynamic Response of Structures with Uncertain Parameters," 1989. (PB–91–154187/AS)	26.50
EERL 89–03	Thyagarajan, R.S., "Modeling and Analysis of Hysteretic Structural Behavior," 1989. (PB–91–154195)	18.50
EERL 89–04	US-China Joint Project on Strong Ground Motion Measurements, "Digital Near Source Accelerograms Recorded by Instrumental Arrays in Tangshan, China," (PB–91–154112)	26.00
EERL 90–01	Hou, Z., "Nonstationary Response of Structures and Its Application to Earthquake Engineering," 1990. (PB–91–170092)	21.50
EERL 90–02	Levine, M., "Accelerogram Processing Using Reliability Bounds and Optimal Corrections Methods," 1990. (PB–91–170209/AS)	29.00
EERL 90–03	Papadimitriou, K., "Stochastic Characterization of Strong Ground Motion and Applications to Structural Response," 1990. (PB–91–170217/AS)	21.00
EERL 91–01	Katafygiotis, Lambros S., "Treatment of Model Uncertainties in Structural Dynamics," 1991.	19.50
EERL 91–02	Hall, John F., Michael J. Dowling and Bahaa El-Aidi, "Defensive Design of Concrete Gravity Dams," 1991.	12.00
EERL 91–03	Beck, Robert T., "Fundamental Problems in the Application of Structural Identification Procedures to Damage Detection," 1991.	16.50
EERL 92–01	Challa, M.V.R., "Nonlinear Seismic Behaviour of Steel Planar Moment-Resisting Frames," 1992.	26.50
EERL 92–02	Chiang, Dar–Yun, "Parsimonious Modeling of Inelastic Structures," 1992.	18.50
EERL 95-01	Pich, Peter, "Nonlinear Rigid Block Dynamics," 1995.	18.50

Disaster Research Center (DRC)

DRC 72–01	Whitney, A.W., "On Insurance Settlements Incident to the 1906 San Francisco Fire," 1972. (PB 213 256)	7.50
DRC 73–01	Housner, G.W., "Earthquake-Resistant Design of High-Rise Buildings," 1973.	8.00
DRC 73–02	"Earthquake and Insurance," Earthquake Research Affiliates Conference, 2–3 April, 1973, 1973. (PB 223 033)	16.00

Dynamics Laboratory (DYNL)

DYNL–100	Yang, I-M., "Stationary Random Response of Multidegree-of-Freedom Systems," 1970.	13.00
DYNL–101	Patula, E.J., "Equivalent Differential Equations for Non-linear Dynamic Systems," 1970.	22.00

DYNL–102	Prelewicz, D.A., "Range of Validity of the Method of Averaging," 1970.	10.00
DYNL–103	Vijayaraghavan, A., "Free and Forced Oscillations in a Class of Piecewise-Linear Dynamic Systems," 1971.	10.50
DYNL–104	Stahl, K.J., "Dynamic Response of Circular Plates Subjected to Moving Massive Loads," 1971.	18.50
DYNL–105	Furuike, D.M., "Dynamic Response of Hysteretic Systems With Application to a System Containing Limited Slip," 1971.	14.00
DYNL–106	Kim, B.-K., "Piecewise Linear Dynamic Systems with Time Delays," 1972.	16.50
DYNL–107	Viano, D.C., "Wave Propagation in a Symmetrically Layered Elastic Plate," 1972.	13.00
DYNL–108	Irvine, H.M., "Studies in the Statics and Dynamics of Simple Cable Systems," 1974.	17.00
DYNL 73–01	Moeller, T.L., "The Dynamics of a Spinning Elastic Disk with Massive Load," 1973.	12.00
DYNL 74–01	Blevins, R.D., "Flow Induced Vibration of Bluff Structures," 1974.	15.00
DYNL 77–01	Edwards, D.B., "Time Domain Analysis of Switching Regulators," 1977.	21.00
DYNL 86–01	Jones, N.P., "Flow-Induced Vibration of Long Structures," 1986. (PB–88–106646/A08)	14.50
DYNL 89–01	Smith, P.W., Jr., "Considerations for the Design of Gas-Lubricated Slider Bearings," 1988. (PB–91–170126)	24.00

Soil Mechanics Laboratory (SML)

SML 82–02	Ortiz, L.A., "Dynamic Centrifuge Testing of Cantilever Retaining Walls," 1982. (PB–84–162312)	36.00
SML 83–01	Bardet, J.P., "Application of Plasticity Theory to Soil Behavior: A New Sand Model," 1983. (PB–84–162304)	20.50
SML 83–02	Hushmand, B., "Experimental Studies of Dynamic Response of Foundations," 1983. (PB–86–115383/A)	31.50
SML 85–01	Tan, T.-S., "Two Phase Soil Study: A. Finite Strain Consolidation, B. Centrifuge Scaling Considerations," 1985. (PB–87–232864/CC)	15.50
SML 87–01	Burridge, P.B., "Failure of Slopes," 1987. (PB–89–194401/AS)	25.50
SML 90–01	Allard, M.A., "Soil Stress Field Around Driven Piles," 1989. (PB–91–170084)	19.50
SML 90–02	Tan, P., "Numerical Simulations of Two-Dimensional Saturated Granular Media," 1989. (PB–91–170255/AS)	21.50
SML 91–01	Yan, Liping, "Seismic Deformation Analysis of Earth Dams: A Simplified Method," 1991.	19.00

Other Reports

Alford, J.L., G.W. Housner and R.R. Martel, "Spectrum Analysis of Strong-Motion Earthquake," revised 1964.	11.00
Housner, G.W., "Intensity of Ground Motion During Strong Earthquakes," 1952.	4.00
Hudson, D.E., J.L. Alford and G.W. Housner, "Response of a Structure to an Explosive Generated Ground Shock," 1952.	5.00
Housner, G.W., "Analysis of the Taft Accelerogram of the Earthquake of 21 July 1952."	3.50
Housner, G.W., "A Dislocation Theory of Earthquakes," 1953.	4.00
Caughey, T.K. and D.E. Hudson, "An Electric Analog Type Response Spectrum," 1954.	4.00
Hudson, D.E. and G.W. Housner, "Vibration Tests of a Steel-Frame Building," 1954.	3.00
Housner, G.W., "Earthquake Pressures on Fluid Containers," 1954.	4.50
Hudson, D.E., "The Wilmot Survey Type Strong-Motion Earthquake Recorder," 1958.	3.00
Hudson, D.E. and W.D. Iwan, "The Wilmot Survey Type Strong-Motion Earthquake Recorder, Part II," 1960.	5.00
Caughey, T. K., D.E. Hudson and R.V. Powell, "The CIT Mark II Electric Analog Type Response Spectrum Analyzer for Earthquake Excitation Studies," 1960.	5.00
Keightley, W.O., G.W. Housner and D.E. Hudson, "Vibration Tests of the Encino Dam Intake Tower," 1961.	5.00
Merchant, H.C., "Mode Superposition Methods Applied to Linear Mechanical Systems Under Earthquake Type Excitation," 1961.	12.50
Iwan, W.D., *"The Dynamic Response of Bilinear Hysteretic Systems," 1961.*	15.50
Hudson, D.E., "A New Vibration Exciter for Dynamic Test of Full-Scale Structures," 1961.	4.00
Hudson, D.E., "Synchronized Vibration Generators for Dynamic Tests of Full-Scale Structures," 1962.	8.00
Jennings, P.C., "Velocity Spectra of the Mexican Earthquakes of 11 May and 19 May 1962," 1962.	5.00
Jennings, P.C., "Response of Simple Yielding Structures to Earthquake Excitation," 1963.	20.00
Keightley, W.O., "Vibration Tests of Structures," 1963.	24.00
Caughey, T.K. and M.E.J. O'Kelly, "General Theory of Vibration of Damped Linear Dynamic Systems," 1963.	11.50
O'Kelly, M.E.J., "Vibration of Viscously Damped Linear Dynamic Systems," 1964.	23.00
Nielsen, N.N., "Dynamic Response of Multistory Buildings," 1964.	19.00
Tso, W.K., "Dynamics of Thin-Walled Beams of Open Section," 1964.	19.00
Keightley, W.O., "A Dynamic Investigation of Bouquet Canyon Dam," 1964.	8.00
Malhotra, R.K., "Free and Forced Oscillations of a Class of Self-Excited Oscillators," 1964.	9.50
Hanson, R.D., "Post-Elastic Response of Mild Steel Structures," 1965.	28.00
Masri, S.F., "Analytical and Experimental Studies of Impact Dampers," 1965.	9.00
Hanson, R.D., "Static and Dynamic Tests of a Full-Scale Steel-Frame Structures," 1965.	7.00
Cronin, D.L., "Response of Linear, Viscous Damped Systems to Excitations Having Time-Varying Frequency," 1965.	17.00
Hu, P.Y.-F., "Analytical and Experimental Studies of Random Vibration," 1965.	18.00
Crede, C.E., "Research on Failure of Equipment when Subject to Vibration," 1965.	20.00
Lutes, L.D., "Numerical Response Characteristics of a Uniform Beam Carrying One Discrete Load," 1965.	10.00

Rocke, R.D., "Transmission Matrices and Lumped Parameter Models for Continuous Systems," 1966.	16.50
Brady, A.G., "Studies of Response to Earthquake Ground Motion," 1966.	16.50
Atkinson, J.D., "Spectral Density of First Order Piecewise Linear Systems Excited by White Noise," 1967.	20.00
Dickerson, J.R., "Stability of Parametrically Excited Differential Equations," 1967.	8.50
Giberson, M.F., "The Response of Nonlinear Multi-Story Structures Subjected to Earthquake Excitation," 1967.	24.00
Hallanger, L.W., "The Dynamic Stability of an Unbalanced Mass Exciter," 1967	7.50
Husid, R., "Gravity Effects on the Earthquake Response of Yielding Structures," 1967.	16.50
Kuroiwa, J.H., "Vibration Test of a Multistory Building," 1967.	10.00
Lutes, L.D., "Stationary Random Response of Bilinear Hysteretic Systems," 1967.	19.50
Nigam, N.C., "Inelastic Interactions in the Dynamic Response of Structures," 1967.	21.00
Nigam, N.C. and P.C. Jennings, "Digital Calculation of Response Spectra from Strong-Motion Earthquake Records," 1968	7.50
Spencer, R.A., "The Nonlinear Response of Some Multistory Reinforced and Prestressed Concrete Structures Subjected to Earthquake Excitation," 1968.	7.50
Jennings, P.C., G.W. Housner and N.C. Tsai, "Simulated Earthquake Motions," 1968.	6.00
"Strong-Motion Instrumental Data on the Borrego Mountain Earthquake of 9 April 1968," (USGS and EERL Joint Report), 1968.	12.00
Peters, R.B., "Strong Motion Accelerograph Evaluation," 1969.	12.00
Heitner, K.L., "A Mathematical Model for Calculation of the Run-Up of Tsunamis," 1969.	13.00
Trifunac, M.D., "Investigation of Strong Earthquake Ground Motion," 1969.	16.00
Tsai, N.C., "Influence of Local Geology on Earthquake Ground Motion," 1969.	21.00
Heitner, K.L., "Additional Investigations on a Mathematical Model for Calculation of Run-Up of Tsunamis," 1970.	13.00
Hudson, D.E. (Editor), "Strong-Motion Instrumental Data on the San Fernando Earthquake of February 9, 1971," (Seismological Field Survey, NOAA, C.I.T. Joint Report), 1971. (PB 204 198)	26.00
Daly, W., W. Judd and R. Meade, "Evaluation of Seismicity at U.S. Reservoirs," USCOLD, Committee on Earthquakes, 1971. (PB 270 036/AS)	3.00
Morrison, P., R. Maley, G. Brady and R. Porcella, "Earthquake Recordings on or Near Dams," USCOLD, Committee on Earthquakes, 1977. (PB 285 867/AS)	13.00
Helmberger, D.V. and P.C. Jennings (Organizers), "Strong Ground Motion: N.S.F. Seminar-Workshop," 1978.	10.50
Iwan, W.D. (Editor), "Proceedings of the U.S. National Workshop on Strong-Motion Earthquake Instrumentation, April 12–14,1981 Santa Barbara, California." California Institute of Technology, 1981.	free
National Academy Press, "Earthquake Engineering Research—1982."	N/A
National Academy Press, *"Earthquake Engineering Research—1982, Overview and Recommendations."*	*free*
Iwan, W.D. (Editor), "Proceedings of the International Workshop on Seismic Design and Reassessment of Offshore Structures, December 7-9, 1992." California Institute of Technology,1993.	20.00

updated February 9, 1995